1 Introduction

1.1 Current status of the iron and steelmaking industry

Current world iron production comprises of 600 million tons per year (MTPY) of hot metal and pig iron, 37.1 MTPY of direct reduced iron (DRI) and hot briquetted iron (HBI), and approximately 2 MTPY of hot metal produced by direct smelting. Most hot metal is produced in blast furnaces, which are operated in conjunction with mining beneficiation plants, pelletizing plants, sinter plants, coke batteries, limestone plants, oxygen plants, fuel gas plants and power stations[1].

Virtually all the steel in the world is either produced in an oxygen steelmaking converter (such as a BOF, LD or OBM (Q-BOP)) or an electric arc furnace (EAF)[2]. Most of these steelmaking equipment was built or rebuilt between 1955 and 1975. The BOF and EAF were the best technologies available at that time to further process blast furnace hot metal and relatively inexpensive scrap, into steel.

During the last three decades, more efficient blast furnaces, oxygen steelmaking, continuous casting and hot metal- and ladle metallurgy practices were developed. However, technology drivers are currently changing. At present, the most important technology drivers are[2,3,4]:

- **Lower capital and fixed cost:** The capital cost to value added ratio for integrated steelmaking is the highest of any major industry. Existing facilities are therefore expanded and renewed to optimise their useable life[1]. Both ore-based production and scrap-based production are accompanied by high fixed, labour and raw material cost. Producers therefore tend towards lower capital costs as well as lower and more flexible fixed costs.
- **Energy and environmental:** Environmental drivers are usually in response to national or international regulation, with reduction of greenhouse gasses and recycling of steelmaking waste materials the major drivers. The reduction of energy consumption goes hand in hand with reduction of CO_2 emissions. Although reduction of energy consumption may be limited (due to the laws of conservation of energy), CO_2 emissions can be reduced by using fossil fuels to replace electrical energy. Note that electrical energy is only about 30-40% effective when considering production and transmission.

- **Flexibility:** In order to be responsive to market conditions, steelmakers need flexibility regarding raw materials, energy and production. Flexibility regarding the use of scrap, hot metal, direct reduced iron (DRI), waste oxides and iron carbide, and the substitution of coke with coal[5], will allow the producer to minimize input costs. The use of fossil fuel as well as electrical energy will optimise the process with respect to energy, cost and productivity. Finally, processes that can reduce or increase production economically will enable producers to respond to market conditions.
- **Competitive forces:** New technologies need to be competitive with existing technologies. The production cost of liquid steel therefore needs to be reduced continuously.

Industry's response to these technology drivers will probably result in incremental improvements in existing technologies as well as in major developments in certain areas (of which one is direct iron and steelmaking processes)[6]. During the next 20 years the blast furnace will continue to produce most of the iron requirements, while direct reduced iron (DRI) could represent 20% of the virgin iron units by 2015[3]. Direct smelting may be commercialised, initially for treatment of waste oxides and to supplement scrap or to increase hot metal in integrated plants[6].

1.2 Direct reduction processes

Direct reduction processes are methods for reducing iron ore directly to metallic iron[7]. These methods bypass several of the steps currently used in conventional steelmaking. Direct reduction processes can be separated into two major categories: i.e. gas-based- and coal-based processes.

1.2.1 Gas-based DRI processes

Gas-based processes dominate the direct reduced iron (DRI) market, with **shaft furnace gas-based processes** accounting for 94% of world DRI production. From this, the Midrex process accounts for 70% (with 50 operational furnaces), the HYL processes accounts for 23% (with 29 operational furnaces) while the Arex accounts for approximately 1% (with 5 operational furnaces). The contribution of the Purofer furnace is negligible[1] while the Danarex process is still at pilot plant stage. The major differences between these processes are the way in which reducing gas for the

process is generated. The Midrex uses a natural gas reformer, the HYL uses a steam reformer, and the Arex is based on direct injection of natural gas into a reduction shaft. All of these processes require the use of high grade, sized iron ore lumps and/or pellets as feedstock. Typical process parameters for shaft furnace gas-based processes are shown in **Table 1**.

Table 1: *Process parameters for shaft furnace gas-based processes* [1,8].

Parameter	Unit	Midrex	HYL (shaft process)	HYL (self-reforming)	Arex	Danarex
Ore/pellets	**t/t DRI**	1.45	1.45	1.42	1.45	1.42
Natural gas	**Gcal/t**	2.42	2.42	2.23	2.2-2.4	2.4
Oxygen	**Nm^3/t**			41		38
Pressure	**atm**	1	5		2	1
Metallization	**%**	92-95	92-95	92-95	92-95	91-94
%C in DRI	**%**	1.0-3.5	1.2-4.5	1.0-5.0	1.8-2.0	1.0-4.0
Capital cost	**USD/t**	125	170	140		

In addition to shaft furnace gas based processes are **fluidised bed gas based technologies** such as the Fior-, Finmet-, Iron carbide- and Circored processes. These processes were developed to use iron ore fines as feedstock and are mostly multi-stage processes.

The **Finmet process** was derived from the Fior process (of which a plant is operational in Venezuela). Two Finmet plants are currently operational: one at Port Hedland, which was commissioned in 1999, and another that was commissioned at Orinoco Iron C.A in 2000. The Finmet is a 4-stage process, operating at a pressure between 11 and 13 atm, and temperatures between 550°C and 800°C. The main problems encountered with this process were difficulties in achieving high degrees of reduction due to temperature control as well as problems with briquetting of the product.

The **Iron carbide process**, which was developed by Hazen Research Institute, uses iron ore fines to produce 80% Fe_3C. The single vessel process is essentially a two-stage batch process. During the first stage the ore is reduced at temperatures between 570°C and 600°C with hydrogen (from a steam reformer), after which the metal is carburised with methane. Although the design capacity of the plant was 300000 tons per annum (tpa), the Trinidad plant had an actual capacity of 120000 tpa and was therefore shut down in 1999.

The **Circored process**, which was developed by Lurgi and commissioned in 1999, produces HBI from iron ore fines. For this, the process uses almost pure hydrogen, which is produced in a steam reformer with natural gas as heat source. The process comprises of two reduction stages, i.e. a circulating Fluidized bed as well as a fixed fluidised bed. The Fluidized bed operates at 630°C and a pressure of 4 atm to achieve between 92 and 93% metallisation. Due to the use of hydrogen as reductant the carbon content of the product is virtually zero. Although the process uses readily available ore fines, the operating cost of the process is relatively high.

1.2.2 Coal-based DRI processes

Coal-based DRI processes comprise the following:

- Rotary kiln based processes
- Rotary hearth based processes
- Fluidised bed based processes

The coal-based processes are less environmentally friendly than gas-based processes, due to higher CO_2 emissions. The production of fine ashes containing sulfur compounds, which requires treatment before disposal, is another potential problem of these processes[(1)].

Coal based DRI production is mainly accounted for by rotary kiln processes such as the SL/RN process (with commercial plants in South Africa, India and New Zealand), the Davy process (with commercial plants in South Africa and China), and the Accar process (with a commercial plant in Norway).

The SL/RN process is schematically shown in ***Figure 1***

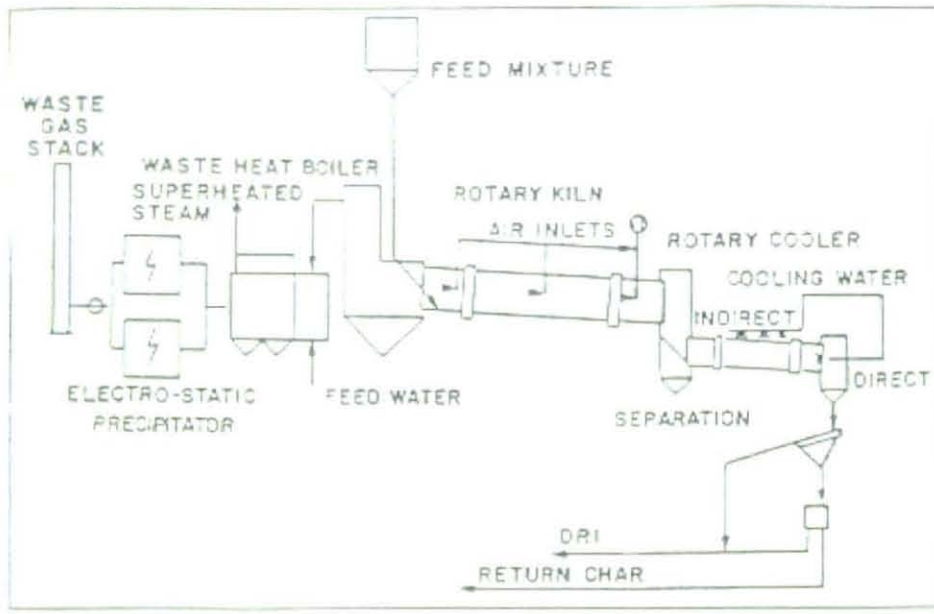

Figure 1: *Schematic illustration of the SL/RN process*[1]

Rotary kilns (such as the SL/RN) typically have capacities ranging between 150000 and 200000 tpa. These processes charges lump ore, pellets and fines (1.42 t/t HBI), fine coal (0.85 t/t HBI) and limestone and dolomite (mainly for sulphur removal) into an inclined kiln that rotates at speeds less than 1rpm. The ore is dried, pre-heated and reduced as it moves along the length of the kiln. Between 92 and 93 % metallization of the iron ore is achieved within 14 hours, due to solid state reduction in the composite bed. The heat for reactions is provided by combustion of coal and part of the CO and H_2 that evolves from the reduction reactions, as well as from air-fuel burners. The process is operated at atmospheric pressure in the temperature range 1000°C to 1100°C. At the discharge end DRI is separated from char and ash to yield metal with a carbon content of 0.5% and sulphur content less than 0.02%. The major weaknesses of the process are the high capital cost, limited plant size, possible environmental impact, complex handling procedures at the exit end of the kiln and quality limitations of the DRI due to the presence of sulphur and gangue.

Rotary hearth coal-based processes include the Fastmet, Inmetco, Comet, Primus, IDI, Redsmelt and Itmk3 processes. The Fastmet process is schematically shown in ***Figure 2.***

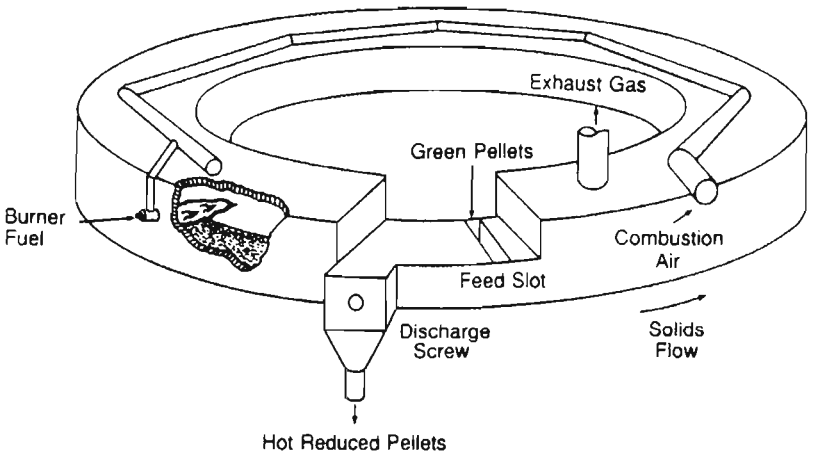

Figure 2: *Schematic illustration of Midrex's Fastmet process*[1].

In the Fastmet and Inmetco processes, pellets containing ore fines (1.34 t/t DRI) and coal fines (0.38 t/t DRI) are charged onto a rotary hearth where they are dried, pre-heated and reduced in the solid state. Carbon in the agglomerate is the reductant, with various air-fuel burners providing heat for the reactions. The process is operated at atmospheric pressure in the 1200°C to 1350°C range. 92% Metallization is achieved within 12 to 15 minutes to produce metal with a carbon content between 1.5 and 5%, and sulphur content between 0.12 and 0.2%. The design capacity regarding iron production is 450000 tpa. However, the two operational plants that were commissioned in 2001 at Kobe steel (for processing of waste oxides) have capacities of 50000 tpa.

The Comet process is similar to the Fastmet and Inmetco processes, but ore and coal fines are charged as discrete layers. Since the excess char and ash can be removed from the final product, the DRI produced has lower carbon (0.5 to 0.7%) and sulphur (0.02 to 0.06%) content.

The **fluidising bed coal-based Circofer process** (developed by Lurgi) is similar to the Circored process. The difference however is that instead of using natural gas, the process uses gas generated (at 1000°C in a gasifier) from coal. The main inputs

to the process consist of iron ore fines (1.42 t/t HBI), coal (0.8 t/t HBI) and oxygen (205 Nm^3/t HBI). The iron ore fines (in the size range 0.03 to 1.00 mm) are pre-heated to between 800 and 900°C and pre-reduced during the first stage in a circulating fluidised bed, after which final reduction occurs in another fluidised bed. The process produces 92 % metallized HBI with carbon content about 2% and sulphur content less than 0.02%. The design capacity for this plant is 500000 tpa.

1.3 Direct Smelting processes

1.3.1 Two stage processes

Two stage direct smelting processes are processes such as the Corex, Finex, Hismelt, AISI, DIOS, CCF (which is similar to cleansmelt), IDI, Redsmelt, Fastmelt, Inmetco etc. These processes use an ore pre-reduction step followed by a smelting step.

Pre-reduction occurs either in shaft furnaces (Corex and AISI), fluidised beds (DIOS and Hismelt), rotary hearth furnaces (Redsmelt) or melting cyclones (CCF). In these processes, ore is charged to the pre-reduction furnace where off gas from the smelter unit is used for partial reduction of the ore. The partially reduced ore, coal, fluxes, oxygen and/or air are fed to the smelter unit, containing hot metal and slag. The furnace is operated at a pressure of 4 atm with the temperature of the pre-reduction shaft and smelter approximately 900°C and 1500°C respectively. Since the cleaned product gas from these processes has considerable value, the gas is either consumed as fuel for the plant, utilised in direct reduction plants, or used to produce electricity.

The Corex process (developed by Voest Alpine) is schematically shown in ***Figure 3***. This is the only smelting reduction technology in commercial use, with four of the five plants currently operational.

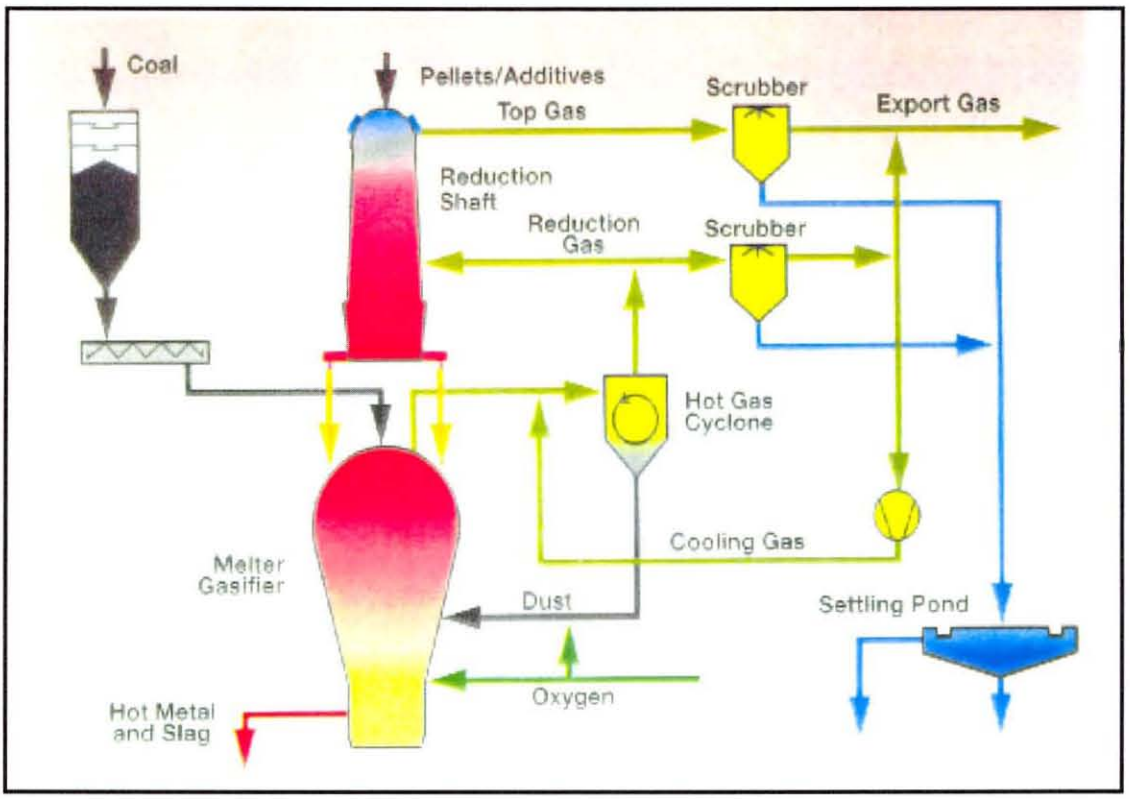

Figure 3: *Schematic illustration of the Corex process*[1].

Typical consumption rates for the Corex are as follows: lump ore and pellets:1.48 t/t hot metal (HM), coal: 0.98 t/t HM (of which 10% is usually coke) and limestone: 0.242 t/t HM. The carbon content of the metal produced is typically 4 to 5% and the sulphur content between 0.05 and 0.1%. The slag typically has a CaO/SiO_2 ratio between 1 and 1.3, with a FeO content between 1 and 2. Typical production rates are between 600000tpa and 1.1 MTPY. The major weaknesses of the process are high capital cost, limited size compared to blast furnaces and the need to utilize off gas to be competitive.

1.3.2 One stage processes

One stage direct smelting processes are processes such as the Romelt (also Vanyukov), Technored, Ausmelt and Ifcon® The Romelt process is schematically shown in ***Figure 4***.

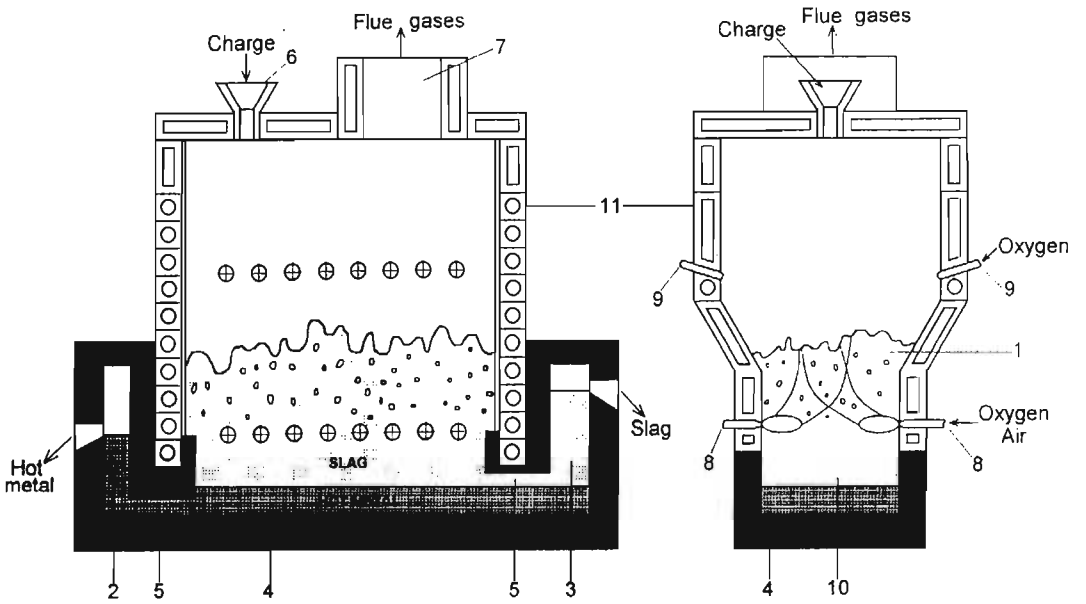

1- foaming slag; 2- siphon for hot metal; 3- siphon for slag; 4 – refractory lined hearth; 5 – orifice; 6 – feed hopper; 7 – flue gas duct; 8 – lower tuyeres; 9 – upper tuyeres; 10 – calm slag; 11 – water-cooled panels

Figure 4: *Schematic illustration of the Romelt process*[1].

In **Romelt** and **Ausmelt** processes, lump or fine ore, coal and fluxes are charged directly into the smelter containing hot metal and slag. The Romelt process uses tuyeres located in the vessel sidewalls for air/oxygen injection, while the Ausmelt (which was developed for non ferrous metals) uses a top lance system. Fine coal is also injected through the lance in the Ausmelt process.

The Romelt process consumes 1.5 to 2.0 tons of iron ore fines, 0.8 to 1.1 tons of coal, 0.1 tons of limestone, 850 to 1100 Nm^3 of oxygen and 450 to 700 Nm^3 of air to produce a ton of hot metal. The hot metal contains 4 to 5 % carbon and 0.025 to 0.05 % sulphur, while the slag produced has a CaO/SiO_2 ratio between 1 and 1.3, with a FeO content between 1.5% and 3%.

The **Technored** process (which is shown schematically in ***Figure 5***) uses unfired green pellets (1.5 to 1.6 t/t HM) and coal (0.74 t/t HM) to produce hot metal with carbon contents between 3.5% and 4.5%, and sulphur contents between 0.05% and

0.1%. The slag produced has a CaO/SiO_2 ratio between 1 and 1.3, and a FeO content of approximately 0.5%.

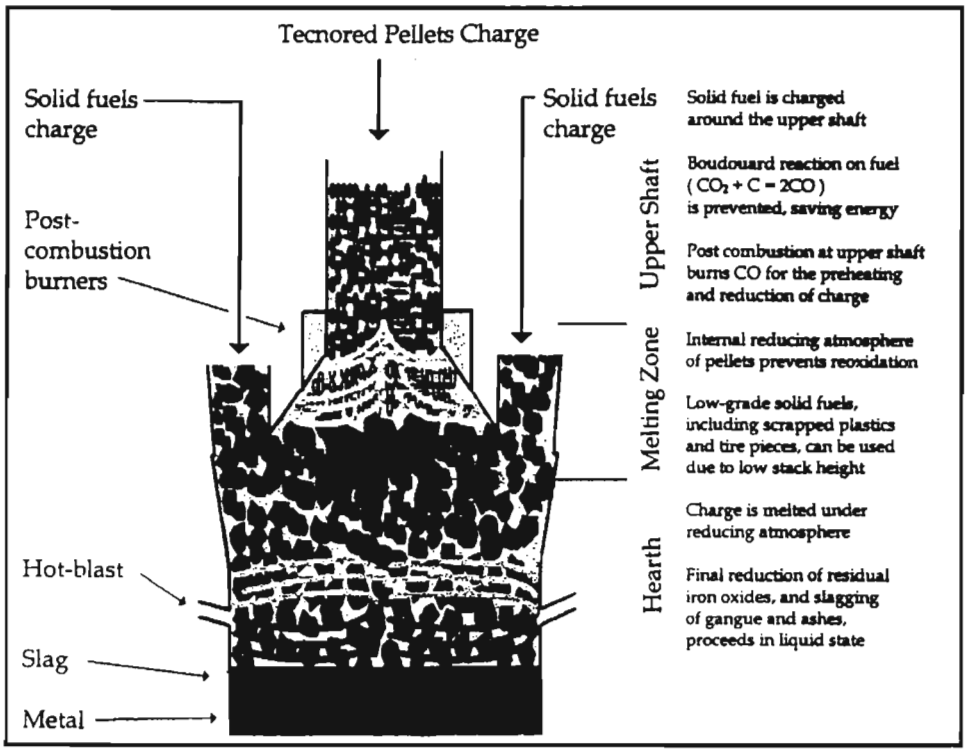

Figure 5: *Schematic illustration of the Technored process*[1].

While other direct smelting processes produces either hot metal or high carbon steel, the **Ifcon**® process[9] produces liquid crude steel with carbon content ±0.05 %, and phosphorus content ±0.007%. Other advantages of the process is that it uses ore fines, non-coking coal, and unburnt fluxes (dolomite and limestone) as feed materials. Energy for the process is supplied as a combination of fossil fuel and electrical energy, thereby reducing the electrical energy consumption significantly. The disadvantages of the process are the relatively slow production rate, and high sulphur content ±0.1 % combined with high oxygen content of the bath. Although the original plant was a horizontal cylindrical vessel, the current reactor is a vertical cylindrical vessel, as shown schematically in ***Figure 6***.

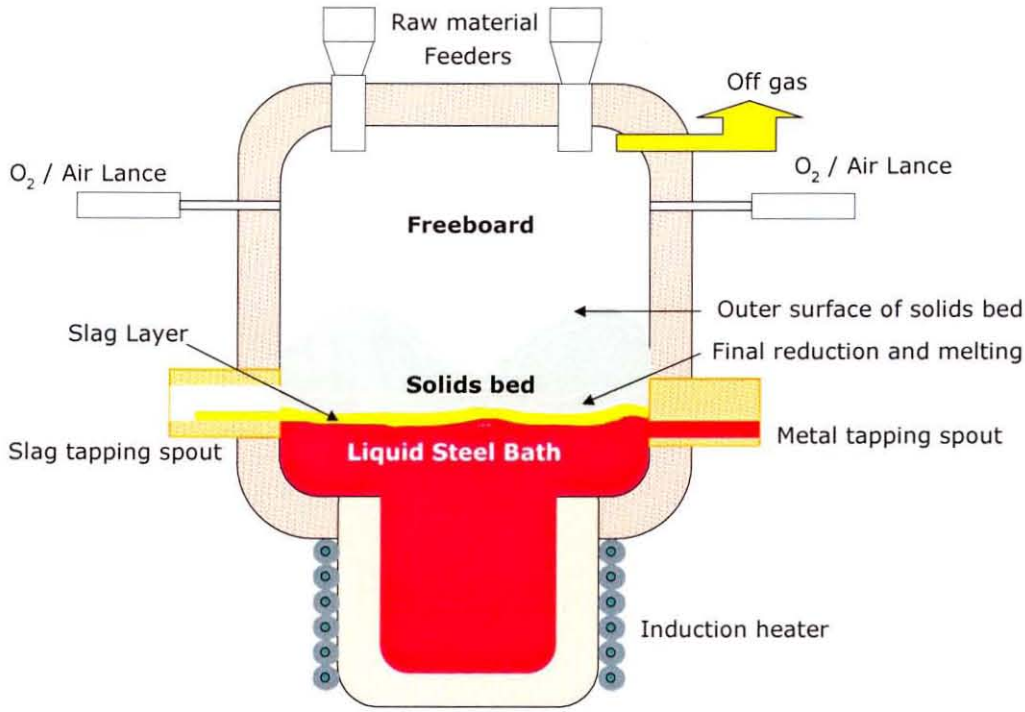

Figure 6: *Schematic representation of the current configuration of the Ifcon® furnace.*

1.4 Process description of the Ifcon® process

The feed material is a composite mixture of iron ore fines, coal, dolomite and limestone. The material mixture is fed from the top of the furnace, through the freeboard, onto a solids bed. The solids bed, which floats on top of the metal bath, covers most of the planar surface of the bath.

The bath is heated from below with induction heaters. Molten metal and slag are tapped intermittently through tapping spouts, by tilting the vessel.

Combustible gasses (such as CO and H_2)[10] are released into the freeboard, from the solids bed. Additional heat for the process is provided by post-combustion of these gasses with oxygen enriched air.

The amounts of ore and coal fed into the furnace, is controlled in such a way that there is always a slight excess of iron oxide in the slag. This means that the burden

at the bottom of bed is almost depleted of carbon. This results in the production of low carbon crude steel.

The Ifcon® process can be divided into three characteristic horizontal zones: the freeboard, the solids bed and the liquid bath, which are schematically shown in ***Figure 7***. The main material and energy flows are also indicated in the figure.

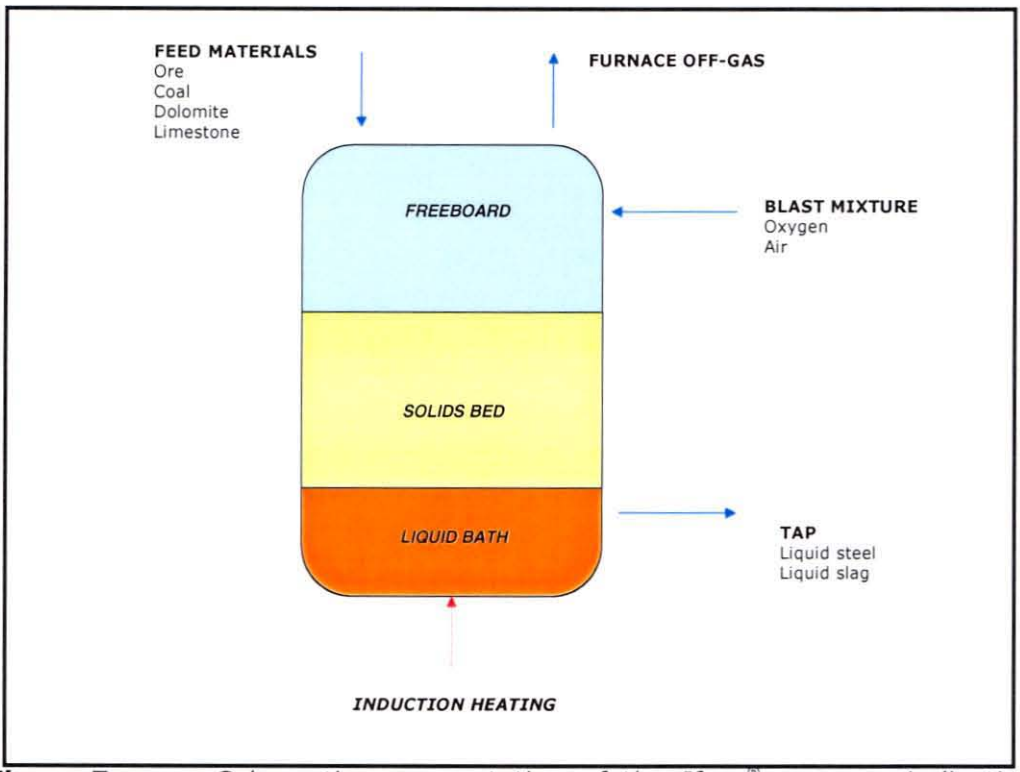

Figure 7: *Schematic representation of the Ifcon® process, indicating the most significant mass and energy input and output streams.*

1.4.1 The Freeboard

The main purpose of the freeboard is to generate heat by post-combustion of process gasses and other combustibles. This is achieved with oxygen-enriched air.

The heat generated is transferred to the upper part of the solids bed, where it is used to drive the overall endothermic reduction reactions.

The rate at which heat is generated for a specific air oxygen mixture is mainly determined by the rate at which combustible gasses evolve from the solids bed and the degree of post-combustion achieved in the freeboard[11,12,13].

1.4.2 The solids bed

The heat generated in the freeboard of the furnace is transferred to the upper part of the solids bed, mainly by radiation. This heat is used for heating material at the top of the bed. As this material reaches temperatures in excess of 700°C, the carbon gasification (or Boudouard) reaction sets in, and reduction of the iron oxides commences[14]. During heat-up, several other endothermic reactions occur, such as drying, devolatilization, and calcination of dolomite and limestone.

The temperature in the upper part of the solids bed is determined by the rate at which heat is transferred to (and into) the bed, as well as the rate at which heat is used to drive the endothermic reactions in the bed[12].

Since bulk melting does not occur in the top part of the bed[15,16], reduction in this area occurs mainly as solid-state reduction. (Solid-state reduction implies solid metal oxide being reduced with solid carbon, but with CO as intermediate gas.) The area is therefore referred to as the "solid-state reduction I" zone. The amount of liquid in the top part of the bed should be low enough, not to influence the solid-state reduction kinetics significantly[15,16].

The atmosphere inside the solids bed is reducing, as opposed to the freeboard gas, which is oxidizing[16].

Under steady state conditions, the bottom layer of the solids bed is continuously melted. Since material is fed to the top of the solids bed with the simultaneous melting of the bottom layer, the thickness of the solids bed remains constant. This implies that the process is operated with material continuously descending through the bed. As the original top layer of material descends through the solids bed, the material cools as a result of the endothermic reactions. This eventually results in the ceasing of reactions, hence creating a "dead" zone in the bed. In this area, the temperature gradient through the bed is negligible and reaction rates are very slow[16].

Below the dead zone, the temperature of the solids bed gradually increases, due to heat transfer from the bath below the bed. In this area, the endothermic calcination, Boudouard, and reduction reactions recommence. At temperatures below the temperature where bulk melting of the feed mixture occurs, reduction occurs as

solid-state reduction. This area is therefore referred to as the "solid-state reduction II" zone.

This study will investigate reduction occurring in the solids bed.

1.4.3 The molten bath

As the material at the bottom of the solids bed is heated to a temperature exceeding the liquidus of the slag, bulk melting of the material (as well as dissolution of solids into the slag) occurs. It is therefore expected that reduction, in this area, will occur as liquid-solid-state reduction. (Liquid-solid-state reduction implies reduction of molten metal oxide (which is dissolved in a slag) with carbon, which is either solid or dissolved in the metal, with CO as intermediate gas.) The mixing reaction regarding slag formation, as well as the reactions between metal and slag, is also expected to occur in this zone[16]. This is where final reduction and melting of bed material occurs and is referred to as the "final reduction and melting" zone.

Electrical energy input to the bottom of the furnace is required to supply energy for the reduction reactions occurring in the "solid-state reduction II" and "final reduction and melting" zones. Electrical energy is also required for melting of the slag and metal produced. The metal bath acts as a transport medium for this energy[13]. The bath also serves as a reservoir for the produced metal and slag.

The slag chemistry of the process is controlled by changing the feed mixture. Slag-metal equilibrium is however not achieved[17].

By considering the discussion above, the process can be re-divided into six zones, as shown in ***Figure 8.***

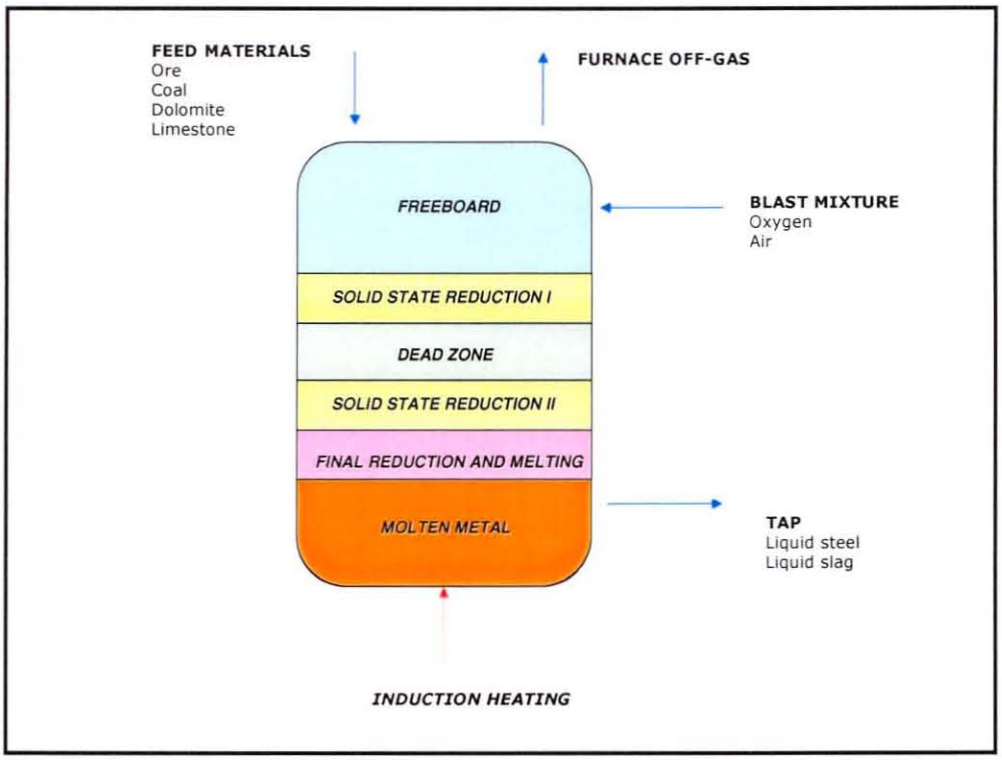

Figure 8: *Schematic representation of the IFCON process, indicating the most significant mass and energy input and output streams*

1.5 Hypothesis statement

During the first Ifcon test work[18] 80% reduction was achieved in the upper part of the solids bed, at a feed rate of 135 Fe/m^2/h (which corresponds with a production rate of 56 kg Fe/m^2/h). During pilot plant trails, crude steel was produced at a rate of 100 kg Fe per m^2 (scaled to the planar surface area of the bath). Additional investigations[10,12,19] showed that approximately 30% reduction was achieved (as solid state reduction) in the "solid state reduction I" zone of the solids bed. At the time it was assumed that the rate of reduction was controlled by a combination of the rate of heat transfer from the freeboard to the solids bed and the rate of the gasification reaction. It was also assumed that volatiles did not contribute to the reduction reaction in the solids bed[15].

Regarding the bottom of the solids bed, it was assumed that final reduction (up to 80% reduction) was achieved as solid-state reduction. The reduced burden was then melted, to form slag and liquid metal.

1.5.1 Objective of this study

This study aimed to test the assumptions stated above, by investigating the following:

- Is the rate of reduction in the solids bed influenced by the rate of heat transfer to the solids bed ?
- Is the rate of reduction in the solids bed influenced by the reactivity of the coal ?
- Is the rate of reduction in the solids bed influenced by the reducibility of the ore ?
- Does volatiles contribute to the rate of reduction in the solids bed ?
- Is final reduction (up to 80%) achieved as solid-state reduction at the bottom of the solids bed, when producing at a rate of 100 kg Fe per m^2 of planar bath surface area, per hour ?
- If final reduction is not achieved as solid-state reduction, at a rate of 100 kg Fe/m^2/h, what is the extent of reduction achieved as solid-state reduction ?

Ifcon® is a very complex and integrated process, which cannot be duplicated in a single laboratory experiment. The investigation was therefore done in two phases.

1.5.1.1 Phase 1: Rate determining step investigation

The main aim of the first phase of this investigation was to determine the optimum feed materials (and criteria for the selection of optimum feed material) for the "Solid-state Reduction I" zone. From literature, it was not clear what the rate-determining steps are during reduction in a solids bed (comprising of ore coal and fluxes). The influence of changes to specific material characteristics and process parameters on the extent of reduction achieved in a mixed solids bed was therefore determined experimentally.

Process parameters that were varied included:

- Ore type (to achieve changes to the reduction rate constant).
- Coal type (to achieve changes to the Boudouard rate constant).
- The temperature to which the material mixture was exposed.

A modelling approach combined with experimental results was used to do the investigation.

Note that the accent of this study was to confirm whether specific process parameters influenced the rate of solid-state reduction of a composite material mixture, and therefore results were more of a qualitative, than quantitative nature.

1.5.1.2 Phase 2: production rate investigation

The second phase of the investigation focussed on solid-state reduction at the bottom of the solids bed. The main objective of this phase of the study was to investigate the extent to which final reduction occured as solid-state reduction at the bottom of the solids bed. Secondary objectives were to back calculate the heat transfer coefficient in the solids bed and to determine the rate at which final reduction can be achieved as solid-state reduction (in the solids bed of the Ifcon® process). For this, a modelling approach combined with experimental results was also used.

2 Phase 1: Rate determining step during solid state reduction

2.1 Solid state reduction in a mixed bed: Theoretical aspects

2.1.1 Basic reactions and thermodynamic considerations

When a composite material mixture (such as the material mixture fed into a rotary kiln- or Ifcon process) heats up to temperatures in excess of 100°C, drying of the mixture occurs and devolatilization of the coal[20] is initiated. Once the temperature of the material increases beyond 300°C, the rate of devolatilization increases significantly[21,22]. Devolatilization products (such as CO and H_2) initiate reduction of iron oxides[23], according to the following reaction:

$$Fe_xO_y\ (s) + CO\ (\text{or } H_2)(g) \Rightarrow Fe_xO_{y-1}\ (s\ ) + CO_2\ (\text{or } (H_2O)(g) \qquad (2.a)$$

At temperatures above 306°C[14] calcination of the magnesite component of the dolomite occurs according to the following reaction:

$$MgCO_3(s) \Rightarrow MgO(s) + CO_2(g) \qquad (2.b)$$

As the material is heated to temperatures in excess of 700°C[14] the carbon gasification (or Boudouard) reaction sets in, and reduction of the iron oxides with CO proceeds [7,14].

$$CO_2(g) + C(s) \Rightarrow 2CO(g) \qquad (2.c)$$

In addition to the Boudouard reaction, carbon can also be gasified by water vapour to produce hydrogen gas. This reaction, which is called the water-gas reaction, is shown below.

$$H_2O(g) + C(s) \Rightarrow CO(g) + H_2\ (g) \qquad (2.d)$$

(This part of the study aims to test whether the hydrogen produced, contribute to the reduction reaction).

At temperatures above 895°C calcination of calcite (limestone) occurs according to the following reaction[14].

$$CaCO_3(s) \Rightarrow CaO(s) + CO_2(g) \quad (2.e)$$

Note that the overall reduction reaction (when combining ***equations 2.a*** and ***2.c***) is as follows:

$$Fe_xO_y\ (s) + C(s) \Rightarrow Fe_xO_{y-1}\ (s\ ) + CO\ (g) \quad (2.f)$$

To study the various reduction steps, ***equation 2.a*** can be subdivided into the following equations:

Reduction of hematite with carbon monoxide (or hydrogen):

$$3Fe_2O_3(s) + CO(\text{or } H_2)(g) \Rightarrow 2Fe_3O_4(s) + CO_2(\text{or } H_2O)(g) \quad (2.g)$$

Reduction of magnetite with carbon monoxide (or hydrogen) below 564°C:

$$Fe_3O_4(s) + CO(\text{or } H_2)(g) \Rightarrow 3Fe(s) + CO_2(\text{or } H_2O)\ (g) \quad (2.h)$$

Reduction of magnetite with carbon monoxide (or hydrogen) above 564°C:

$$Fe_3O_4(s) + CO(\text{or } H_2)(g) \Rightarrow 3FeO(s) + CO_2(\text{or } H_2O)\ (g) \quad (2.i)$$

Reduction of wustite with carbon monoxide (or hydrogen):

$$FeO(s) + CO(\text{or } H_2)(g) \Rightarrow Fe(s) + CO_2(\text{or } H_2O)\ (g) \quad (2.j)$$

From the thermodynamic data of Kubaschewski et al[14], the equilibrium iron oxide diagram (in a CO/CO_2 atmosphere) and carbon stability diagram[7] is constructed (as shown in ***Figure 9***). The equilibrium iron oxide diagram (in a H_2/H_2O atmosphere) [7] is shown in ***Figure 10***.

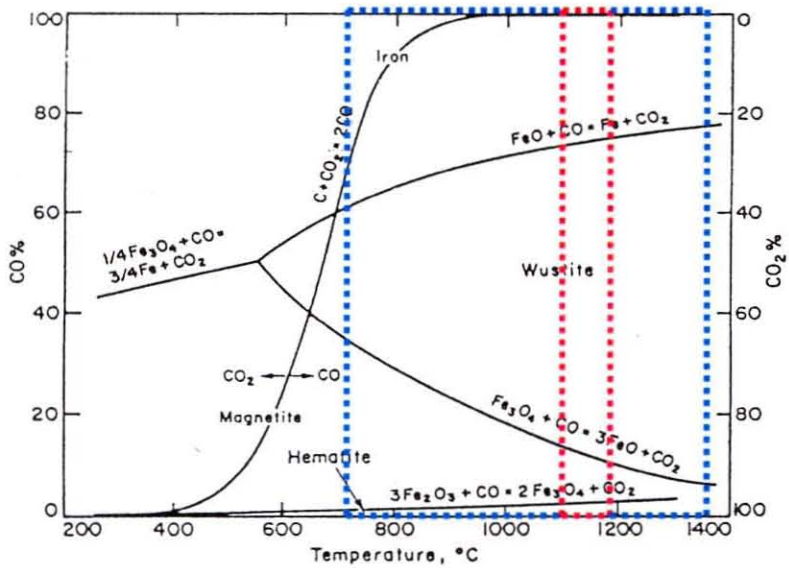

Figure 9: *Equilibrium iron oxide- and carbon stability diagrams in a CO/CO_2 atmosphere[7]. The anticipated operational window for the solids bed in the Ifcon process is shown as a blue rectangle. The operational window where tests regarding the first phase of the investigation were done is indicated with a red rectangle.*

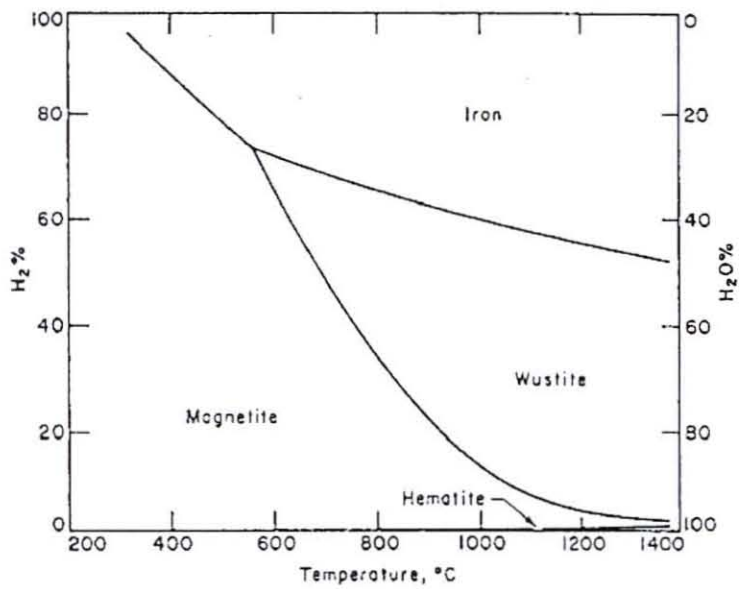

Figure 10: *Equilibrium iron oxide diagram in a H_2/H_2O atmosphere[7].*

Figure 9 shows the extent to which reduction of iron oxide with CO, and the oxidation of carbon with CO_2, will tend to proceed, while ***Figure 10*** shows the extent to which reduction of iron oxide will tend to proceed with H_2 under specific conditions. These diagrams also indicate the stable phases that will be present at a specific temperature and gas composition (with $p_{CO} + p_{CO_2} = 1$ for ***Figure 9*** and $p_{H_2} + p_{H_2O} = 1$ for ***Figure 10***). Accordingly, at typical temperatures between 700°C and 1400°C (in the solids bed of the Ifcon process) and anticipated CO/CO_2 ratios of 0.5 to 1.0[15], the stable oxide phases will be wustite and iron.

2.1.2 Reaction mechanisms and rate controlling steps

To investigate the rate at which reactions occur, the reaction mechanisms must be considered. According to the overall reduction reaction ***(2.f)***, iron oxide in the ore is reduced by solid carbon to produce metallic iron and CO gas.

Although the overall reaction is between iron oxide and carbon, literature shows that reduction predominantly occur via intermediate CO gas, rather than by direct contact between iron oxide and carbon[7,23,24]. The reduction mechanism for reduction occurring via intermediate CO gas is schematically shown in ***Figure 11***.

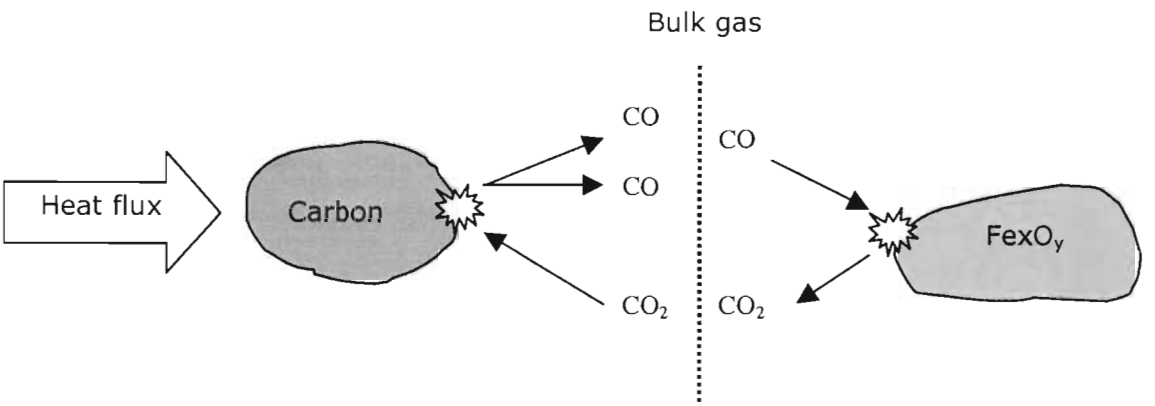

Figure 11: *Schematic representation of solid-state reduction via CO as intermediate gas.*

Figure 11 shows that reduction is performed by the gaseous species CO, while the product gas (CO_2) is regenerated by the Boudouard reaction to carbon monoxide, which in turn reacts with the iron-ore specie. Note that the average composition of the gas, which evolves from such an ore-carbon mixture, will depend on the relative rates of the reduction and Boudouard reactions. The same argument also holds when reduction is achieved with H_2 while the product gas (H_2O) is regenerated by the water-gas reaction.

The individual reaction steps by which the overall reaction (presented in ***Figure 11***) proceeds are[7,24]:

a. Diffusion of CO from the bulk gas to the iron oxide particle.
b. Diffusion of CO inward through the reduced product layer.
c. Chemical reduction reaction of iron oxide with CO gas.
d. Diffusion of CO_2 outwards through the reduced product layer.
e. Diffusion of CO_2 from the iron/iron oxide particle to the bulk gas.
f. Diffusion of CO_2 from the bulk gas to the carbon particle.
g. Heat transfer to the carbon particle.
h. Chemical oxidation of carbon with CO_2.
i. Diffusion of CO from the carbon particle to the bulk gas.

In order to quantify the rate of the overall reaction, each reaction step must be quantified, or eliminated (as not being rate controlling). (This is finalised in the second phase of this investigation.)

Of the above steps, a, e, f and i are **mass transfer** steps, and their rates can be described by equations such as ***(2.k).*** If any one of these steps governs the rate of the overall reaction, the reaction is mass transfer controlled.

The rate of mass transfer between the bulk of a phase and the interface with another phase can be quantified with the following equation:

$$J = m(C_{bulk}-C_{interface}) \qquad (2.k)$$

where, *J* (with units: $mol.m^{-2}.s^{-1}$) is the flux of the given species towards an interface, *m* (with units: $m.s^{-1}$) is the mass transfer coefficient, and *C* (with units: $mol.m^{-3}$) is the concentration of the species.

Steps b and d are **diffusion** steps[25,26], and their rates can be described by equations such as ***(2.l).*** If diffusion governs the rate of the overall reaction, the reaction is referred to as diffusion controlled.

The rate of diffusion transfer between the surface of a particle and the reaction interface or site where the actual chemical reaction takes place, can be quantified with the following equation[27]:

$$J = D\left(\frac{C_{\text{particle surface}} - C_{\text{reaction interface}}}{dx}\right) \qquad (2.l)$$

where J (with units: $mol.m^{-2}.s^{-1}$) is the flux of the given species towards an interface, *D* (with units: $m^2.s^{-1}$) is the diffusivity, $C_{particle\ surface}$ *and* $C_{reaction\ interface}$ (with units: $mol.m^{-3}$) are the concentration of the species on the particle surface and reaction interface respectively and *dx* (with unit: m) is the product layer thickness or distance over which the concentration gradient exists.

Steps c, and h are chemical reactions, and their rates are described by equations such as ***(2.m)***[28]. If the rate of the overall reaction is governed by the rate of either of the chemical reactions, the rate at which the chemical reactions occur must be quantified.

For the general reaction

$$bB + cC \quad \Leftrightarrow \quad dD + eE$$

where b, c, d, and e are stoichiometric coefficients of reagents B, C, D and E respectively, the rate of the reaction is typically given by the following rate expression:[28]:

$$J = k\left[\left(a_B^b \times a_C^c\right)_{\text{int erface}} - \left(a_B^b \times a_C^c\right)_{equilibrium}\right] \qquad (2.m)$$

where J (with units $mol.m^{-2}.s^{-1}$) is the flux of one of the species (*B, C, D* or *E*) to or away from the interface, a_i is the activity of species i, and k is the reaction rate constant.

If the gasification and reduction reactions have similar rates, they both would be controlling. This implies that neither of the two reactions would be at their equilibrium values, but that a quasi-equilibrium would be established, somewhere between these two equilibrium values.

When two of the above rate mechanisms (mass transfer, diffusion transfer or chemical reaction rate) influence the rate of reduction, the overall mechanism is referred to as "mixed control"[7].

Steps g is a heat transfer steps, and it's rate can be described by the rate of conduction-, convection- or radiation heat-transfer. If the rate of the overall reaction is governed by the rate of either of these steps, the overall reaction is heat transfer controlled. Heat transfer control therefore occurs when heat for the reactions is supplied at a slower rate than the rate at which the reactions consume the heat. The rate of heat transfer depends on the heat transfer mechanism (i.e. conduction, convection or radiation), which is influenced by the configuration of the material (e.g. packed bed or fluidised bed). The rates of heat transfer are mathematically expressed in ***(2.n)*** to ***(2.p)***[29].

General rate expression for conduction heat transfer:

$$q = k\,A\left(\frac{T_{heat\ source} - T_{particle}}{dx}\right) \qquad (2.n)$$

General rate expression for convection heat transfer:

$$q = h\,A\left(T_{heat\ source} - T_{particle}\right) \qquad (2.o)$$

General rate expression for thermal radiation heat transfer:

$$q = F_{\varepsilon}\,F_{G}\,\sigma\,A\left(T^{4}_{heat\ source} - T^{4}_{particle}\right) \qquad (2.p)$$

In these equations, q is the heat flux (with units: $W.m^{-2}$), A is the area through which the heat flux is transferred (with unit: m^2), $T_{heat\ source}$ and $T_{particle}$ are the temperatures of the heat source and particle respectively (with units: K), k and h are the thermal conductivity and convection heat transfer coefficients respectively, F_ε is the emissivity function, F_G is the geometric "view factor" function and σ is the Stefan-Boltzmann constant (with a value of $5.669 \times 10^{-8}\ W.m^2.K^4$).

2.1.3 Relevant studies

Various studies investigated the mechanisms and rate-determining steps during reduction of composite iron ore-reductant mixtures (with graphite, coke, coal char and coal used as reductant). During these investigations, the analyses of product gas, the influence of reductant content and particle size, and the magnitude of the apparent activation energy were used to evaluate the rate-determining step during reduction. Most authors concluded that the rate of the gasification reaction governed the overall rate of the reaction[30].

2.1.3.1 Carbon gassification

For the reduction of ore-coal mixtures, Bryk and Lu[24] noted that the overall reduction rate is controlled by the oxidation of carbon at temperatures below 1100°C, while at higher temperatures the reaction rate is controlled by a combination of the reduction and Boudouard reactions. They also found that when small coal particles were used (<150µm), changes to the particle size did not influence the degree of metallization achieved in 15 minutes, but increasing the coal size beyond 150µm decreased the metallization rate.

Shivaramakrishna[31], who reacted composite pellets in a bed of coal between 950°C and 1050°C, concluded that the Boudouard reaction governed the overall reduction reaction. Note that the Boudouard reaction is highly endothermic and may be limited by heat transfer limitations.

Fruehan[32] showed that the reactivity of different carbon sources differs from one another. Different authors used different types of carbon sources including coconut charcoal, coal char, petroleum coke, and graphite, but a clear correlation between activation energy and type of carbon was not found[33,34,35].

The activation energies for gasification of carbon with CO_2 mostly ranged from 215 to 310 kJ/mol[30], while the activation energies for gasification of carbon with steam ranged from 120 to 245 kJ/mol[30].

2.1.3.2 Reduction reaction

Srinivasan and Lahiri[36] measured the CO/CO_2 ratio of the product gas when composite pellets were reacted. They found that the CO/CO_2 ratio decreased with decreasing carbon content of the pellet, thereby changing the rate controlling reaction from carbon gasification to wustite reduction.

Reported activation energies for reduction of FeO with CO usually ranged from 116kJ/mol to 151 kJ/mol[37], while the activation energies for reduction of Fe_2O_3 and FeO with H_2 was mostly reported as 64-74 kJ/mol and 52-77kJ/mol respectively[30].

Sun and Lu[38] developed a mathematical model to describe the non-isothermal reduction of magnetite-coal mixtures. For reduction with CO and H_2, they found activation energy values in the ranges 65 - 74 kJ/mol, and 61 – 69 kJ/mol respectively.

2.1.3.3 Temperature and Heat transfer

Bryk and Lu[24] reacted large masses of ore-coal mixtures at 900°C, 1100°C and 1300°C. From their results, they concluded that heat transfer to the sample as well as conduction within the sample affected the reaction kinetics significantly.

Huang and Lu[23] reacted ore–coal mixtures at 1200°C in a muffle furnace. Their results suggested that heat transfer limited the kinetics of their system, due to the heat demand from endothermic reactions occurring in the mixture.

In an experiment, similar to that of Huang and Lu, Sun and Lu[39,40] found that heat transfer to, as well as conduction within, the material mixture was rate limiting due to the endothermic nature of the reactions. They also concluded that heat transfer within the solids bed was mainly due to conduction, rather than convection or radiation, for furnace temperatures below 1300°C

Wang *et al.*[41] inferred from heat transfer and kinetic calculations that, during fast heating, reduction rate of composite pellets is initially controlled by the chemical reduction reaction, where after the rate is controlled by heat transfer.

2.1.3.4 The influence of volatiles

Wang *et al.*[42] reduced composite ore-coal pellets and noted that significant devolatilisation only started at 400°C. They also found that volatiles significantly influence the rate of reduction at temperatures above 700°C. Similar results were also obtained by Dutta and Gosh[43], Dey *et al.*[44], and Shivaramakrishna *et al.*[31] Dutta and Gosh proposed an explanation for the reactions occurring, and noted that devolatilisation of coal in an iron-coal mixture is different to devolatilisation of unmixed coal.

Sun and Lu[39], Sharma[45], Huang and Lu[23] and Bryk and Lu[24] all observed some contribution of volatiles to the reduction of iron ore in a packed bed. Bryk and Lu[24] showed that when coal was replaced with graphite, the rate of metallization of iron ore composites at 1150°C decreased.

Coetsee *et al.*[30] modelled the reduction of magnetite-coal pellets, and predicted that volatile matter contribute to reduction of pellets.

2.2 Experimental aspects

A thermo gravimetric study was done to investigate the influence of changes to feed material characteristics and exposure temperature, on the reduction rate of composite material mixtures. The experimental apparatus mainly comprised of a high temperature tube furnace and associated gas flow rate control system.

2.2.1 Experimental apparatus

2.2.1.1 High temperature furnace.

The tests were performed in a vertical tube resistance furnace. A mullite tube (one end closed) of 60mm inside and 70mm outside diameter, served as work tube. The furnace was heated by eight silicon carbide heating elements and the furnace was equipped with a PID (proportional integral derivative) controller, for furnace temperature control. A schematic representation of the furnace arrangements is shown in ***Figure 12***.

A water-cooled brass ring was fitted onto the open end of the work tube. The interface between the brass ring and the work tube was made gas tight with two rubber O-rings and vacuum grease.

Purge gas entered the work tube, through an alumina tube (that extended through the brass ring). Product-gas exited the furnace through a copper tube, which also passed through the brass ring

A mullite 3A crucible with inside diameter of 32 mm and outside diameter of 35 mm, and height 50 mm was used to contain the sample. (The dimensions of the crucible were chosen to ensure that the sample was representative of the bulk material[46].) The crucible, which was contained in a molybdenum basket made from 0.5mm molybdenum wire, was suspended from a scale with a molybdenum wire of 2mm diameter. The crucible was lowered into the work tube by lowering the scale (which was contained in the scale car). A DC drive was used to lower the scale.

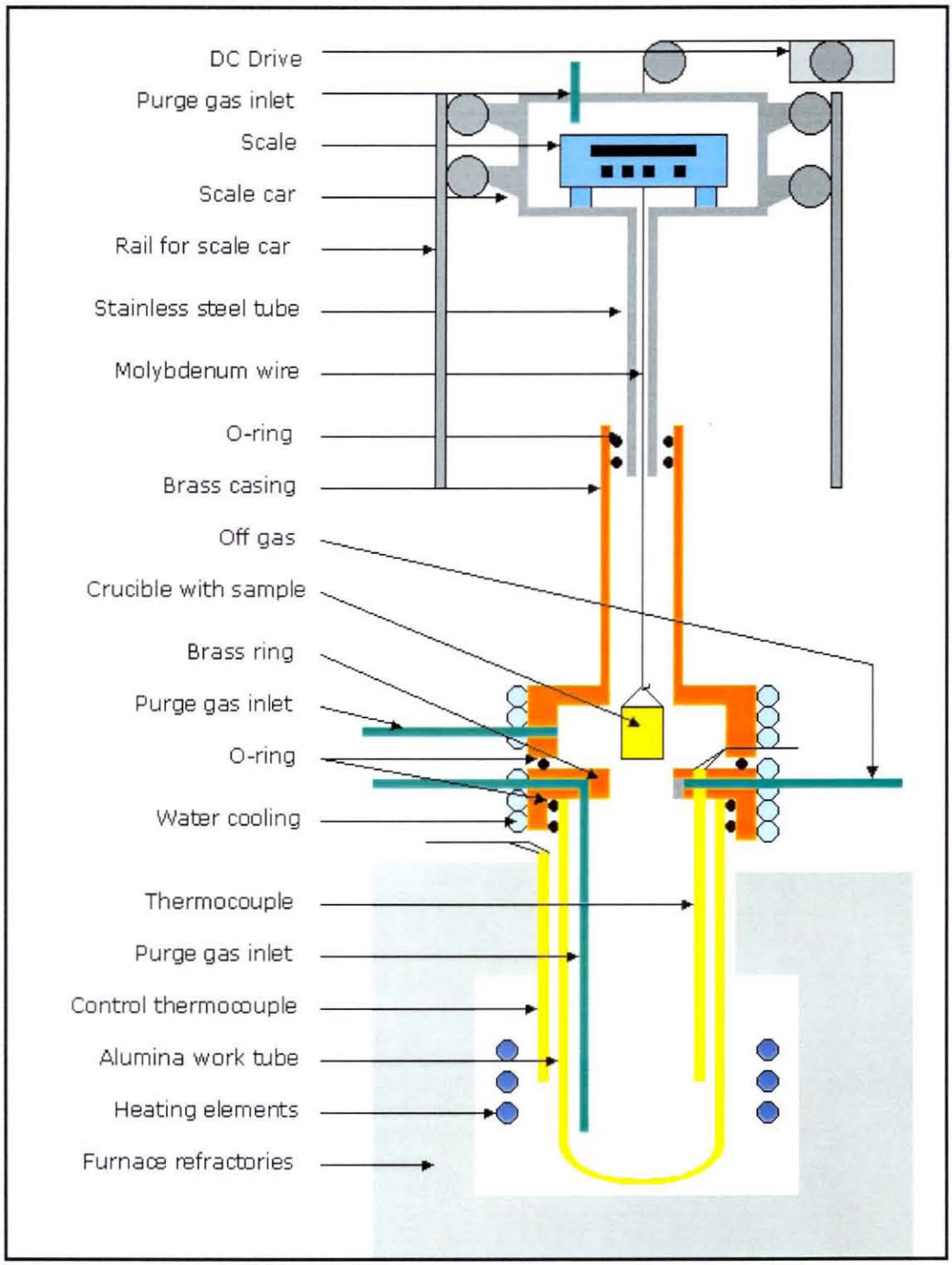

Figure 12: *Schematic illustration of the TGA furnace configuration.*

During lowering of the scale, the stainless steel tube below the scale car (of 28mm inner and 31mm outer diameter and length of 520 mm) slid into a brass casing that was clamped onto the brass ring. Two rubber O-rings and vacuum grease ensured a gas-tight seal between the stainless steel tube and brass casing. A rubber O-ring ensured a gas-tight seal between the brass casing and brass ring. The casing could be removed from the brass ring, thereby providing access to the work tube for loading and removal of samples.

2.2.1.2 Gas system

The work tube and scale car assembly was continuously purged with Argon. A schematic diagram of the gas preparation and control system, (including gas lines, purification trains, connecting gas-lines and stopcocks) is shown in ***Figure 13***.

The gas passed through Drierite ($CaSO_4$) to remove excess moisture. The argon was further purified by passing through copper turnings in a fused silica tube, which was heated to 600°C. The copper turnings have a large surface area and react with excess oxygen in the gas, to form copper oxide. The copper was periodically replaced.

From the copper turnings the gas line split into three separate gas lines. They were: a line leading to the work tube, a line to the scale car and a line to the brass casing. The gas line to the work tube was used for flushing of the tube, while the line to the brass casing was to assist with cooling of samples after testing. The gas fed to the scale car forced downward flow of gas in the stainless steel tube and brass casing, thereby protecting the scale from furnace gasses and soot. The flow rate of the argon through each line, was measured with a calibrated rotameter, thereby enabling control of the flow rate of the gas supplied to the furnace. (Calibration of rotameters are discussed in ***Appendix A.1***.) From the rotameters, the gas line led directly to the work tube, brass casing and scale car. Gas lines, which by-passed the rotameters, were included in order to flush the furnace assembly at high gas flow rates, prior to each test.

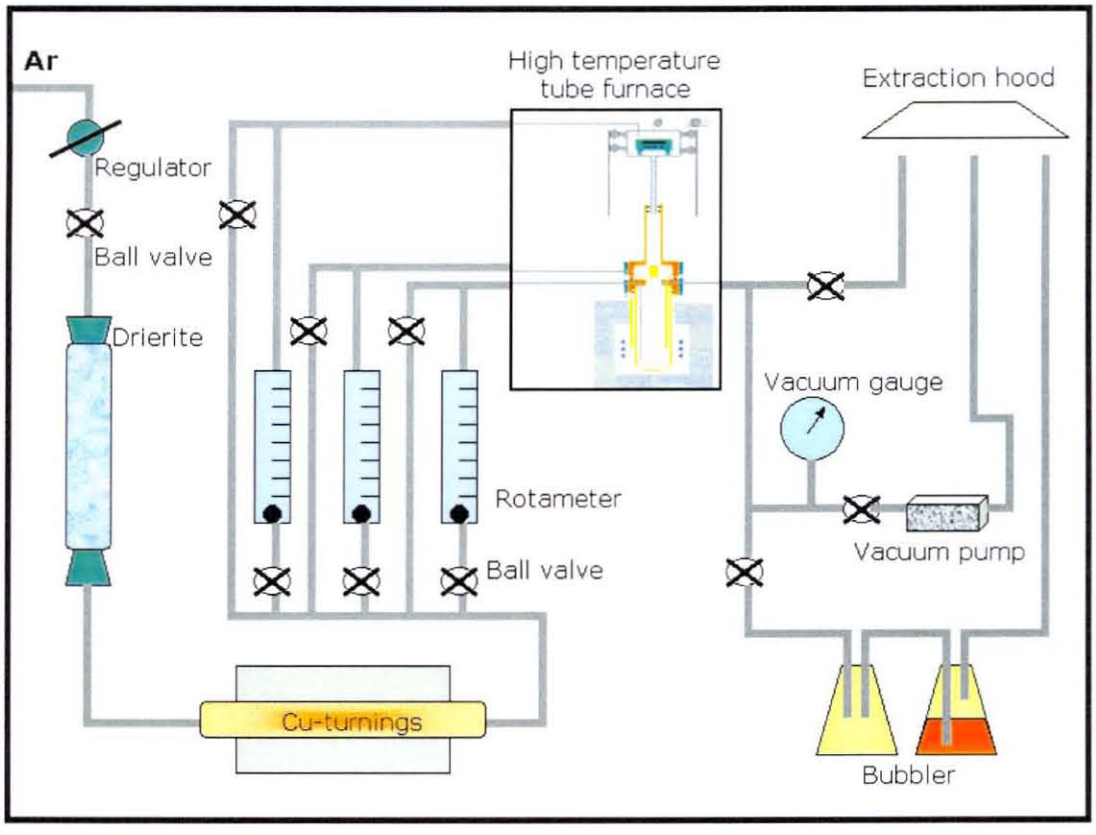

Figure 13: *Schematic illustration of the gas preparation and control system for the TGA.*

The exit gas line from the work tube was divided into three lines. One line lead to a bubbler, one to a vacuum pump and the third was a bypass, which lead directly to the extraction hood.

Oxygen entering the reaction tube assembly, could result in oxidation of species associated with the sample mass. Accordingly, leaking of air into the system had to be prevented. In addition, poisonous CO was produced during the test. All the gas that exited the system therefore had to be extracted in the gas extraction system of the laboratory for safe expulsion.

Gas-tightness of the furnace tube was checked by applying a vacuum of 15 mm Hg and noting the stability of the vacuum with time, as measured by a vacuum gauge. A significant pressure-drop in a period of two minutes indicated a leak. Serious leaks

could be found easily with a soap and water solution, but minor leaks were sometimes not traceable by this technique. A Helium snifter probe, as used in chromatography for leak detection, was obtained and minor leaks were detected by flushing and pressurising the system with helium gas and then searching along the gas-line for leaks with the snifter probe. In the event of a leakage, the relevant gas line was dismantled and reassembled.

2.2.2 Experimental procedure.

2.2.2.1 Temperature control of the heat zone

The furnace temperature was controlled by a proportional-integral-derivative (PID) controller. A Pt/Pt10%Rh (or type S) thermocouple, positioned in the hot zone of the furnace, outside the mullite work tube, served as control thermocouple (as shown in ***Figure 12***). (The method used to determine the position of the hot zone of the furnace, is discussed in ***Appendix A.2***)

The temperature inside the work tube was measured with a Pt/Pt10%Rh (or type S) thermocouple that was fixed to the brass ring, and positioned in the hot zone of the furnace at the same height as the control thermocouple. For gas-tightness, the point of entry of the thermocouple sheath into the brass ring, was sealed with silicone rubber.

A minor difference was observed between the temperature measured by the control thermocouple and the thermocouple inside the reaction tube. The difference was about 2°C at 1100°C and 4-5°C at 1400°C, with the control thermocouple reading higher then the temperature measured inside the tube. The temperature on the PID controller was therefore set at a temperature that yielded the required temperature inside the work tube.

2.2.2.2 Sample preparation

Each sample was made-up to test specific material characteristics. In order to benchmark the influence of a material characteristic on the reduction rate, a reference sample was used. The reference sample comprised of a material mixture similar to that used at the Ifcon pilot scale facility that was erected at Kumba's pilot plant. The reference sample comprised of Sishen iron ore fines, duff coal from Eikeboom collieries, dolomite from Mooiplaas and limestone from PPC lime. The

ingredients of the reference mixture are summarised in ***Table 2***. The recipe of the reference mixture was referred to as the "base mixture".

Table 2: *Ingredients of the reference mixture (base mixture recipe).*

Ore type	Mass (g)	Mass% (%)
Sishen iron ore fines	27.8	69.5
Eikeboom coal (-2mm)	7.3	18.3
Dolimite	2.2	5.5
Limestone	2.7	6.7

Raw material preparation that was done is discussed in ***Appendix A.3,*** while the chemical compositions of the various raw materials and analytical techniques used, are presented in ***Appendix A.4*** and ***Appendix A.5*** respectively.

The base mixture as well as other test mixtures were all made up in such a way that 15 grams of metal could theoretically be produced from a sample, when 80% reduction was achieved. The amount of limestone and dolomite added to each sample was such that the CaO/SiO_2 ratio of the inset material was 1.4 while the MgO content of the slag species (that remained after 80 % reduction was achieved) would be 8%. These numbers represent the characteristics of the feed mixture that was used during trails done at the Ifcon pilot plant facility. This is discussed in more detail in ***Appendix A.6.***

Material mixtures, other than the base mixture, were made up so that one material characteristic was changed for each consecutive sample. By doing this, the influence of changes to a specific material characteristic, on the degree of reduction achieved, could be determined. The degree of reduction achieved with each sample could therefore be compared to the degree of reduction achieved with the base mixture (as a function of time).

The various samples that were tested against the reference sample are listed in ***Table 3***. The changes made to material characteristics or operational conditions are also indicated in the table.

Table 3: *Experimental program that was followed to determine the influence of specific material characteristics on the reduction rate of the material mixture.*

Test no	Test objective
1	Reference samples (made up according to the "base mixture") were tested repeatedly under similar conditions to determine the repeatability of results
2	Sishen ore was replaced with Thabazimbi ore (which has a higher CO reducibility than Sishen ore) to investigate the influence of changing CO reducibility of the ore on reduction rate.
3	A mixture containing large Sishen ore particles was compared to a mixture containing smaller Sishen ore particles.
4	Eikeboom coal was replaced with Leeuwpan coal to investigate the influence of changing CO_2 reducibility of the coal
5	Coal was replaced with char to investigate the influence of volatile matter in the material mixture on the reduction rate.
6	All of the above tests were done at 1100°C and 1200°C to determine the influence of varying exposure temperature on the reduction rate.

2.2.2.3 Test procedure

Mullite crucibles (A3) were used to contain the samples. The crucible dimensions were OD 35mm, ID 32mm and height 50mm, with inner height of about 48mm. Prior to testing, the mass of each crucible was measured.

Each sample was intimately mixed, placed into a crucible, and the mass of the crucible containing the sample was measured. The crucible was placed in a basket that was made from 0.5 mm molybdenum wire, which was suspended from the scale with molybdenum wire of 2 mm diameter.

Access to the reaction tube was obtained by lifting the brass casing from the brass ring. During testing, the brass casing was fastened to the brass ring with quick-release clams. To ensure that no carbon was lost during the initial stages of the test

(due to oxidation with air), the sample was inserted into the alumina work tube at a position where the temperature in the tube was approximately 100 °C. The alumina work tube was then flushed with nitrogen for 2 minutes before the sample was lowered into the constant heat zone of the work tube.

The crucible- assembly was lowered into the work tube, by lowering the scale car with the DC drive. The crucible was lowered at such a rate that the crucible reached its final position within 10 seconds. The crucible was lowered to exactly the same height during each experiment. This was accomplished by installing a ruler next to the rail of the scale car to measure the relative height of the scale.

The alumina work tube was continuously flushed with nitrogen (at a flow rate of 0.5 litre per minute) for the duration of each experiment. The system was operated at a slight positive pressure by continuously bubbling the exiting gas through an oil trap (or bubbler).

From the moment the crucible was inserted into the furnace the mass of the crucible assembly (and therefore the rate of mass loss of the sample) was measured. Once the rate of mass loss slowed down significantly, the sample was elevated from the hot zone (into the brass ring) and left to cool to approximately 100°C (in an nitrogen atmosphere) before being removed from the work tube. Finally the mass of the crucible containing the reduced sample was measured and the total mass loss of the sample was calculated and compared to that of the reference sample. Since the analyses of the input materials were known, the apparent degree of reduction achieved for each sample was calculated as a function of time, and compared to that of the reference sample. Note that this is an apparent degree of reduction, based on assumptions made during calculations. Assumptions made during these calculations are discussed in ***Appendix A.7***.

2.3 Kinetic modelling of the TGA experiment

The model, which was developed by Pistorius *et al.*[30], was used to simulate reduction of the TGA samples. The main assumptions and calculation procedure of the model are presented below.

2.3.1 Sample configuration:

The model simulates heating of a composite sample similar to that of the TGA experiment. The samples in the TGA experiment had cylindrical shapes (with diameter of 32 mm and 45 mm high). However, in order to simplify heat transfer calculations, the samples were modelled as spheres, so that heat flux in a sample was one-dimensional towards the centre of the sample. The radius of the spherical model-samples were taken as 20 mm, so that model samples and samples that were actually tested had similar volumes.

Another advantage of modelling the samples as spheres (rather than infinitely long cylinders) is that heat entering the samples through the top and bottom sides was accounted for.

Spherical symmetry was assumed around the centre point of each sample, with the solid- and gas temperatures assumed to be the same at a given position in the sample[15,30].

Each sample was divided into ten hollow spherical nodes (except for the centre node which was a solid sphere). The thickness of each node was similar to the radius of the centre node.

The total reaction time was divided into various time steps. A mass-and energy balance was performed for each node during each time step, to yield the change in temperature of the node as a function of time.

The equilibrium constants were found from simplified expressions[15] fitted to the equilibrium constants that were calculated with the data of Kubaschewski et.al.[14]

2.3.2 Heat transfer

Since the thermal conductivity of the crucible was about 6[47] compared to a conductivity of about 1 for the sample[15], the effect of conduction through the crucible was not accounted for. Heat transfer to the sample was assumed to be by radiation only with the surface of the sample (crucible) having an emissivity of 0.8. The rate of radiation heat transfer followed the expression[30]:

$$q = \sigma \varepsilon A(T_f^4 - T_s^4) \qquad (2.q)$$

where q is the rate of heat transfer (in W), σ is the Stefan-Boltzmann constant, ε is the emissivity of the crucible (taken to be 0.8), A is the outer surface area of the sample, T_f is the furnace temperature, and Ts is the surface temperature of the crucible.

Heat transfer inside the sample occurred as conduction as well as by bulk movement of the gas[30]. For this, the effective thermal conductivity was estimated with the following relationship:

$$k_e = k_s \frac{1 - 2e(\kappa - 1)/(2\kappa + 1)}{1 + e(\kappa - 1)/(2\kappa + 1)} \qquad (2.r)$$

where e is the porosity of the sample, and $\kappa = k_s / k_g$, where k_s is the average thermal conductivity of solids in the sample, k_g is the thermal conductivity of gas in the pores, and k_e is the effective thermal conductivity of the solids bed. During each time step, the sample porosity was calculated using known densities of the species present[15]. The sizes of the nodes were assumed to remain constant with time.

The average conductivity of the solid phases in the sample was calculated, with the following geometric mean expression: [30]

$$k_s = \prod_{i=1}^{n} k_i^{f_i} \qquad (2.s)$$

where f_i is the volume fraction of the solids occupied by solid species i.

Equations and constants that were used to calculated to conductivities of the solid phases, are presented in ***Appendix B.1***.

2.3.3 Reaction rate expressions

2.3.3.1 Reduction reaction:

Stepwise reduction of hematite to magnetite, magnetite to wüstite and wustite to iron (above 564°C) or alternatively hematite to magnetite and magnetite to iron (below 564°C) was assumed. Reduction occurred by CO and H_2 in parallel. (564°C is the temperature where wustite becomes thermodynamically unstable when iron oxide is reduced with CO, assuming unit activity for all species[14].)

The reaction rates were assumed to be first-order with respect to all reactants, and the rate expressions were as follows[30]:

$$r = k_R M_{Fe} (1\text{-}F) (p_i - p_i^{equilib})/RT \qquad (2.t)$$

where r is the reduction rate (moles of O removed per unit time), k_R is the reduction rate constant (with units: $m^3\ s^{-1}\ kg^{-1}$), M_{Fe} is the mass of Fe per sample volume (with units: kg/m^3), F is the degree of reduction, p_i is the partial pressure of reductant i (H_2 or CO) (in Pa), $p_i^{equilib}$ is the equilibrium partial pressure of the reductant, R is the ideal gas constant, and T is the absolute temperature.

The rate constants were assumed to follow Arrhenius-type temperature dependences, with constants presented in ***Appendix B.1***.

2.3.3.2 Carbon gasification reaction:

Carbon gasification occurred by both the Boudouard-and the water-gas reactions. The rate of the Boudouard reaction is given by:

$$r_B = k_B M_C (p_{CO_2} - p_{CO_2}^{equilib})/RT \qquad (2.u)$$

where r_B is the Boudouard reaction rate (with units: moles of C gasified per unit time), k_B is the Boudouard reaction rate constant (with units: $m^3\ s^{-1}\ kg^{-1}$), M_C is the mass of carbon per sample volume (with units: kg/m^3), p_{CO_2} is the partial pressure of reductant CO_2 (in Pa), and $p_{CO_2}^{equilib}$ is its equilibrium partial pressure.

The water gas reaction rate is similarly given by:

$$r_{wg} = k_{Wg} M_C (p_{H_2O} - p_{H_2O}^{equilib})/RT \quad (2.v)$$

where r_{wg} is the rate of the water gas reaction (with units: moles of carbon gasified per unit time), and p_{H2O} is the partial pressure of H_2O (in Pa), and $p_{H2O}^{equilib}$ is its equilibrium partial pressure.

Expressions for equilibrium constants and enthalpies are presented in ***Appendix B.2*** and ***Appendix B.3*** respectively. Rate constants and activation energies used in the model are presented in **Appendix B.4**.

2.3.3.3 Devolatilisation

Devolatilisation was assumed to occur in two steps (in series). Each step was assumed to be first-order with respect to the amount of volatile matter remaining in the coal[15]. The rate constants and activation energies for the two steps are given in ***Appendix B.4.*** Each of the two devolatilisation steps was assumed to remove half of the volatile matter.

Default conditions for the model calculations are presented in ***Appendix B.5***.

Model predictions are presented in support of experimental results in ***Section 2.4***.

2.4 Results and discussion

2.4.1 Repeatability of results

Four tests were done with the "base mixture" to test repeatability of results. Two of the tests were done at 1100°C and two were done at 1200°C. The sample masses recorded from these tests are shown as black dotted lines in ***Figure 14***. To ensure that results were comparable, only the sample masses (excluding the masses of the crucible and crucible basket) were reported. Note that the initial masses of the base mixture samples were the same.

Figure 14 shows that the masses of the base mixture samples that were exposed to 1100°C for 20 minutes varied between 29.8 and 29.5 g, while the masses of the samples that were exposed to 1200°C for 20 minutes varied between 27.5 and 27.6 g. The variation between results from similar tests were therefore less than 5% of the difference between results from samples exposed to different conditions. This was considered repeatable enough to obtain qualitative results. The apparent degree of reduction was also calculated from these data (as shown in ***Appendix C.3 and***).

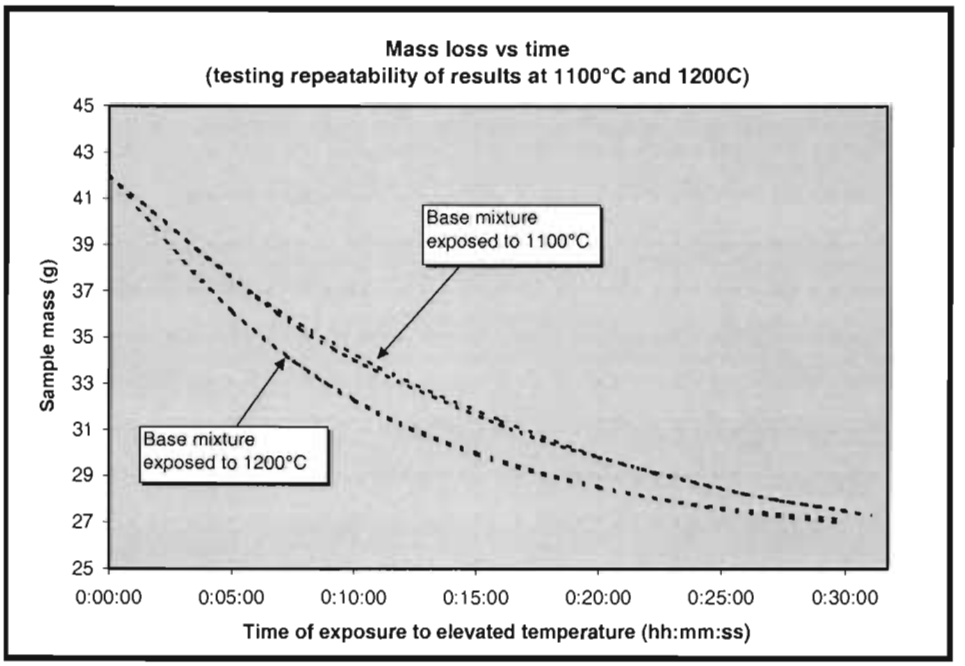

Figure 14: *Masses of base mixture samples exposure to 1100°C and 1200°C respectively as a function of exposure time, showing the repeatability of results.*

2.4.2 Influence of reducibility of ore on reduction behaviour

The model was used to predict changes to the degree of reduction when the reduction rate constant was changed. Two simulations were done: the first to establish a base line (with model inputs listed in ***Appendix B.1*** *to* ***Appendix B.5***), and the second to simulate an increase of the reduction rate constant. The reduction rate constant was increased with a factor of 10. Results are shown in ***Figure 15.***

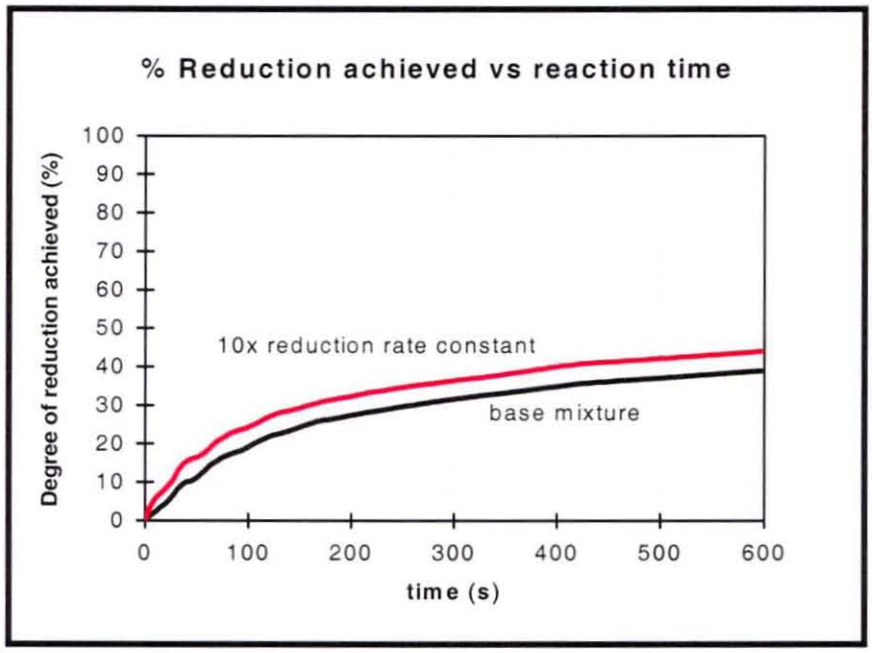

Figure 15: *Model prediction of change in degree of reduction achieved when the reduction rate constant was increased by a factor of 10. (The model prediction for the base mixture is shown as a reference (in black) with the model prediction for the increased rate constant shown in red.)*

From ***Figure 15***, it is clear that an increase in reduction rate constant, increased the degree of reduction achieved. This implies that the rate of reduction (of this specific material mixture when exposed to 1200°C) is to some extent controlled by the reduction reaction.

The extent of reduction achieved in the solids bed will therefore depend on the type of ore selected.

In order to quantify the extent to which reduction occurs (with a model), the rate constants of the ore used must be determined accurately.

The reducibility index of Sishen fine ore was reported as 1.34 percent per minute while the reducibility index for Thabazimbi fine ore was reported as about 1.49 percent per minute[48]. The rate of reduction of a material mixture containing Thabazimbi ore was therefore expected to reduce at a faster rate than the base mixture (containing Sishen ore).

When the mass loss of the mixture containing Thabazimbi ore (when exposed to 1200°C) was compared to that of the base mixture, the mass losses were similar for similar exposure times. This implies that similar reduction rates could be expected for mixtures containing Sishen ore and Thabazimbi ore. The mass vs time curves for these tests are shown in ***Figure 16.***

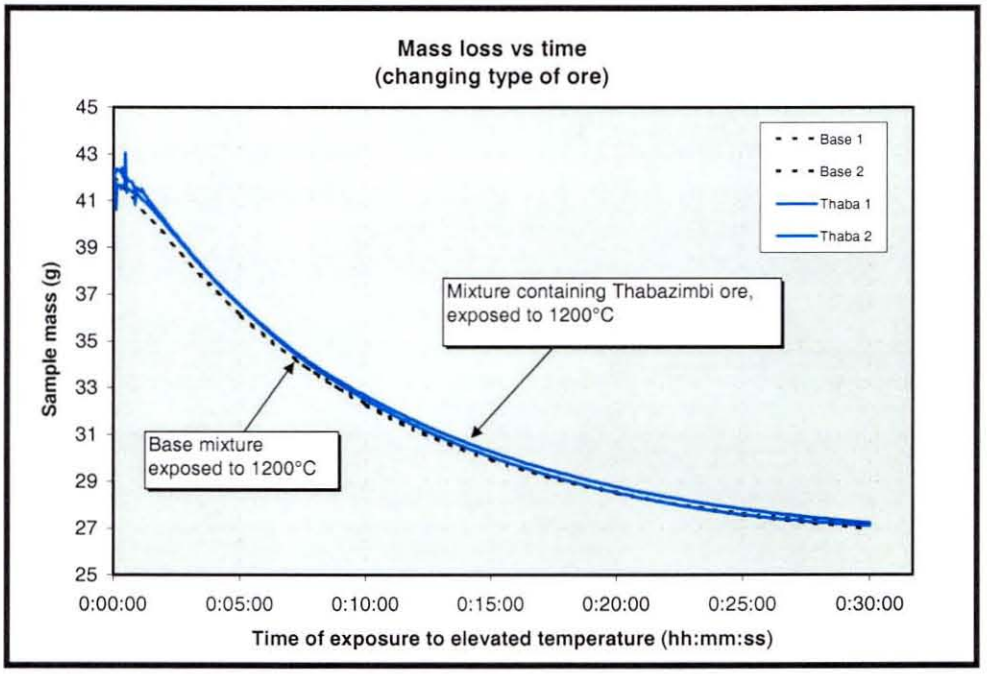

Figure 16: *Masses of base mixture samples exposure to 1200°C as well as masses of mixtures containing Thabazimbi ore exposed to 1200°C respectively, as a function of exposure time.*

The reducibility of Thabazimbi ore is about 10% higher than that of Sishen ore. To test the results, the influence of a 10% increase in the rate constant of the reduction reaction was simulated. Results (presented in **Figure 17**) showed that after 10

minutes, the mixture containing Thabazimbi ore achieved 39.3% reduction while the base mixture (containing Sishen ore) achieved 39.0% reduction. This implies that the extent to which reduction rate can be increased by increasing ore reducibility, is limited.

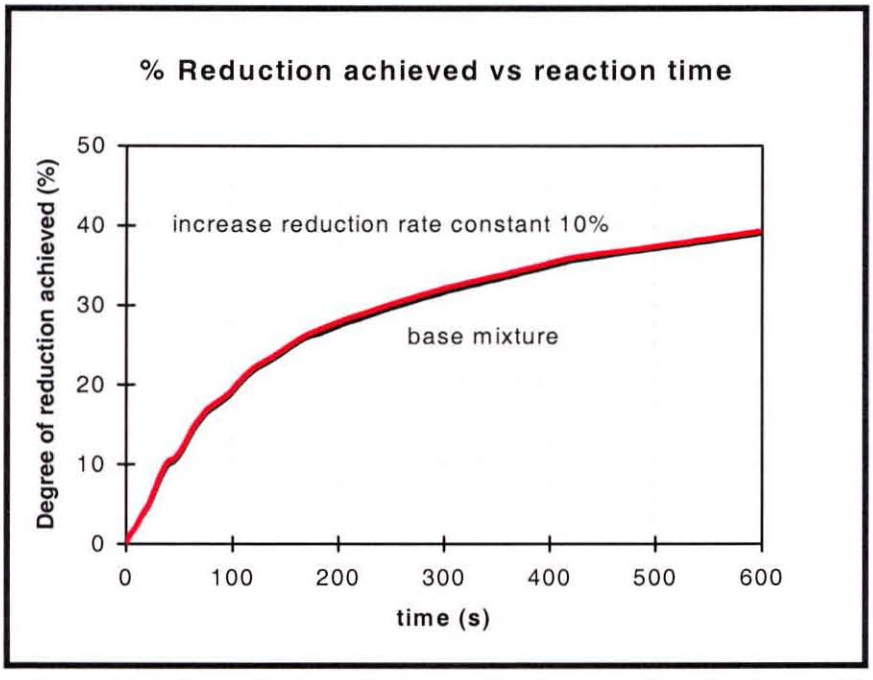

Figure 17: *Model prediction of change in degree of reduction achieved when the reduction rate constant is increased by 10%. (The model prediction for the base mixture is shown in black as a reference with the model prediction for the increased rate constant shown in red.)*

To confirm repeatability of the test, two experiments were conducted with mixtures containing Thabazimbi ore at 1100°C. ***Figure 16*** shows that the two curves obtained were similar, thereby indicating repeatability

2.4.3 Influence of ore size on reduction behaviour

Figure 18 shows the reduction rate of a material mixture containing specific size fractions, when exposed to 1200°C.

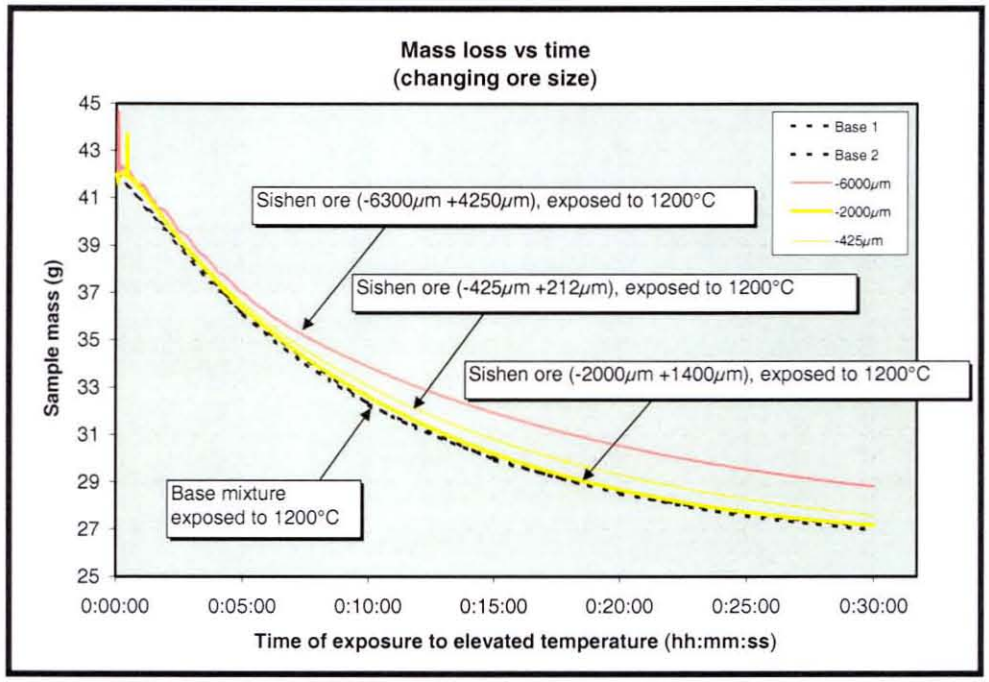

Figure 18: *Mass losses as a function of time for base mixture as well as mixtures containing various size fractions of Sishen ore during exposure to 1200°C*

Figure 18 shows that the base mixture, the mixture containing –425 +212 µm particles, and the mixture containing –2000 +1400 µm particles showed mass losses of 13.4, 13.4 and 12.7 g respectively during the first 20 minutes, while the +4750 – 6300 µm particles however only showed 11.5 g mass lost during the same time. This means that the mass loss achieved by particles smaller than 2000 µm, deviated 4.5% from the base mixture (after 20 minutes), while the +4750 µm deviated from the base mixture by 14%. From these figures it seems that the reduction rate of particles smaller than 2000µm was independent of particle size, while the reduction rate of particles larger than 4750 µm was slower. To investigate this, samples of partially reduced ore (reduced at 1200°C) was set in resin, polished and investigated with an optical microscope. (The method used for setting and polishing of the samples is similar to the procedure discussed in ***paragraph 3.4.2.2***.)

Typical images obtained are shown in **Figure 19** and **Figure 20**. **Figure 19** shows a "shrinking core" texture that was observed in some of the larger particles (+4750 µm). Most of the large particles and all of the small particles showed homogeneous reduction occurring throughout each particle. (This is shown on the right-hand-side of **Figure 20**). **Figure 20** shows two adjacent particles in the sample, one with a "shrinking core" structure and one with a homogeneous structure.

No correlation was found between the position of particles in the sample and the particle texture (shrinking core or not). This implies that the tendency of the ore particles to react according to a shrinking core, was a result of material characteristics rather than sample configuration.

From the above it was concluded that the rate of reduction in some of the larger particles (mostly larger than 4.7 mm), was controlled by the rate of diffusion of gaseous species in the particle.

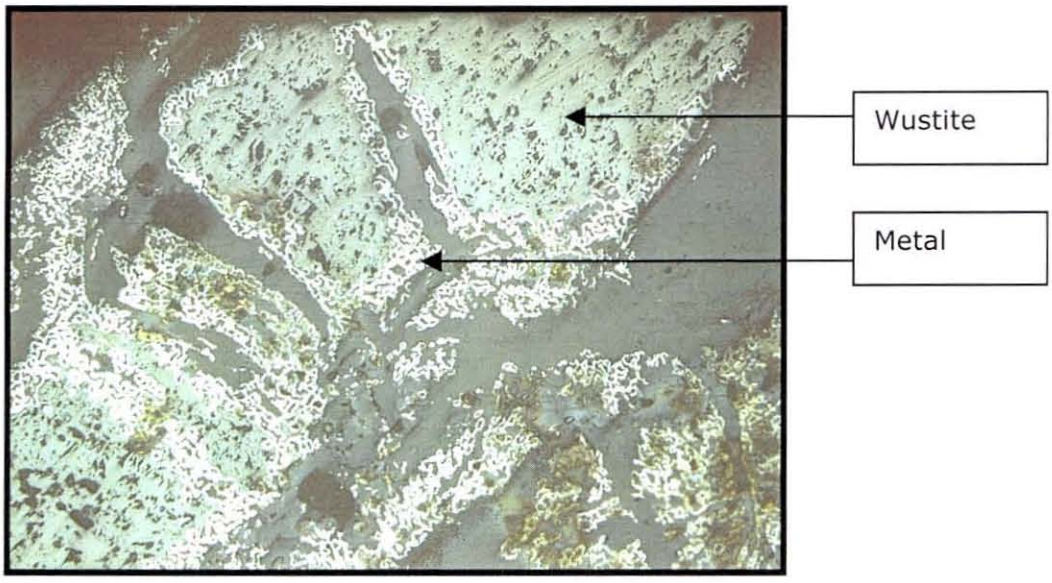

Figure 19: *Optical image of a polished section of a partially reduced +4750 µm – 6300 µm ore particle. (Width of field of view = 2 mm.)*

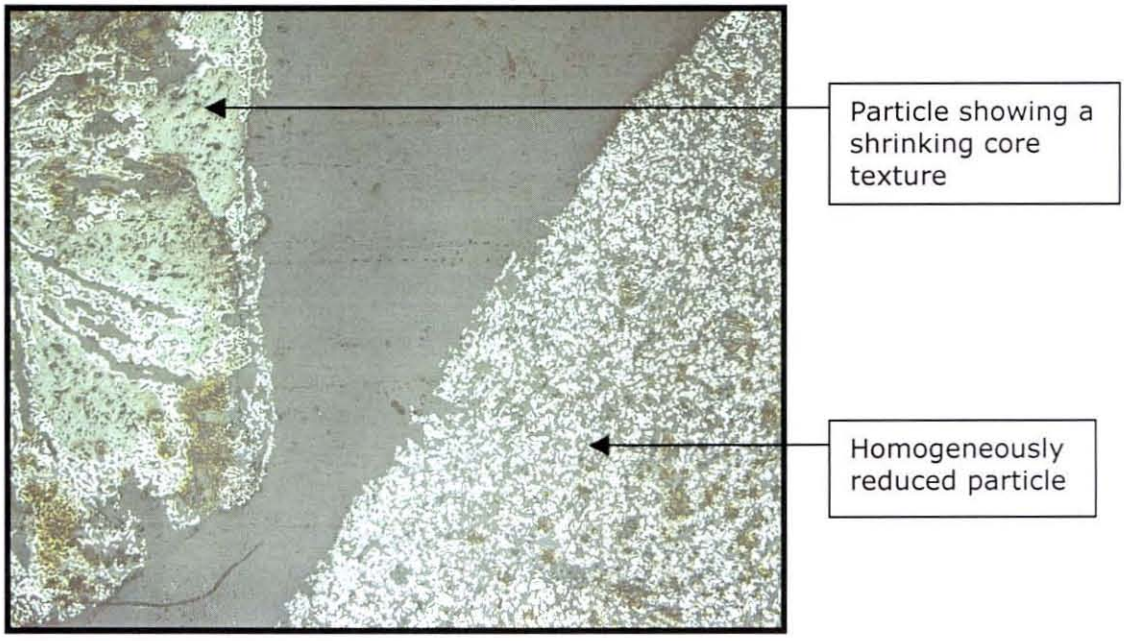

Figure 20: *Optical image of a polished section of adjacent particles that were partially reduced. (+4750 µm –6300 µm ore particle) (Width of field of view = 2 mm.)*

2.4.4 Influence of type of coal on reduction behaviour

The CO_2 reactivity of coal is the rate at which carbon in coal is oxidised by CO_2 at 1000°C. CO_2 reactivity is expressed in terms of mass of carbon reacted per unit time.

The influence of changing the CO_2 reactivity of a material mixture was modelled, by changing the rate constant for the Boudouard reaction. The results from the model are shown in ***Figure 21***.

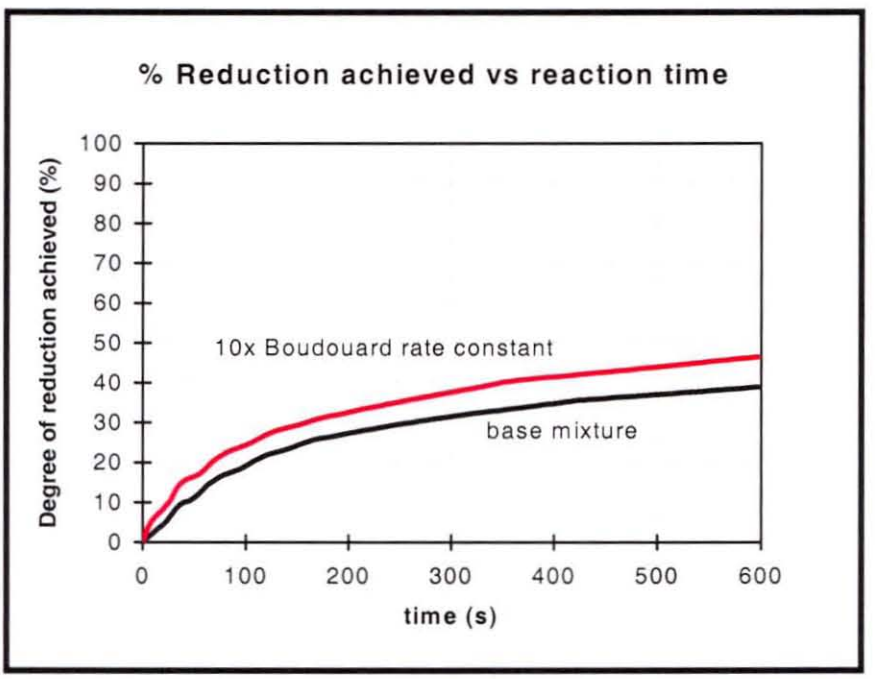

Figure 21: *Model prediction of change in degree of reduction achieved when the gasification rate constant is increased by a factor of 10. This is for a sample exposed to 1200°C. (The model prediction for the base mixture is shown as a reference (in black) while the model prediction for the increased rate constant shown in red.)*

The model results show that the degree of reduction achieved, is influenced by the CO_2 reactivity of the coal. The effect of changing the gasification reaction rate is predicted to have a similar effect as changing the rate of the reduction reaction (for this specific mixture, exposed to 1200°C).

The model predictions were experimentally tested. For the experimental investigation, Eikeboom and Leeuwpan coal, with CO_2 reactivities of 2.06 and 1.64

g/min were respectively used[48]. From the CO_2 reactivity values it can be seen that the CO_2 reactivity of the Leeuwpan coal was about 20 % higher than that of Eikeboom coal. The base mixture contained Eikeboom coal.

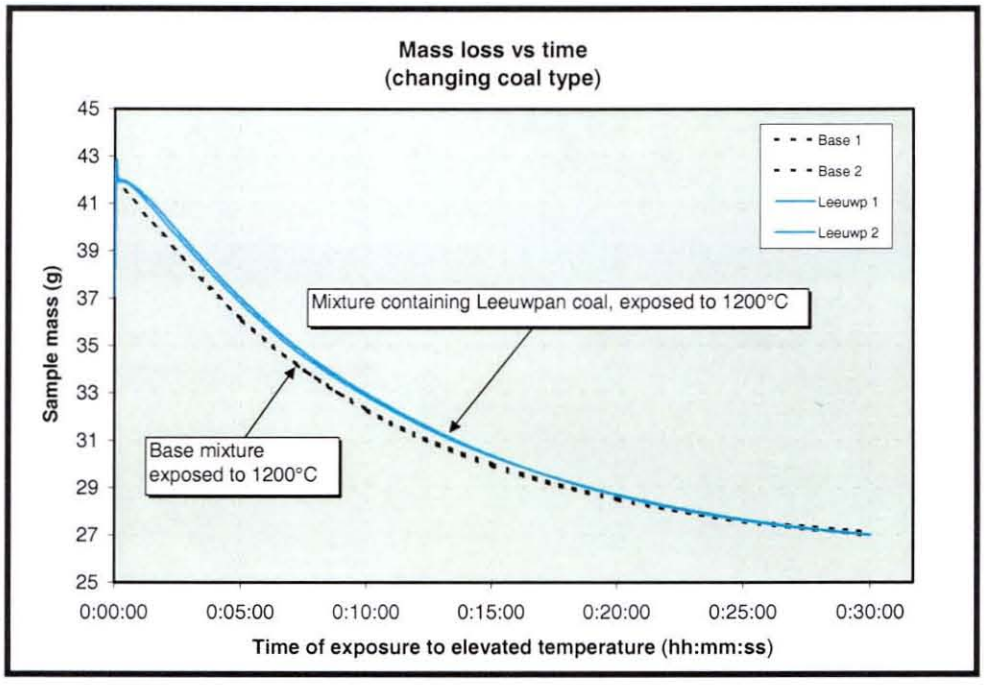

Figure 22: *Masses of base mixture samples and masses of mixtures containing Leeuwpan coal exposed to 1200°C respectively, as a function of exposure time.*

Figure 22 shows no significant change to the mass loss achieved, when the CO_2 reactivity of the material mixture changed (for exposure to 1200°C). ***Figure 22*** shows that even though the graphs in ***Figure 22*** *are* not identical, the mass loss achieved after 30 minutes of exposure was similar. Accordingly, the degree of reduction was expected to be similar. However, similar changes to the reduction rate constant and the Boudouard rate constant yielded similar changes to the overall reduction rate. This implies that the rates of the reduction- and Boudouard reaction, are similar, and the reaction may be under mixed control at some point in time. (This conclusion only holds for the specific material mixture investigated, exposed to 1200°C).

The influence of changes to the reduction and gasification rate constants on the overall reduction rate was marginal. A change in exposure temperature (as shown in ***Figure 22***) had a more prominent effect than changing rate constants.

2.4.5 Influence of amount of volatile matter of coal on reduction behaviour.

The model prediction showed that the volatile matter in coal does contribute to reduction. The presence of volatile matter increases the rate at which the composite mixture is reduced. This is shown in ***Figure 23***. Calculations were done for a furnace temperature of 1200°C.

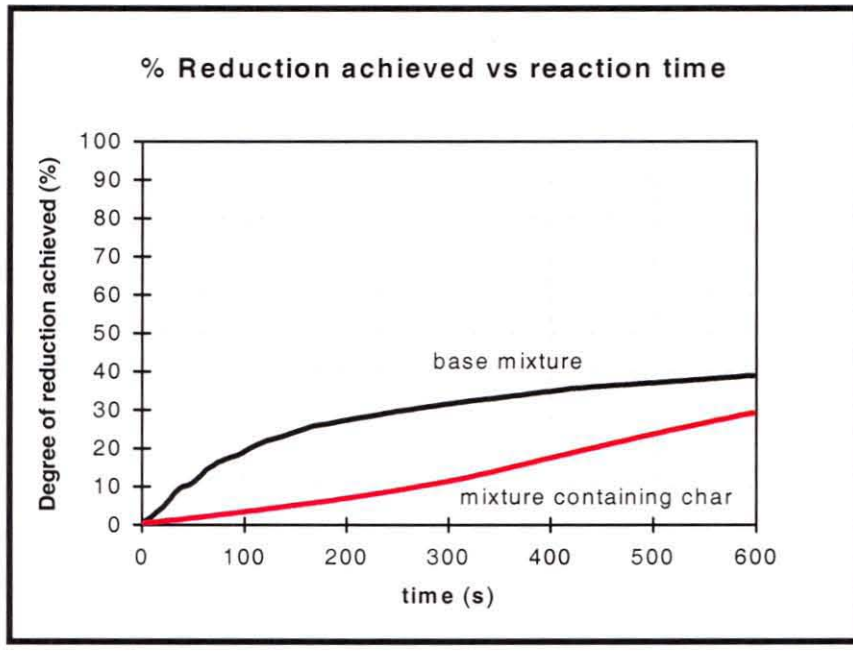

Figure 23: *Model prediction comparing the reduction rate of a mixture containing coal (with 23% volatiles) with that of a mixture containing char.*

The experimental results, shown in ***Figure 24*** (as well as ***Appendix C.2*** *and* ***Appendix C.3***), confirmed model prediction-trends. ***Figure 24*** shows that the rate at which the mass of the base mixture decreased was higher than the rate at which the mass of the sample containing coal char decreased. Although the contribution of volatile matter to the rate of reduction was not obvious from ***Figure 24***, ***Appendix C.2*** and ***Appendix C.3*** clearly show that volatile matter increased the rate of reduction. This was assumed to be a result of hydrogen reduction (noting that the rate of reduction of iron oxide with hydrogen is significantly faster than that with carbon monoxide)[50,51].

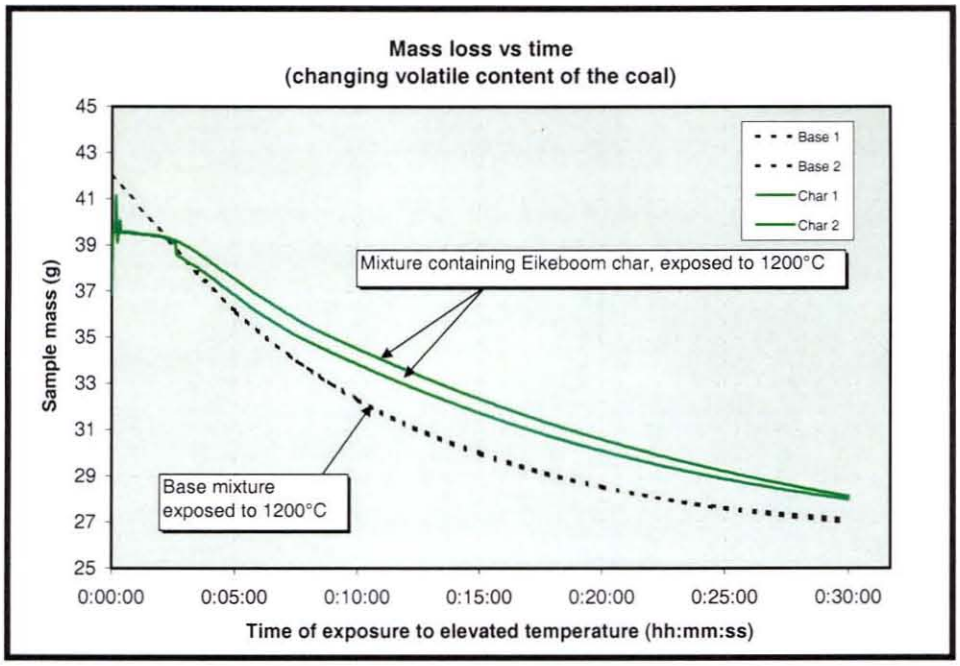

Figure 24: *Reduction rate of base mixture and a mixture containing Eikeboom char exposed to 1100°C and 1200°C respectively.*

2.4.6 Influence of exposure temperature on reduction behaviour

The model prediction showed that the rate of reduction increased when the temperature (to which the material mixture was exposed) increased. This is shown in ***Figure 25***. The model prediction was confirmed by experimental results, as shown in ***Figure 14***.

When a sample is exposed to 1200°C instead of 1100°C, the model predicted an increase from 38 to 40 % reduction (achieved after 10 minutes). Actual measurements showed that the degree of reduction that was achieved, changed from 24 to 38% (after 10 minutes exposure). Although the values were not the same, model predictions were qualitatively confirmed.

In addition, the model predictions showed that the rate of reduction increased when the conduction heat transfer coefficient increased. This implies that the rate of reduction is influenced by the rate of conduction in the material mixture. The model prediction is shown in ***Figure 26***.

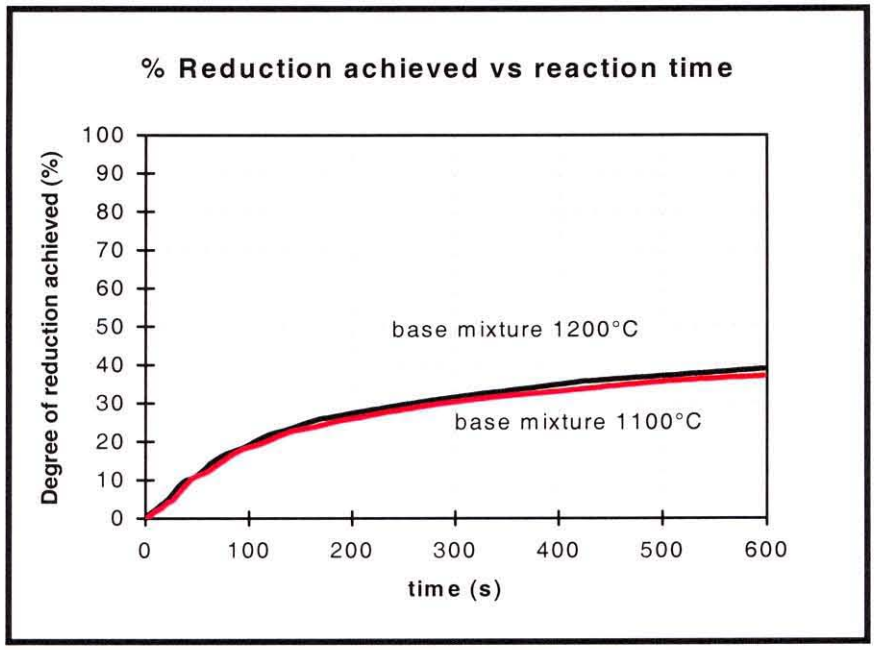

Figure 25: *Model prediction comparing the reduction rate of a mixture exposed to 1200°C to that of a mixture which was exposed to 1100°C.*

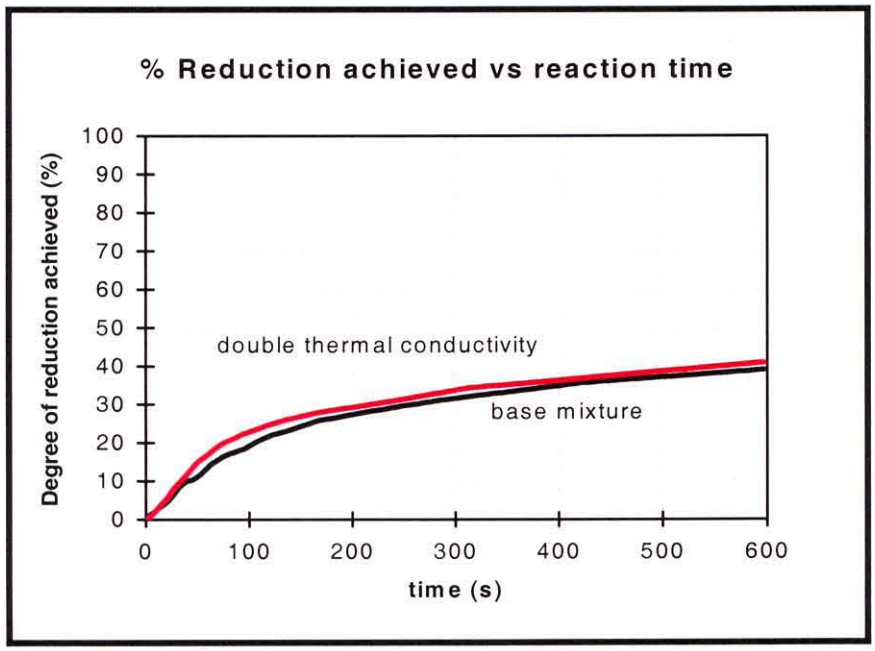

Figure 26: *Model prediction comparing the reduction rate of a base mixture to that of a mixture for which the heat transfer coefficient was doubled.*

The predicted temperature in the centre of the sample, as well as the predicted temperature of the outer surface of the sample are shown in ***Figure 27.*** This figure shows a significant temperature difference between the outer surface and the centre of the sample during the first 180 seconds of the test. The reduction occurring during this time, was therefore governed (to a great extent) by heat transfer limitations. In addition, the centre of the sample reached 700 °C after about 190 seconds. This means that there was a period at the start of each test during which the Boudouard reaction did not proceed and reduction would have been slow (especially at the centre of the sample). Actual measurements also show a period (between 240 and 360 seconds) during which reduction did not occur. (This is shown in ***Figure C.1*** *to* ***Figure C.12*** *in* ***Appendix C.2*** *and* ***Appendix C.3***.) During calculations it was however assumed that devolatilization and calcination of carbonates was completed before reduction started. This also contributed to the period of no reduction that was observed at the start of each test.

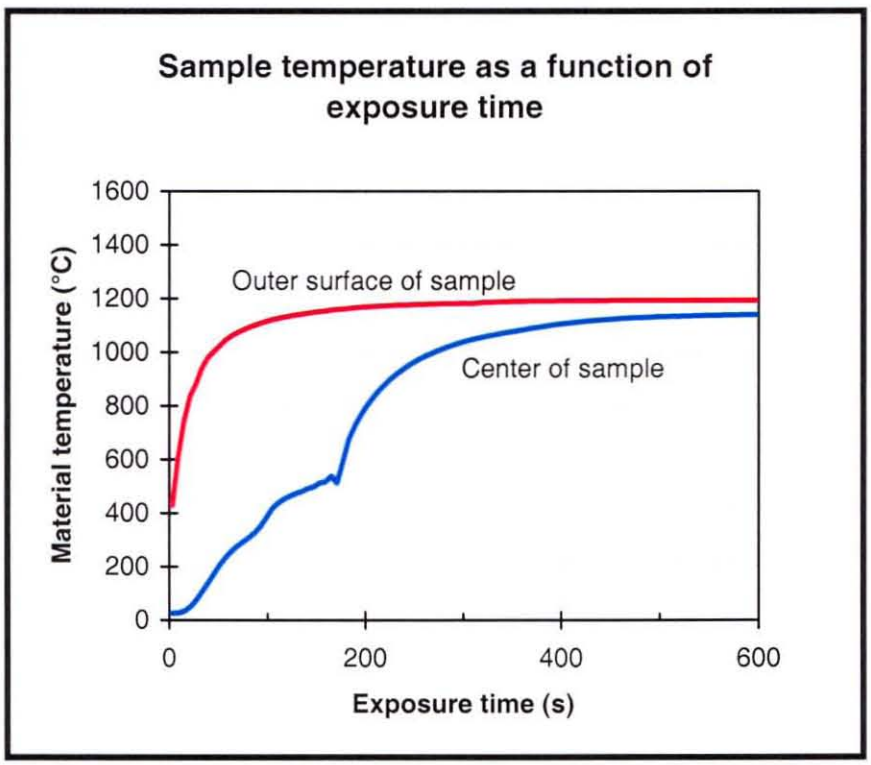

Figure 27: *Model prediction comparing the temperatures of the centre and outer surface of the sample as a function of exposure time. The centre of the sample is shown in blue, while the outer surface is shown in red.*

However, the steep temperature gradient in the sample showed that reduction was governed by the rate of heat transfer, at least during the first three minutes of each test.

2.4.7 Extent of influence of various parameters

All the tested parameters are shown on the same graph in **Figure 28.**

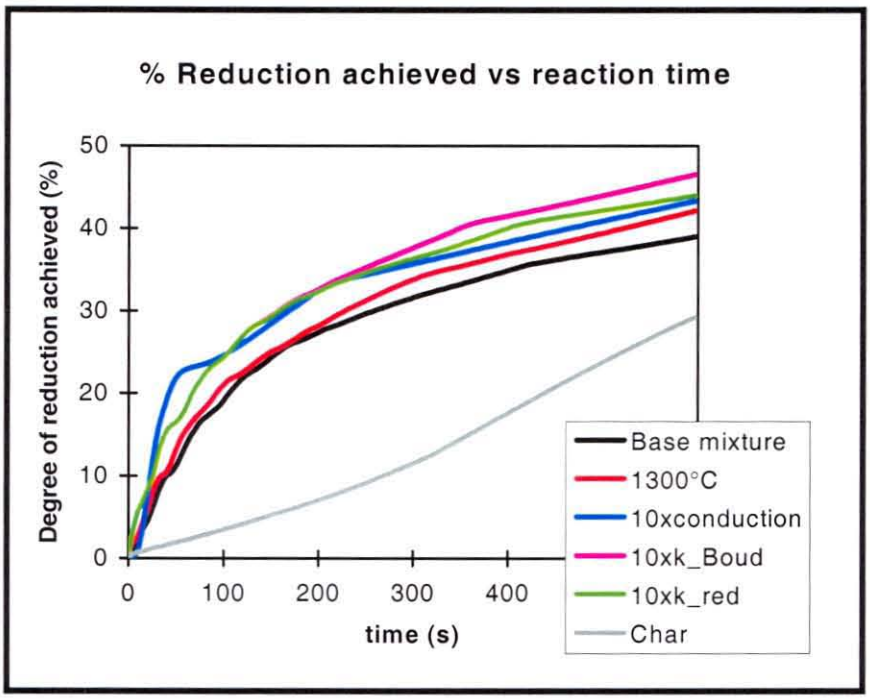

Figure 28: *Model prediction comparing the influence the exposure temperature, reduction rate constant, gasification rate constant, heat transfer coefficient and the volatile content of the material mixture on the degree of reduction achieved.*

From the graph it can be seen that increasing the exposure temperature by 100°C had a similar effect as increasing the heat transfer coefficient or rate constants by a factor of 10. The temperature to which the mixture was exposed therefore appeared to be the most significant in governing the reduction rate.

The increased reduction rate is due to better heat transfer to drive the Boudouard reaction and/or it may be due to reactions occurring faster at higher temperatures.

Volatile matter from the coal influenced the rate of reduction significantly.

The reduction rate constant, the Boudouard reaction rate constant and the conductivity of the material affected the degree of reduction achieved.

The original experimental data is presented in ***Appendix C.1***.

2.5 Conclusions

To optimise production in the solids bed of the Ifcon process, **ore and coal** should not only be selected according to chemical composition but also according to CO reducibility and CO_2 reactivity. Both of these parameters influenced the overall rate of reduction, which implies that the rates of the reduction and Boudouard reactions were of the same magnitude. The effect of changes to CO reducibility and CO_2 reactivity was however limited.

The **use of coal instead of char** increases the rate of reduction in the material mixture. This is probably due to the reduction of iron ore with hydrogen.

When the conductivity of the solids bed is increased, the extent of reduction that is achieved in the bed, also increases. This indicates that heat transfer may govern the rate of reductions (especially when the size of the sample increases). From a practical perspective, material should be fed in such a way that **conduction heat transfer is avoided**. Material will typically be fed in thin layers, so that more material is exposed to the freeboard. This will cause more heat to be transferred from the freeboard to the solids bed directly by radiation, and not via conduction through the bed material.

The degree of reduction achieved increased with increasing exposure temperature. This may be due to better heat transfer (as a result of a larger driving force for heat transfer), or it may be the result of a higher temperature region in the bed where reactions occur faster. **The temperature to which the mixture is exposed should be as high as possible**, within the limits of solid state reduction.

3 Phase II: Production rate in the packed bed of the Ifcon process

3.1 Background

3.1.1 Objective

The origin of the Ifcon process was based on results from an experiment[18] that showed that 80% reduction could be achieved in a solids bed, at a material mixture feed rate of 135 kg/m^2/h. This correlated with an iron feed rate of about 60 kg Fe/m^2/h (and a production rate of 56 kg Fe/m^2/h [17]). Based on the result of 80% reduction achieved in the solids bed, it was assumed that the reduced bed is melted from below to produce metal and slag. In practice however, reduction can occur as a combination of solid-state reduction in the solids bed and solid-liquid-state reduction in the slag [1,17]:

The objective of this part of the study was to determine the extent of reduction achieved as solid-state reduction. For this, the following was done:

- Information from related studies was investigated.
- A kinetic model was used to predict the temperature profile and reduction profile through the solids bed.
- Experimental data was used to determine the applicable rate constants to be used in the model.
- The temperature profile through a solids bed was measured and compared to model predictions.
- Finally, the model was used to calculate the extent of reduction achieved, as solid-state reduction, in the solids bed.

3.1.2 Related studies and test approach

This investigation was done in conjunction with another study[19]. Both studies aimed at gaining information that complimented each other.

In the other study[19], the degree of reduction achieved (in the upper part of the solids bed) was estimated as a function of exposure time. For this, typical Ifcon-material-mixtures were exposed to elevated temperatures in a muffle furnace. Conditions in this muffle furnace simulated conditions in the freeboard of the Ifcon

process. The material mixtures were contained in identical alumina fibre crucibles that insulated the samples from all sides but one. The open end of each crucible was exposed to the muffle furnace (at an elevated temperature), for a specific time. After exposure, the degree of reduction achieved was determined for each sample. Results for 40 mm thick samples exposed to 1500°C are shown in ***Figure 29.*** The size of each sample was known and so was the time for which the sample was exposed. The cross-sectional area of each sample was also known. When the mass of the sample is divided by the time of exposure and the cross-sectional area, a specific feed rate (with units: $kg/m^2/h$) is obtained. Once the Fe content of the material mixture is known and a Fe yield is estimated, the feed rate can be expressed as a production rate. The results of the abovementioned investigation[19] were expressed in terms of production rate, rather than exposure time.

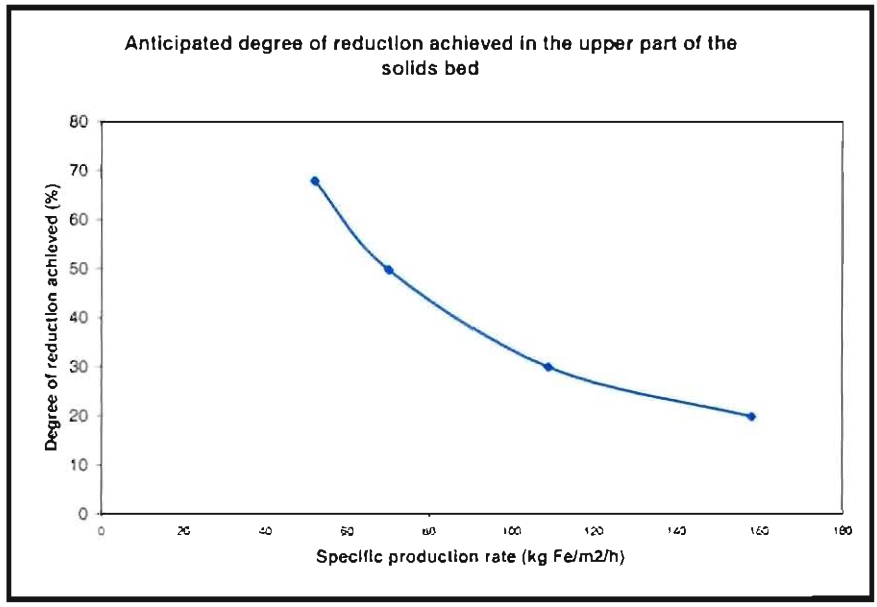

Figure 29 : *Results from muffle furnace experiments showing the anticipated degree of reduction achieved in the top 40 mm of the solids bed, as a function of production rate, for a freeboard temperature of 1500°C*[19].

As discussed in ***paragraph 1.4.2***, the solids bed can conceptually be divided into a top and bottom part, so that the top part only receives energy from above the solids bed, while the bottom part only receives energy from below the solids bed. ***Figure 29*** shows the anticipated degree of reduction in the top part of the solids bed, which was driven by energy from above the solids bed. Since the material that is partially reduced in the upper part of the solids bed, descends to the bottom part of the bed,

Figure 29 also shows the anticipated degree of reduction of material that enters the bottom part of the solids bed, as a function of production rate. This study investigated the rate at which partially reduced material, which entered the bottom part of the solids bed, was reduced by solid-state reduction.

The achievable production rate was calculated using a kinetic model (discussed in the next paragraph). To confirm model predictions, the results were tested experimentally.

Figure 29 shows that between 20% and 68% reduction can be achieved in the upper part of the solids bed. Data obtained from pilot plant campaigns[12] showed that the degree of reduction achieved on the outer surface of the solids bed was about 30%[12]. Accordingly, a material mixture containing 30 % pre-reduced iron ore was used as input material during the experimental investigation. Material mixtures containing 0% and 50% pre-reduced iron ore was also used as input material to test the sensitivity of the results. The experimental investigation is discussed in detail in ***paragraph 4.4***.

The production rate was also varied during the experimental investigation. Production rates of 30, 80 and 120 kg Fe/m^2/h were aimed for. This was done by varying the electrical energy input to the experimental set-up. The experimental procedure is described in detail in ***paragraph 3.4***. ***Table 4*** summarizes the experiments that were planned for this investigation.

Table 4: *Experimental program of phase II of the investigation*

Specific Production rate (kg Fe/m^2/h)	% Pre-reduction		
	0 %	30 %	50 %
30	X	X	X
80		X	
120		X	

The temperature profile that was predicted by the model was compared to experimentally measured temperature profiles. Point-counts were also done on

selected samples to identify the amounts of phases present at specific positions in the solids bed. This was done as reference to model predictions.

3.1.3 Other relevant studies

Huang and Lu[23] exposed ore–coal mixtures to 1200°C while measuring the temperature profile through the mixed burden. Their results indicated temperature gradients of between 10 and 40°C/mm.

Sun and Lu[39] also measured the temperature profiles through composite ore-coal mixtures. They found that the temperature gradients are steeper near the hot surface and for shorter reaction times (lower degrees of metallization). They also suggested that the low effective thermal conductivity of the mixture and the strong endothermic nature of carbon gasification may be the main determinants of the temperature gradients. Their results also indicated temperature gradients between 10 and 40°C/mm.

The main difference between this study and the studies mentioned above, are that none of the above studies investigated the effect of a continuously descending bed due to melting of the reduced or partially reduced product, while sustaining steady state solid-state reduction.

3.2 Determining rate constants for the reduction of iron ore

3.2.1 Solid state reduction kinetics

To eliminate unknowns during modelling of final reduction in the solids bed, representative rate constants for the reduction reactions (of the specific ore used during the investigation) had to be determined. The TGA experiment (discussed in ***paragraph 2.2***) was not designed to yield basic kinetic information and could therefore not be used for this purpose. Accordingly, data from a related study[51] was used to determine the kinetic rate constant for the reduction reactions. The original data from the experimental work was used to calculate the rate constants used in this paper.

The rate constants for the gasification reaction is calculated in a similar way than the reduction rate constant. For this study values recently measured for the specific coal that was used during this investigation, was used [51] .

3.2.1.1 Experimental aspects[51]

Experimental set-up

The experimental set-up consisted of a fluidised bed, which was mounted on a scale. This is schematically shown in ***Figure 30***. The scale enabled mass loss of the sample to be measured while the reactions occurred in the reactor. The reactor comprised of a double-shelled glass reactor. The inner glass reactor, which could be removed from the outer glass reactor, contained a perforated silica disc to allow gas flow from the outer glass reactor to the inner glass reactor. The perforated disc also ensured gas distribution through the sample.

The furnace temperature was controlled by a proportional-integral-derivative (PID) controller. A Pt/Pt10%Rh (or type S) thermocouple, positioned at the height of the sample, outside the outer glass reactor, served as control thermocouple. The outer reactor was mounted on the scale, which recorded mass loss as a function of time throughout each experimental run. Argon (99.999% purity) was used as purging gas, while CO (99.995% purity) was used as reduction gas, and CO_2 was used as oxidation gas. All of the gasses were passed through water vapour and oxygen removal columns (similar to that shown in ***Figure 13***) before introduction into the outer reactor. Gas flow rates were controlled by mass flow meters calibrated for each

specific gas. Flammable gasses CO and H_2 were burnt with a pilot flame at the gas outlet. The experimental set-up is discussed in more detail elsewhere[51].

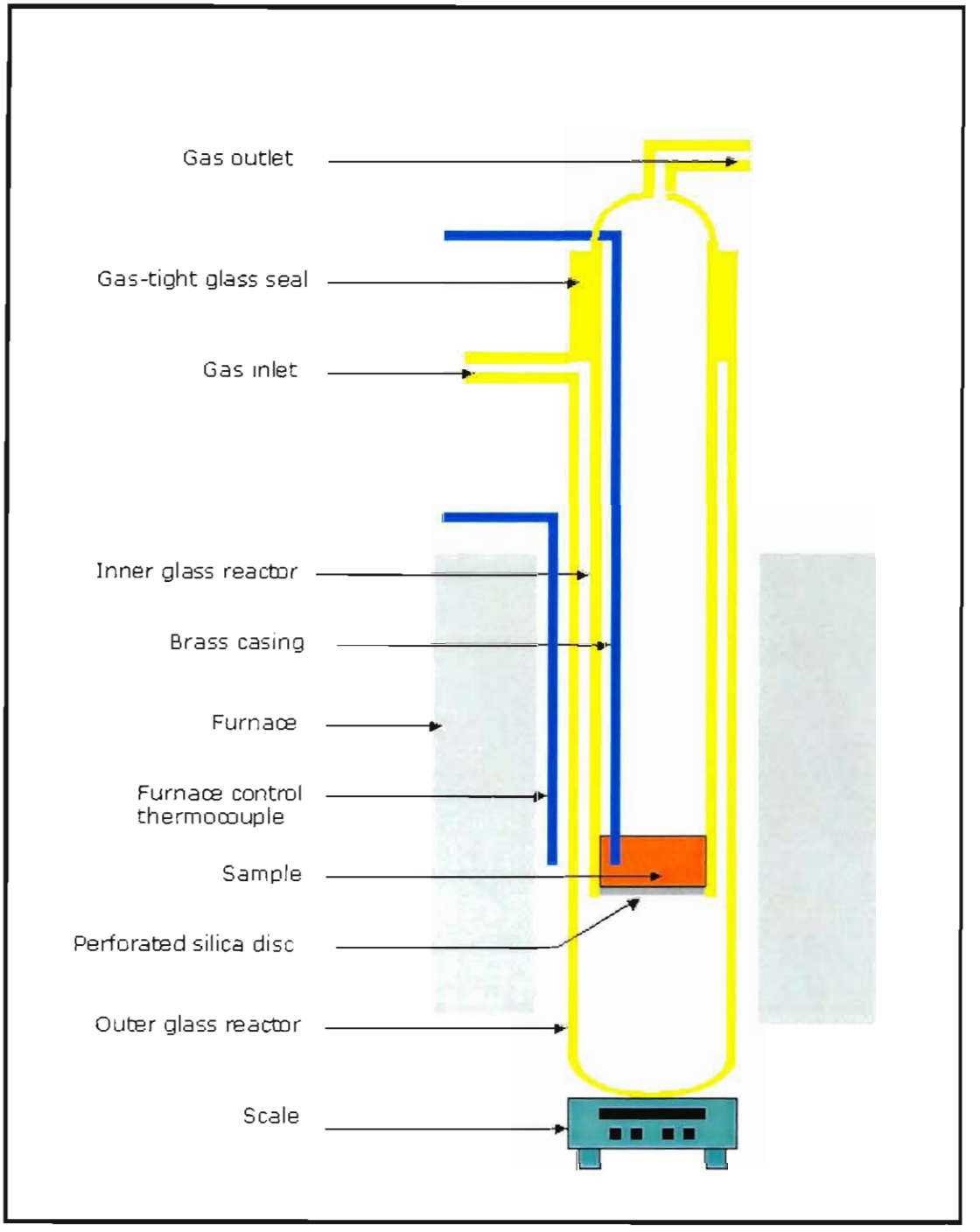

Figure 30: *Schematic presentation of the experimental set-up used for measuring rate constants*

Experimental Procedure[51]

Before the test commenced each sample was weighed. The sample was placed into the inner reactor, which was placed inside the outer reactor. The thermocouple was put in place to measure the sample temperature. The reactor was sealed and purging gas introduced. The mass recording software was activated and the mass of the sample was recorded continuously. The reactor was purged with Argon for 2 minutes, after which the Argon gas flow was terminated, and the reactant gas was introduced into the reactor at the required gas flow rate. The calculation of the required gas flow rate is shown in ***Appendix D.1***.

The sample was reacted for the required period. On completion of this period the reactant gas flow was terminated and the system was purged with Argon. After flushing for 5 minutes the inner reactor, containing the sample, was removed from the reactor assembly and allowed to cool to room temperature. Once the sample cooled to ambient temperature, it was recovered from the inner reactor, weighed, and analysed for degree of reduction.

For measuring of gasification reaction rates the same procedure was followed, but CO was substituted with CO_2. The experimental procedure is discussed in more detail elsewhere[51].

3.2.2 Results and discussion

A summary of the kinetic data from the reduction experiment with CO is shown in ***Table D.1*** to ***Table D.5*** and ***Figure D.2*** to ***Figure D.6*** in ***Appendix D.2.***

Reduction was assumed to proceed in the sequence hematite → magnetite → wustite → iron, with all reactions occurring as first order reactions. (Reduction of hematite to magnetite and magnetite to wustite was taken as one step.) The reaction rate of a first order reaction is described by the following relationship[51]:

$$\frac{dF}{dt} = -c\,(1-F) \qquad (3.a)$$

where *F* is the fraction of oxygen atoms reacted, t is the reaction time (with unit: s), and c is the proportionality constant (with unit: s^{-1}). Integration of ***equation 3.a*** between F and F_0, as well as t_0 and t yields the following equation:

$$\ln \frac{(1-F)}{(1-F_o)} = -c\,(t-t_o) \qquad (3.b)$$

From the experimental data, a plot of $\ln[(1-F)/(1-F_o)]$ vs $(t-t_o)$ was constructed. The slope of this plot yielded the proportionality constant c. This constant was expressed as follows[30]:

$$c = \frac{k_{co}\, m_{Fe}\, C_{co}}{N_0^O} \qquad (3.c)$$

where m_{Fe} was the mass of Fe in the sample (with unit: kg), C_{CO} was the concentration of CO gas in contact with the sample (with unit: mol/m^3) N_0^O was the initial oxygen content of the sample (with unit: mol), and k_{CO} was the rate constant (with units: $m^3.s^{-1}.kg\ Fe^{-1}$).

From ***equation 3.c***, the rate constant (k_{CO}) was calculated. The rate constant (k_{CO}) was expressed as follows:

$$k_{co} = k_o\, e^{(-E_a/RT)} \qquad (3.d)$$

where k_0 was the pre-exponential constant in rate expression (with units: $m^3.s^{-1}.kg\ Fe^{-1}$), E_a was the activation energy (with units: $J\ mol^{-1}$), R was the gas constant (with units: $J\ mol^{-1}\ K$), and T was the temperature (in K).

From a plot of $\log(k_{CO})$ vs 1/T, the value of the pre-exponential constant (k_0) and the activation energy (E_a) was obtained, by considering the intersect with the y-axis and the slope of the graph. Values obtained for the various size fractions of ore are presented in ***Appendix D.3***.

By plotting the ln of the rate constant against 1/temperature (the Arrhenius plot), the apparent activation energies as well as the k_o values of the reduction reaction for each particle size fraction of ore was determined. The Arrhenius plots are shown in ***Figure 31*** and ***Figure 32.***

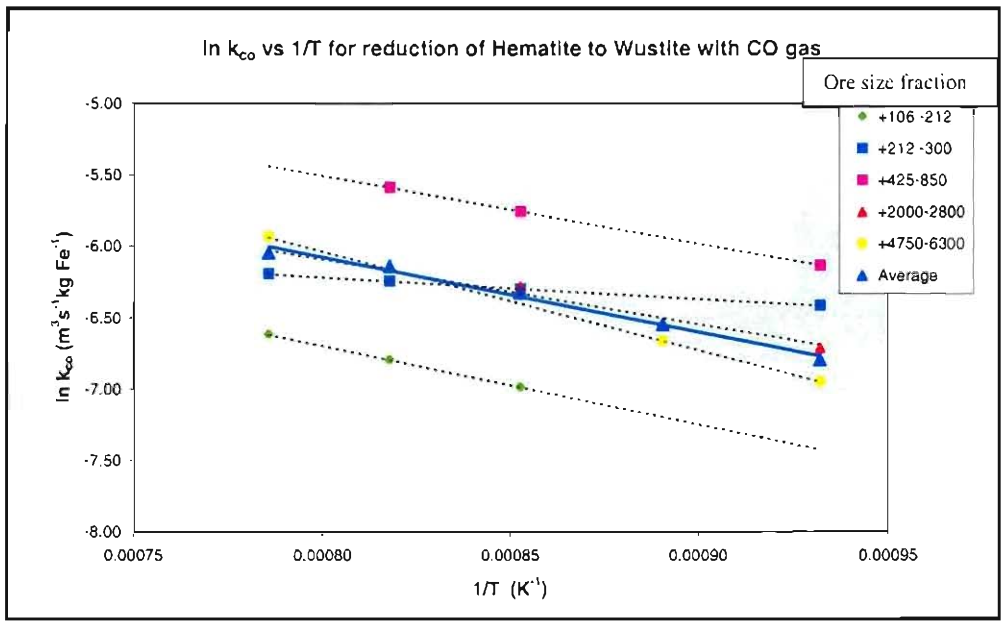

Figure 31: *ln (rate constants) as a function of 1/temperature for the reduction of hematite to wustite.*

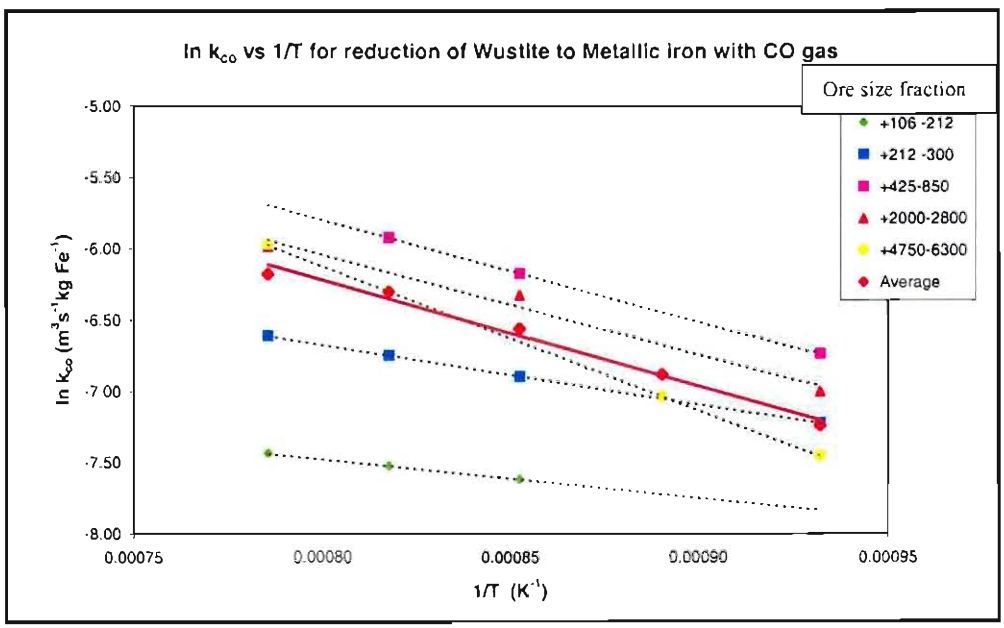

Figure 32: *ln (rate constants) as a function of 1/temperature for the reduction of wustite to metallic iron.*

Since the size distribution of the iron ore was known, the average rate constant and apparent activation energy was calculated from the weighted average plot of the plots for the individual size fractions. ***Figure 31*** and ***Figure 32*** (and ***Figure 33***) also shows the weighted average Arrhenius plot, which represents the plot for the ore fines with size distribution as used during this study.

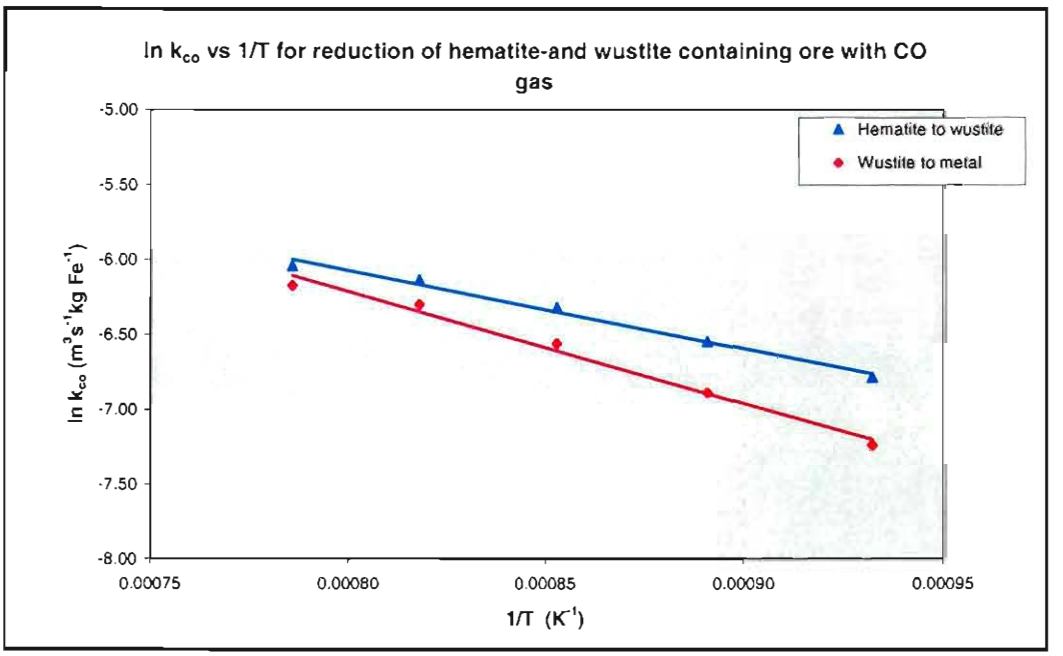

Figure 33: *Weighted averages of ln (rate constants) as a function of 1/temperature for the reduction of hematite to wustite and wustite to metallic iron respectively.*

The proportionality constants, rate constants and activation energies of the various particle sizes are shown ***Appendix D.3.*** The overall results are also shown in ***Table 5.***

Table 5: *Apparent activation energies and rate constants for Sishen ore used during this investigation.*

	0 to 30% reduction		30 to 80% reduction	
	k_o ($m^3s^{-1}kg\ Fe^{-1}$)	E_a ($J.mol^{-1}$)	k_o ($m^3s^{-1}kg\ Fe^{-1}$)	E_a ($J.mol^{-1}$)
Average values	0.535	56520	3.242	77000

The rate constants for the gasification reaction was measured by Pistorius et al[51] for char from the same Eikeboom coal that was used during this investigation. The rate constants for various size fractions of Eikeboom char was measured and the overall rate constant and activation energy was calculated. These values are shown in ***Table 6*** and ***Table 7*** respectively.

Table 6: *Individual activation energies and rate constants for gasification of specific size fractions of Eikeboom char, (which was also used during this investigation)*[51].

Size fraction of char	Carbon gasification	
	k_o ($m^3s^{-1}kg\ C^{-1}$)	E_a ($J.mol^{-1}$)
- 212µm +106 µm	4.588×10^4	182 440
-425µm + 212µm	1.252×10^4	166 769
-850µm + 425µm	6.180×10^2	137 098
-2000µm + 1400µm	8.255×10^4	189 867

Table 7: *Apparent activation energies and rate constants for gasification of Eikeboom char, which was used during this investigation*[51].

	Carbon gasification	
	k_o ($m^3s^{-1}kg\ C^{-1}$)	E_a ($J.mol^{-1}$)
Values used	45780	172401

3.3 Modelling of the bottom part of the solids bed

3.3.1 Basic model description[15]

3.3.1.1 Overview

The area in the solids bed where reduction mainly occurs by solid-state reduction, can be simulated as a plug flow reactor (PFR)[2]. On the other hand, the slag pool where solid/liquid state reduction and bath smelting reactions on be simulated as a continuous stirred tank reactor (CSTR)[2]. Based on the assumption that all material that reached the slag pool moved through the solids bed, final reduction at the bottom of the solids bed can be simulated as a PFR and CSTR in series. The relative amounts of reactions occurring in the PFR and CSTR depends on the respective amounts of solid-state reduction and solid-liquid-state reduction occurring in the process. This split in reduction mechanism was investigated during this study. The rate of reactions in the slag pool was assumed to be much faster than the rate of reactions in the solids bed[5,15].

The bottom of the solids bed was modeled as a PFR, using a kinetic model. The model was a variation of the model that was used by Pistorius[15] to simulate reduction in the top part of the solids bed. Since devolatilisation was expected to occur in the top part of the solids bed, volatiles were not included in the model. Although calcinations may or may not occur in the bottom part of the bed, the complexity of calcinations was excluded from the model. The solids bed therefore consisted of hematite, magnetite, wustite, metallic iron, carbon, and lime, while the gas phase comprised of CO and CO_2.

Since it was assumed that material moved through the solids bed in plug flow[15,16], one-dimensionality of the bed was assumed, i.e. properties varied only in the vertical direction.

The bed was divided into a number of horizontal cross-sections (or nodes). The condition in each node was assumed to be uniform. Coetsee et al.[49] showed that the gas temperature in a node could be assumed equal to the solids temperature in the node.

3.3.1.2 Thermal conductivity of the bed

The porosity of a nodes depended on the amounts of each of the phases present in the nodes, their densities and the node heights. The node height was assumed to remain constant during the reduction process. This means that compacting due to softening of the bed was not accounted for.

The effective thermal conductivity of each node was calculated using the geometric mean thermal conductivity of the solids[51], the conductivity of the gas[29], and the porosity of the node. This calculation was based on the assumption of random distribution of solids in each node (discussed in more detail in ***paragraph 2.3***).

3.3.1.3 Gas flow through the bed

The boundary condition at the bottom of the bed was a net flow of CO and CO_2 into the bottom node. The amount of CO and CO_2 corresponded to the amount of unreduced material leaving the bottom node. The CO/CO_2 ratio of this gas was chosen as 13, which corresponds with a partial oxygen pressure of $4x10^{-10}$, which in turn corresponds with a FeO activity of 0.3 at 1550°C. This correlates with pilot plant data[17].

The temperature of the gas entering each node was assumed to be equal to that of the solids in the node below it[49], while the gas leaves the node at the temperature of the solids in the node. For the bottom node the gas temperature was equal to the bath temperature.

The equilibrium partial pressures of CO_2 for the reduction and Boudouard reactions was calculated from equilibrium constants, which were derived from the free energy data as compiled by Kubaschewski et al.[53]

3.3.1.4 Reaction kinetics

Reduction was assumed to proceed in the sequence hematite → magnetite → wustite → iron, where the rate equation held for all three reduction steps. At temperatures below 564°C however, reduction was assumed to proceed in the sequence hematite → magnetite → iron, where the rate equation held for both reduction steps

The reaction rate expressions of the model were based on the expressions used by Coetsee et al.[30] during modeling of reduction of a composite pellet.

Reduction reaction:

$$r_R = k_R \exp(-E_R / RT)\, M_{Fe}\, (1-F)\, \frac{p_{CO} - p_{CO}^{R}}{RT} \qquad (3.e)$$

Boudouard reaction:

$$r_B = k_B \exp(-E_B / RT)\, M_C\, \frac{p_{CO_2} - p_{CO_2}^{B}}{RT} \qquad (3.f)$$

where r_R and r_B were the reaction rates (with units: moles of O and C reacted per m^2 per second), k_R and k_B were the rate constant for the reduction and Boudouard reactions respectively,(with units: m^3/kg Fe/s and m^3/kg C/s) , F was the degree of reduction achieved, M_{Fe} and M_C were the masses (in kg) of iron and carbon respectively per m^3 of the packed bed, E_R and E_B were the activation energies of the reduction and Boudouard reactions (with units J/mol), T was the absolute temperature, p_{CO} and p_{CO_2} were the partial pressures of CO and CO_2 respectively(with unit: Pa), p_{CO}^{R} and $p_{CO_2}^{B}$ were the equilibrium partial pressures of CO and CO_2 for the reduction and Boudouard reactions (in Pa).

3.3.1.5 Mass transfer and rate constants

Coetsee et al.[49] showed that the interface concentration of CO and CO_2, respectively was similar to the respective CO and CO_2 concentration of the bulk gas. Diffusion of gaseous species through the pores of the bed was therefore not considered in the model. The apparent rate constants (which makes provision for diffusion in the pores of the particle) were determined from experimental data, as discussed in ***paragraph 3.2***.

3.3.1.6 Calculation procedure

The initial conditions in the nodes was defined by the starting temperature, degree of reduction and the mass ratio of carbon and lime to iron.

The new temperature was explicitly calculated, and depended on the heat transfer into the node by radiation and conduction as well as the extent of reactions occurring

in each node. Radiation only took place at the bottom node, while the top node was assumed to be thermally insulated.

By considering an oxygen and carbon balance for each node, the CO/CO_2 ratio which satisfies the rate equations for the reduction and Boudouard reactions were found. The carbon and oxygen balances were written as follows:

Carbon balance: $n = (1 + x)(n_1 + n_2 + n_3)$ (3.g)

Oxygen balance: $n = (2 + x)(n_1 + 2n_2 + n_4)$ (3.h)

Where n_1 and n_2 were the amounts of CO and CO_2 , which respectively entered the node in a time interval (with units: mol/m^2), n_3 was the number of moles of carbon gasified by the Boudouard reaction (with units: mol/m^2), n_4 was the amounts of oxygen removed by the relevant reduction reaction (with units: mol/m^2), and x was the molar CO/CO_2 ratio of the gas leaving the node.

From ***equation 3.g*** and ***equation 3.h***, n_3 and n_4 were written as follows:

$$n_4 = C_1\left(p_{CO} - p_{CO}^{R}\right); \text{ with } C_1 = k_R \exp(-E_R / RT)\, M_{Fe}\, dh\, (1 - F)\, \frac{1}{RT}\, dt \quad (3.i)$$

$$n_3 = C_2\left(p_{CO_2} - p_{CO_2}^{B}\right); \text{ with } C_2 = k_B \exp(-E_B / RT)\, M_C\, dh\, \frac{1}{RT}\, dt \quad (3.j)$$

with dh the height of the node and dt the time interval (with unit: s) and all other symbols as defined for ***equation 3.e*** and ***equation 3.f***.

By combining ***equations 3.g*** and ***3.h***, and substitution of ***equations 3.i*** and ***3.j***, the following expression was obtained:

$$n_1 + 2n_2 + C_1\left(p_{CO} - p_{CO}^{R}\right) = \frac{x+2}{x+1}\left[n_1 + n_2 + C_2\left(p_{CO_2} - p_{CO_2}^{B}\right)\right] \quad (3.k)$$

In order to solve for X, ***equation 3.k*** was written in quadratic form as follows:

$$ax^2 + bx + c = 0 \tag{3.l}$$

with

$$\begin{aligned} a &= -n_2 - C_2 p^B_{CO_2} - C_1 p_{TOT} + C_1 p^R_{CO} \\ b &= n_1 - n_2 + C_2 p_{TOT} - 3C_2 p^B_{CO_2} - C_1 p_{TOT} + 2C_1 p^R_{CO} \\ c &= n_1 + 2C_2 p_{TOT} - 2C_2 p^B_{CO_2} + C_1 p^R_{CO} \end{aligned} \tag{3.m}$$

The quadratic equation was solved to yields a value for x, which was then used to solve for n_3, n_4 and n.

Once the amounts of Fe and C reacting was known for a time interval, an energy balance was performed to calculate the new temperature of the node, at the end of the time interval. The following equations were used:

$$T_{NEW} = (H_{INIT} + (q/A)_{cond\_in} + (q/A)_{Rad\_in} - (q/A)_{cond\_out} - SumA)/SumB \tag{3.n}$$

where T_{NEW} was the absolute new temperature of the node at the end of the time interval, H_{INIT} was the enthalpy of all species entering the node at the start of the time interval, $(q/A)_{cond\_in}$ $(q/A)_{Rad\_in}$ were the amounts of conductive and radiant heat (with units: J/m^2) which respectively entered the node during the time interval, while $(q/A)_{cond\_out}$ was the amount of conductive heat that left the node during the time interval.

$$H_{INIT} = \sum_i n_i \left(A_i + B_i T_{Node}\right) + n_1 \left(A_{CO} + B_{CO} T_{gas}\right) + n_2 \left(A_{CO_2} + B_{CO_2} T_{gas}\right) \tag{3.o}$$

$$SumA = \sum_j n_j \left(A_j\right) + xn\left(A_{CO}\right) + n\left(A_{CO_2}\right) \tag{3.p}$$

$$SumB = \sum_j n_j \left(B_j\right) + xn\left(B_{CO}\right) + n\left(B_{CO_2}\right) \tag{3.q}$$

where n_i is the number of moles of solid species *i* (Fe°, FeO, Fe_3O_4, Fe_2O_3, CaO and C) in the node at the start of the time interval, n_j was the number of moles of solid species j (Fe°, FeO, Fe_3O_4, Fe_2O_3, CaO and C) in the node at the end of the time interval, A_i , A_j, B_i and B_i are the constants in the enthalpy correlation[15] of species *I and j respectively*, n_1 and n_2 are the number of moles of CO and CO_2 respectively which entered the node, at the temperature T_{gas} , while *xn* and *n* were the number of moles of CO and CO_2 which left the node at the new temperature (T_{NEW}). Note that T_{gas} for node (n+1) was assumed equal to T_{Node} for node n.

This procedure was followed for all nodes in the solids bed, to yield the temperature profile of the bed at the end of time interval *dt.* The entire procedure was then repeated for various time intervals to find the change of temperature and degree of reduction with time.

3.3.1.7 Simulating feed rate:

To simulate feeding at the top of the solids bed with the simultaneous melting of the bottom of the bed, the solids bed moved down by a node thickness after a holding time which corresponded with the feed rate of iron ore. Feeding and melting therefore occurred as steps rather than continuous movement of the bed. After each step, the top node comprised of newly fed material , while the rest of the nodes each inherited the properties of the node above it (i.e. temperature, degree of reduction and carbon content).

This procedure was repeated until the change in temperature of the nodes became negligible. The temperatures of the nodes then showed the steady state temperature profile of the bed. Similarly, a reduction profile of the bed was found.

3.3.2 Model predictions

The predicted temperature profile as well as profile for degree of reduction through the solids bed, for a feed mixture containing 30% pre-reduced iron ore, is shown below:

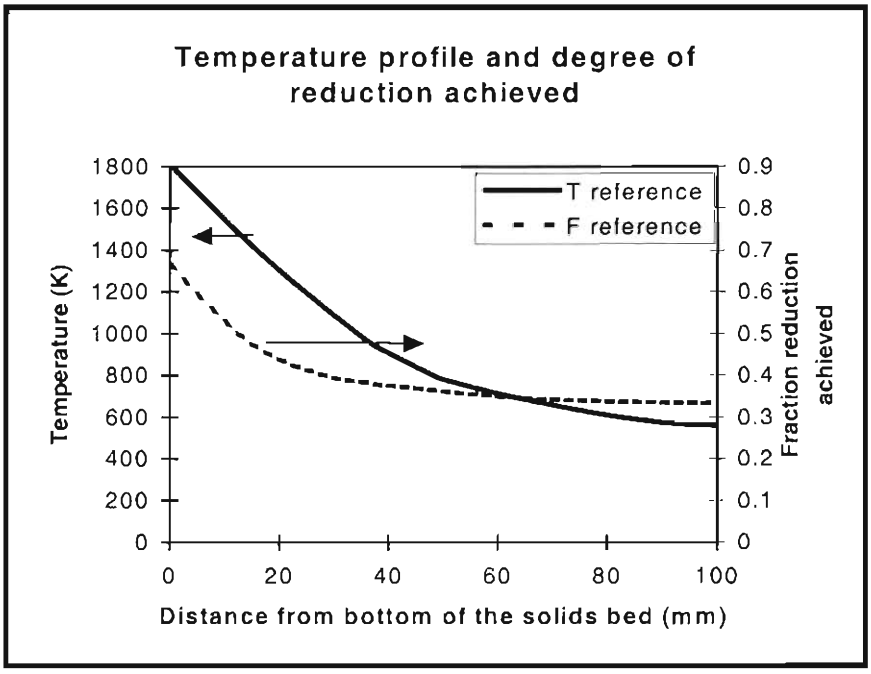

Figure 34: *Theoretical profiles of temperature and fraction reduction achieved through a 100mm high solids bed, for a production rate of 30kg/m²/h.*

Figure 34 shows that reduction mainly occurs in the 50mm above the bottom of the bed. These temperature and reduction profiles were used as basis for comparison when changes were made to the properties of the solids bed.

3.3.2.1 Change in rate constant for the reduction reaction

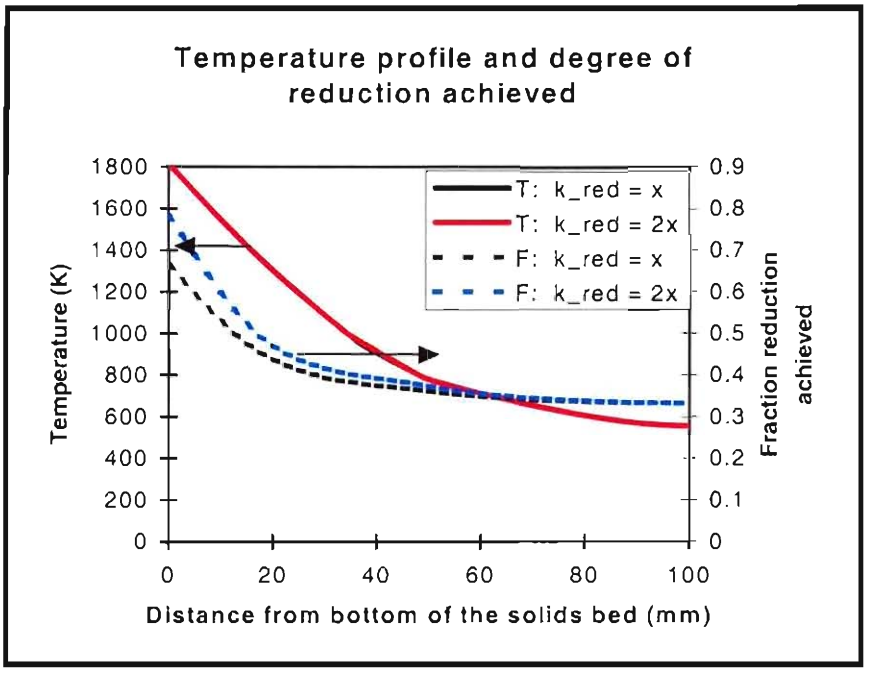

Figure 35: *Theoretical profiles of temperature and fraction reduction achieved through a 100mm high solids bed, for a production rate of 30kg/m²/h, when doubling the rate constant for the reduction reaction.*

Figure 35 shows the effect of doubling the rate constants for the reduction reactions on the profiles of the temperature and reduction achieved. The profiles for temperature and reduction for the increased rate constant are shown in red and blue respectively. The graphs presented in ***Figure 34*** are also shown as reference. The figure clearly indicates that the reduction profile changes. Before the rate constant was changed, 66% reduction was theoretically achieved, while 78% reduction was achieved when the rate constant was doubled. The temperature profile of the bed was not affected by the change in rate constants (the solid red and black lines were exactly the same).

From the above it seems that the degree of reduction achieved is controlled by the rate of the reduction reaction. Accuracy regarding the reduction rate constant (discussed in ***Section3.2***) used during modelling of the solids bed is therefore important.

Figure E 2 in ***Appendix E.1*** shows the theoretical profiles of temperature and fraction reduction through a 100mm high solids bed, for a production rate of 30kg/m^2/h, when the rate constant for the reduction reaction is halved. The effect thereof was that 8% less reduction was achieved, while the temperature profile of the bed was unchanged.

3.3.2.2 Change in rate constant for the gasification reaction

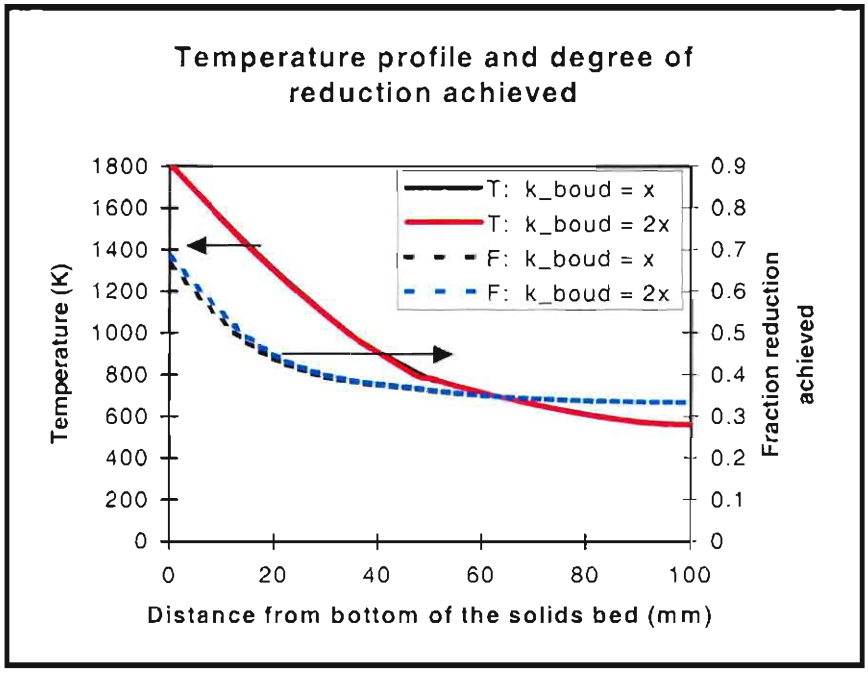

Figure 36: *Theoretical profiles of temperature and fraction reduction achieved through a 100mm high solids bed, for a production rate of 30kg/m^2/h, when increasing the rate constant for the gasification reaction.*

Figure 36 shows the effect of doubling the rate constants, for the gasification reactions, on the temperature and reduction profiles. The profiles for temperature and reduction are shown in red and blue respectively, while the results from ***Figure 34*** are also shown in black. The figure indicates that neither the temperature nor the reduction profiles changed significantly when the gasification rate constant was doubled. This implies that the rate of reduction at the bottom of the solids bed is not governed by the chemical rate of the Boudouard reaction.

Since it appeared that the rate of reduction was not controlled by the rate of the gasification reaction as such, accuracy regarding the rate constant for the gasification reaction was not regarded critical for modelling purposes.

Figure E 4 in ***Appendix E.1*** shows the theoretical profiles of temperature and reduction achieved through a 100mm high solids bed, when the rate constant for the Boudouard reaction is halved. Changing of the gasification rate constant did not change the temperature profile or the reduction profile of the bed.

3.3.2.3 Change in thermal conductivity of the bed

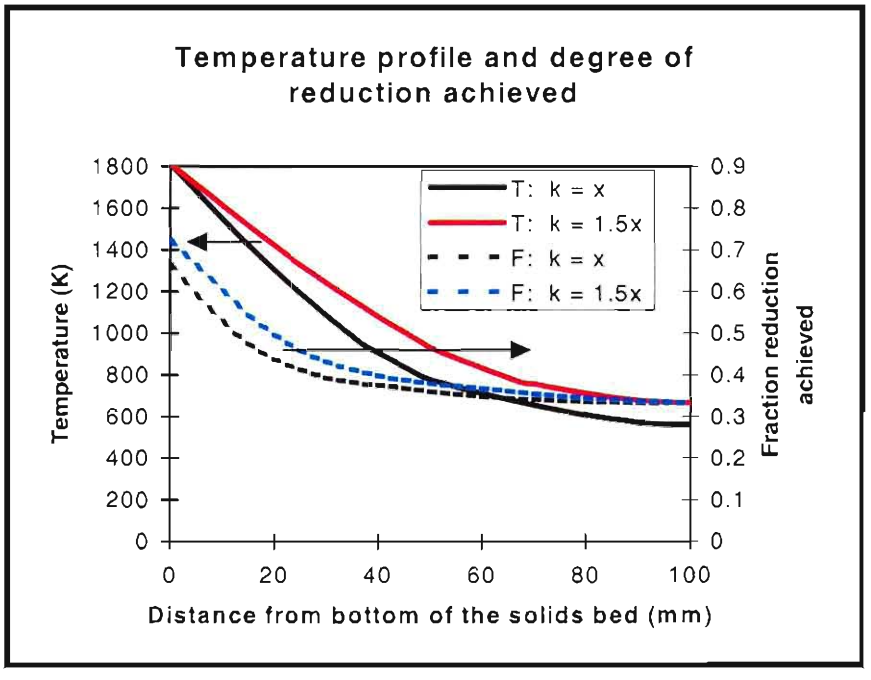

Figure 37: *Theoretical profiles of temperature and fraction reduction achieved through a 100mm high solids bed, for a production rate of 30kg/m^2/h, when increasing the thermal conductivity of the solids bed 1.5 times.*

Figure 37 shows the effect of increasing the thermal conductivity of the solids bed by a factor of 1.5. The figure shows a significant decrease in the slope of the temperature profile (in red) as well as a 7% increase in the degree of reduction achieved (in blue).

From the above it is clear that the overall reduction rate is not only controlled by the rate of the reduction reaction (as discussed in 3.2.2.1) but also by the rate of heat transfer (via conduction) in the solids bed.

Figure E 6 in ***Appendix E.1*** shows that halving of the thermal conductivity resulted in about 10 % less reduction achieved, while the slope of the temperature profile increased .

3.3.2.4 Change in bath temperature

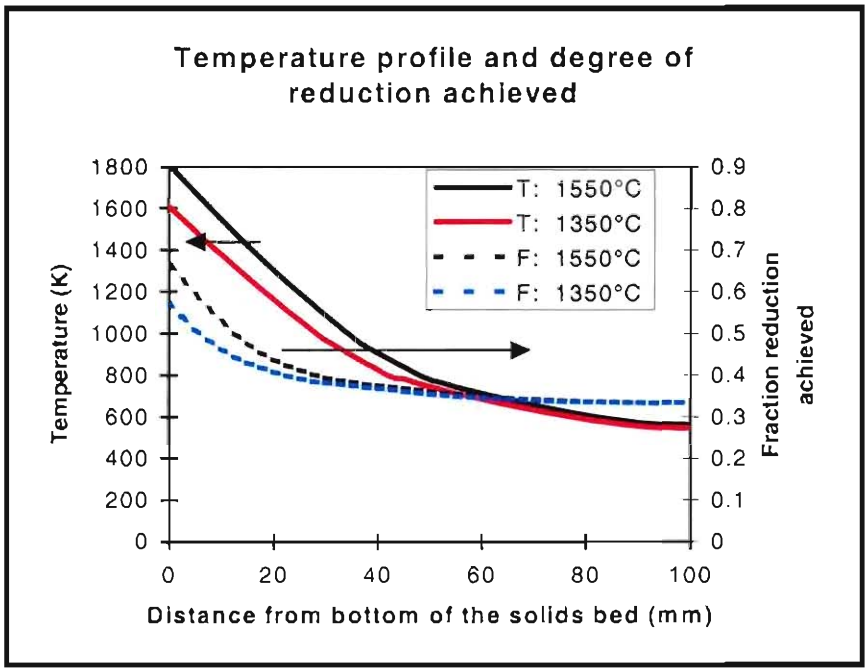

Figure 38: *Theoretical profiles of temperature and fraction reduction achieved through a 100mm high solids bed, for a production rate of 30kg/m²/h, when decreasing the bath temperature.*

Figure 38 shows the effect of decreasing the bath temperature from 1550°C to 1350°C. The figure shows a temperature profile (in red) at a lower position but with similar slope than that of **Figure 34** (shown in black). The reduction profile (shown in blue) also changed with a decrease in bath temperature. This indicated the importance of maintaining a constant bath temperature for comparative purposes.

Figure E 7 in ***Appendix E.1*** showed that when the bath temperature was increased from 1550°C to 1750°C, a larger temperature gradient and a higher degree of reduction was achieved.

3.3.2.5 Change in production rate

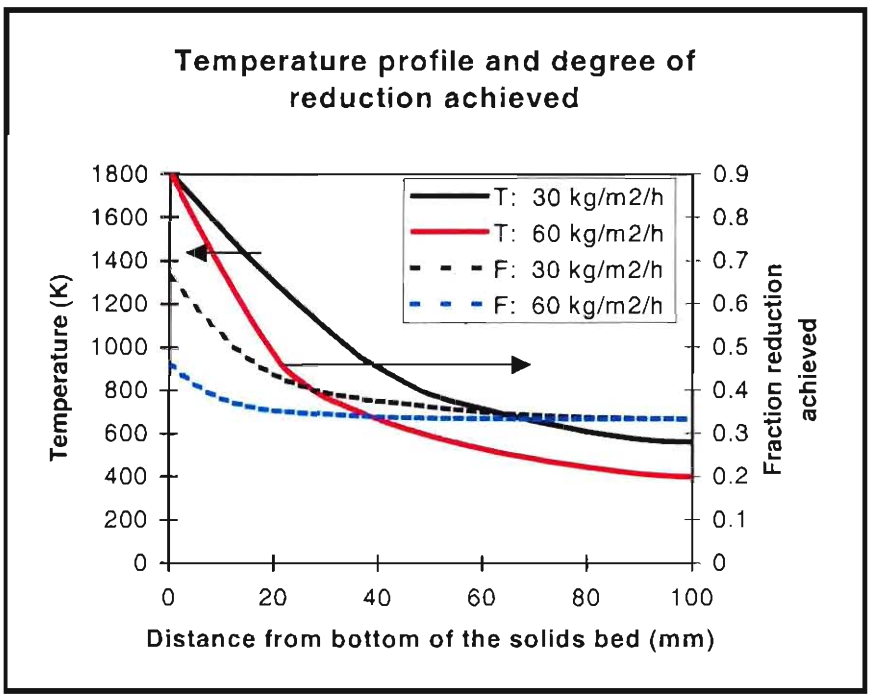

Figure 39: *Theoretical profiles of temperature and fraction reduction achieved through a 100mm high solids bed, for a production rate of 30kg/m^2/h as well as 60kg/m^2/h.*

Figure 39 shows the effect of increasing the production rate from 30 kg/m^2/h to 60kg/m^2/h. The figure shows a significant increase in the slope of the temperature profile, and accordingly, lower temperatures (in red). The figure also shows a significant decrease (about 20%) in the degree of reduction achieved (in blue). This indicated that the degree of reduction achieved in the solids bed strongly depended on the residence time of the particles in the solids bed.

Figure E 10 in ***Appendix E.1*** shows that when the production rate was halved, the degree of reduction achieved increased by about 20%, while the slope of the temperature profile of the bed decreased.

3.3.2.6 Change in degree of pre-reduction of input material

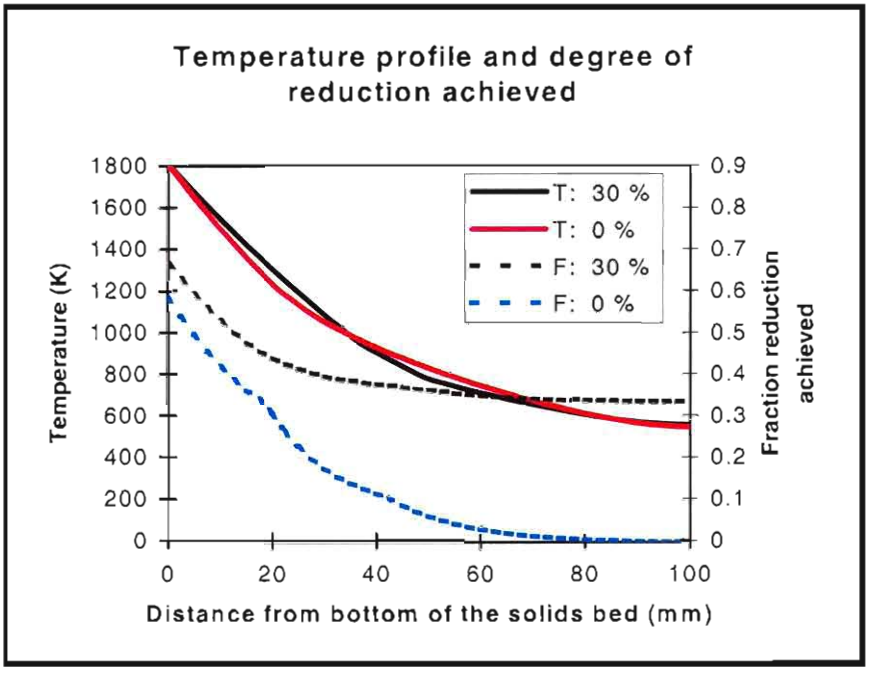

Figure 40: *Theoretical profiles of temperature and fraction reduction achieved through a 100mm high solids bed, for a production rate of 30kg/m²/h when decreasing the degree of pre-reduction of the input material from 30% to 0%*

Figure 40 shows the effect of decreasing the extent of reduction achieved in the upper part of the solids bed (from 30% to 0%). The figure shows little change in the slope of the temperature profile (in red), while the final degree of reduction achieved at the bottom of the solids bed (in blue) decreased (from 66% to 59% reduction).

Figure 41 shows the effect of increasing the extent of reduction achieved in the upper part of the solids bed from 30% to 50%. The figure shows that the slope of the temperature profile decreased, while the final degree of reduction achieved at the bottom of the solids bed (in blue) increased with 10%..

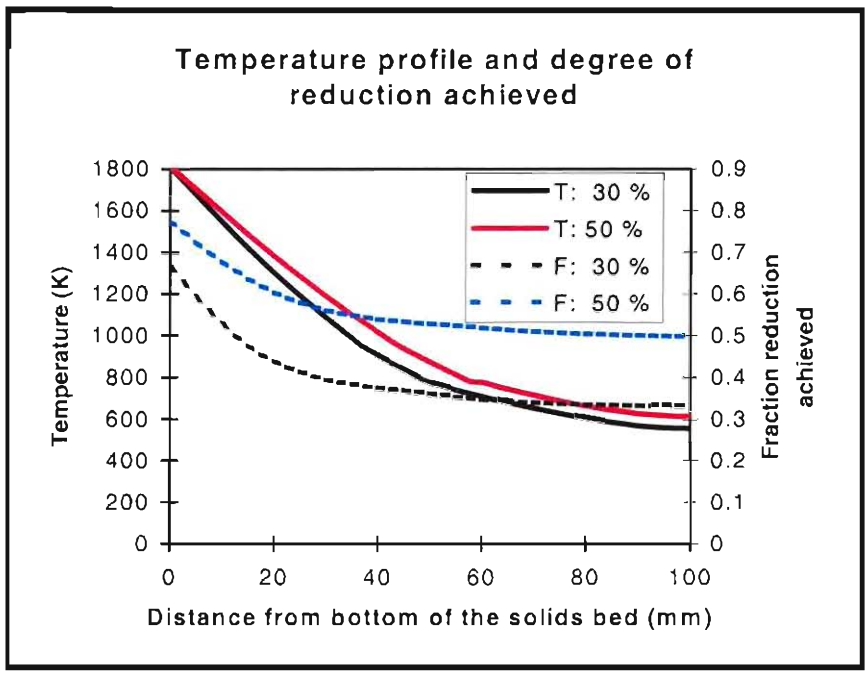

Figure 41: *Theoretical profiles of temperature and fraction reduction achieved through a 100mm high solids bed, for a production rate of 30kg/m^2/h when increasing the degree of pre-reduction of the input material from 30% to 50%*

The next step was to measure these model predictions experimentally.

3.4 Experimental aspects

3.4.1 Experimental apparatus

The experimental equipment mainly comprised of the induction furnace and associated gas flow rate control system.

3.4.1.1 The induction furnace setup.

The tests were performed in a 150kW coreless induction furnace. The furnace consisted of a fixed water-cooled induction coil, a fixed refractory lining, a removable crucible and a crucible lid assembly (shown in ***Figure 42***)

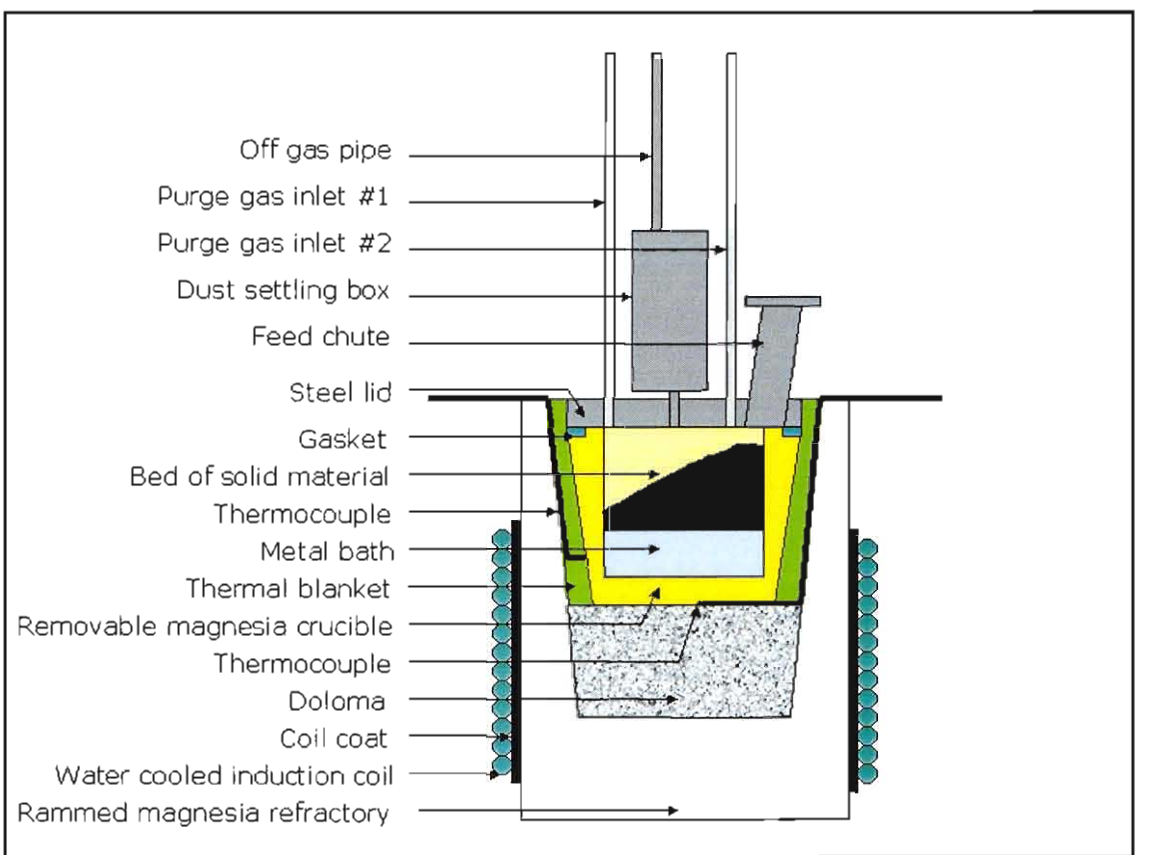

Figure 42: *Schematic illustration of the induction furnace configuration.*

The furnace was heated with a water-cooled, copper induction coil of 340 mm inside and 400 mm outside diameter, with a height of 465 mm. The coil was covered with high temperature insolating paper, to serve as coil coating. Since the furnace refractories expand and contract during heating cycles, the coil had to be separated

from the furnace refractories. This enabled stable coil conditions, despite expansion and contraction of furnace refractories.

The walls of the furnace were rammed, using a high magnesia ramming material (Basiram 95 HK) from Hernic Premier Refractories. Prior to test work, the rammed lining was sintered by establishing, and maintaining a steel bath in the furnace for three hours. The furnace was tapped (by tilting), and after cooling the metal scull was removed.

The floor of the furnace was lined with a layer of doloma (burnt dolomite) of particle size between 2.8 mm and 3.3 mm diameter. This was done to avoid "sticking" of the magnesia crucible to the magnesia furnace refractories (due to sintering), thereby easing removal of the "removable crucible".

The removable crucible was positioned on top of the doloma. (The positioning of the crucible is discussed in more detail in ***Appendix F.2***.) Each crucible had a 160 mm inner diameter and a height between 235 mm and 240 mm, while the outer diameter tapered from 190 mm to ±215 mm. The crucibles were cast with Basiram 95 HK from Hernic Premier Refractories. The water addition needed to obtain the castable was 7% (as specified by the manufacturers). The crucibles were cast in plastic moulds, and dried at 110°C for 36 hours. The crucibles were freed from the mould by breaking (cutting and tearing) the moulds. Sintering of the crucibles was done in a muffle furnace, with temperature control by PID (proportional integral derivative) controller. The sintering cycle comprised of heating from ambient to 1500°C over a period of 60 hours and cooling to ambient over another period of 60 hours.

In the experimental set-up, the crucible was covered with a steel lid. The off gas pipe extended through the steel lid. A gasket, cut from a high alumina thermal blanket (1400°C grade) was placed between the crucible and the lid. Since the steel lid was held in position by its own weight, and could be lifted by pressure inside the crucible (the entire lid acted as an pressure relieve damper) the crucible arrangement could not be made gas tight. A positive pressure was therefore maintained in the crucible to prevent air from leaking into the crucible. This was done by purging the crucible with argon.

The feed system of the furnace consisted of a feed chute, onto which a removable glass lid was fastened with clamps. A rubber packing ensured a gas-tight seal between the glass lid and the chute. The chute extended through the crucible lid, into the crucible.

A 4 mm hole through the crucible lid enabled access of thermocouples to the inside of the crucible, for measuring the temperature profile of the solids bed.

The cavity between the removable crucible and the furnace refractories was filled with an alumina fibre thermal blanket. This improved thermal insulation of the crucible and also served to hold the thermocouples in position.

3.4.1.2 Gas system

The crucible assembly was continuously purged with 99.999% pure Argon. A schematic diagram of the gas preparation and control system is shown in ***Figure 43***. The respective gas lines, their purification trains, connecting gas-lines and stopcocks are indicated.

A ball valve was used to set the flow rate of the purge gas. The argon passed through a hydrosorb cartridge (from Messer Griesheim) to remove traces of moisture. According to specifications the final purity of the gas was < 0.5 ppm H_2O.

To avoid oxidation of the sample (and product gas from the sample) the oxygen potential of the purge gas was regulated. This was done by passing the argon through oxisorb-W (also from Messer Griesheim), which comprises activated chromium trioxide that absorbs traces of oxygen in the gas. According to specifications, the oxygen content of the gas is lowered to below 10ppb (which corresponds to an oxygen potential below 10^{-8} atm). Changes in colour indicated when the cartridges needed replacement.

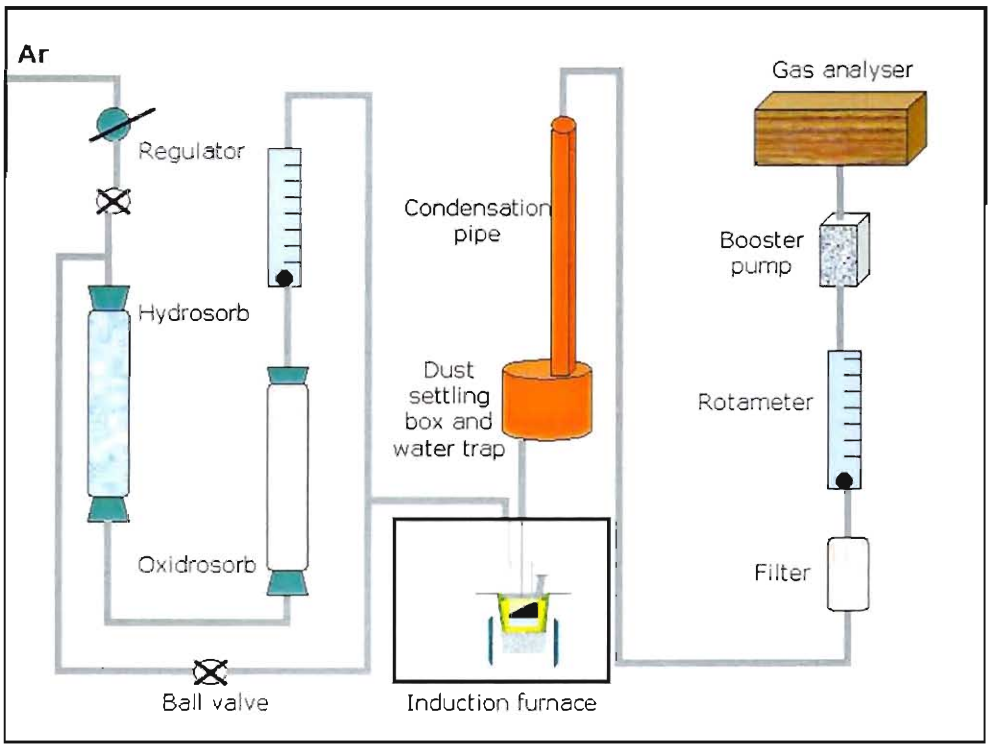

Figure 43: *Schematic illustration of the gas system configuration.*

The flow rate of the Argon was measured with a calibrated rotameter from Fisher Porter (model 10P6132NA). Calibration of flow meters is discussed in ***Appendix F.3***. From the rotameter, the gas line split into two gas supply lines, both leading directly to the crucible lid, for flushing. (Two supply lines were used for the argon in an attempt to induce mixing of the purge gas with the CO and CO_2 that evolves from the solids bed.) Purge gas entered the crucible, through two copper tubes that extended through the crucible lid. Off-gas exited the furnace through a steel tube, which also passed through the lid.

Since the gas analyser needed a gas flow rate of 6 l/min to operate accurately, at least 6 litres of gas had to be either produced inside, or blown into, the crucible. To avoid air from entering the crucible, the crucible was operated with a slight positive pressure. For this, the flow rate of argon into the crucible, was maintained at 6 l/min. The product gas from the reactions in the crucible then resulted in a positive pressure inside the crucible.

The off gas from the crucible passed through a dust-settling box of about 5 dm^3, made from mild steel. From the box, the gas passed through a steel cooling pipe of 25 mm diameter and 1 m long. This was intended to allow water vapour to condense and drip into the dust-settling box. The gas then passed through a Balston (model 9556-1/4) filter, with replaceable filter elements. These filter elements were replaced after each test.

The gas was passed through a calibrated rotameter, from where it went through a booster pump, to the gas analyser. A Prima 600 mass spectrometer was used for analysing of the gas.

3.4.2 Experimental procedure.

3.4.2.1 Raw material preparation

The ore, coal and fluxes used during this investigation were similar to those used for the reference sample for the TGA tests (the first phase of the investigation).

Dolomite and limestone samples were compiled according to the size distributions in ***Table A 2*** in ***Appendix A.3*** To avoid complications associated with the calcinations reactions, calcinated dolomite (doloma) and calcinated limestone (lime) were used. For calcination, the dolomite and limestone were placed in alumina crucibles and exposed to 1000°C for a period of 16 hours (overnight) in a muffle furnace.

Since devolatilization is expected to occur in the upper part of the solids bed, coal char was used in the mixture. The coal was charred at 1000°C. This was done by heating 7 kg batches of coal, at such a rate that 1% mass loss occurred every 10 minutes. The coal was charred until no further mass loss occurred. Charring was done in a nitrogen atmosphere. After cooling, the char was screened and samples were compiled so that the size distribution of each sample matched the size distribution of the coal in ***Table A 2*** in ***Appendix A.3.***

The ore samples were all synthetically compiled to match the size distribution of ore in ***Table A 2*** in ***Appendix A.3***. Three series of ore samples were prepared for testing.

The first sample series comprised of unreduced hematite ore.

The second series comprised of iron ore that was 30% pre-reduced at 800°C. For this a thermo gravimetric analyser (TGA), with a capacity of 7kg, at Kumba's technology department was used. A gas flow rate of 1 l/min was maintained to avoid fluidisation of the material, and a reducing gas comprising 50% CO and 50% CO_2.was used. (The temperature and gas composition was chosen so that the stable phase that formed would be wustite)[7]. The mass of the sample was registered continuously, as indication of the degree of reduction achieved.

The third series was 50% pre-reduced at 1000°C, using a gas containing CO and CO_2 in a 2:1 ratio, so that the stable phase that formed would be metallic iron[7].

The char content of the samples were chosen so that the material mixture comprised a $FC/O_{(ore)}$ ratio of 0.85. The selection of a $FC/O_{(ore)}$ ratio of 0.85 is discussed in more detail in ***Appendix F.1.***

3.4.2.2 Test Procedure

Prior to testing the mass of the removable crucible as well as the mass of the metal (to be melted as metal bath) recorded. The experimental configuration, as described previously, was assembled. A metal bath was established by melting two metal discs of 150mm diameter and weighing about 12kg in the removable crucible, in the induction furnace (see ***Figure 44***). The scrap metal used was cut from the same sheet of grade 300 WA steel, produced at Highveld Steel and Vanadium Corporation Ltd. The certified analysis of the steel is shown in ***Table 8***

Table 8: *Analyses of 300 WA sheet steel used to establish the metal bath.*

	C (%)	S (%)	P (%)	Si (%)	Mn (%)	Cr (%)	Vl (%)
300 WA	0.17	0.02	0.005	0.26	0.91	0.05	0.01

During heating of the discs, the temperatures of the discs and outer surface of the crucible (at the bottom and on the sidewall) were recorded. The power input to the furnace was regulated so that a heating rate of ±300°C/hour was achieved.

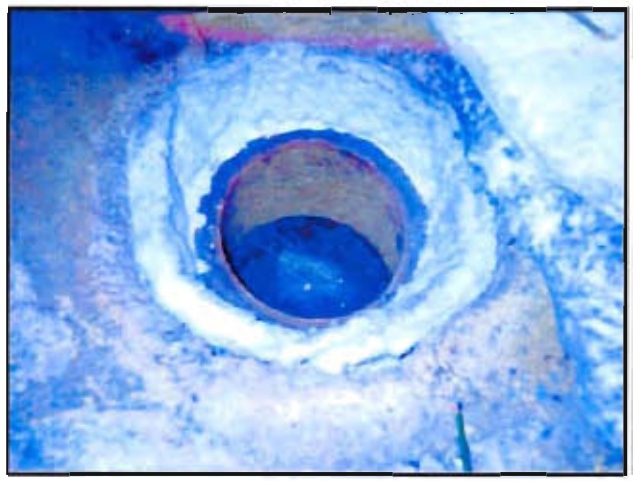

Figure 44: *Crucible with scrap for metal heel in induction furnace.*

Figure 45: *Establishing of a solids bed on top of the molten bath.*

As soon as the discs melted, and a liquid bath was established, ± 1kg of feed mixture was fed onto the liquid bath. This is shown in ***Figure 45***. The lid of the crucible was then positioned on top of the crucible, and the argon gas flow was established to flush the crucible, and establish a positive pressure inside the crucible. An additional ±500 g of feed mixture was fed into the crucible, to establish a solids bed (as a pile) with apex about 2 to 5 cm below the crucible lid. Batches of material mixture (±250g) were then fed onto the solids bed, at such intervals to maintain a constant bed height. Access to the crucible was obtained by a feed chute that extended through the crucible lid. During operation the chute was closed with a removable glass lid, which clamped onto the end flange of the chute. For gas tightness a rubber gasket was placed between the glass lid and the end flange of the chute. This configuration is shown in ***Figure 46.***

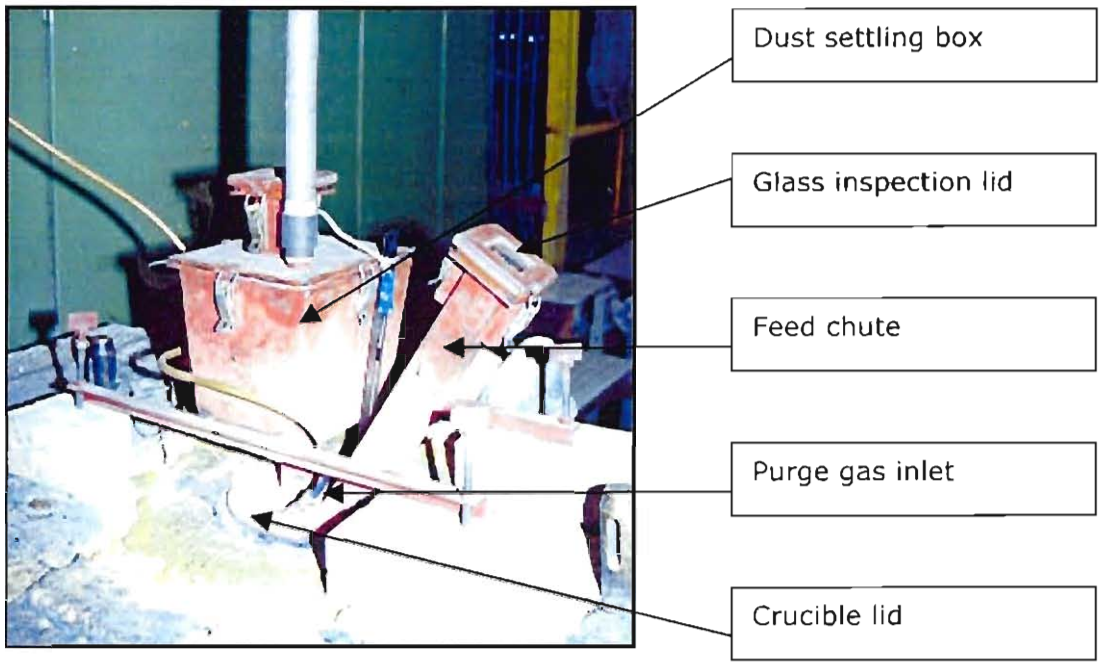

Figure 46: *Lid with feed chute on top of crucible.*

The production rate was estimated from the rate at which material had to be fed to the furnace to maintain constant heap heights, as well as from gas analyses.

A multi-channel Prima 600S gas analyser was used to analyse the off gas. Off gas from the crucible (comprising of product gas and purge gas) was pumped to a gas analyser at a rate of 6 l/min. This is the minimum gas flow rate specified for the gas analyser. Analyses were performed at approximately two-minute intervals, depending on the amount of channels in use during an experiment.

Since the rate at which argon was blown into the "freeboard" of the crucible was known, the rate at which CO and CO_2 entered the "freeboard" of the crucible was calculated from the off gas analyses. (The CO to argon flow ratio in the off-gas is directly shown by the off-gas analysis, when perfect mixing is achieved in the "freeboard" of the crucible.) The rate at which CO and CO_2 leaves the crucible translates to the rate at which oxygen is removed from the crucible and therefore gives the rate of reduction (and metal production) in the crucible

Excess process gas that escaped from the system, were extracted through the roof extractor fans. For safety reasons the CO content of the furnace surroundings were continuously monitored, using a Dräger CO monitor.

The power input to the furnace was manually regulated in an attempt to achieve the desired production rate. Although mass and energy balance calculations showed that approximately 4 kW power input was needed to drive the reduction and melting reactions, about 40 kW power input was needed to prevent solidification of the bath. Accordingly, an estimated 90% of the power input was used to overcome heat losses. The amount of heat losses however varied from one experiment to the next, thereby complicating control of the electrical power input for the process. The capacitor arrangement of the furnace also had to be changed intermittently, to ensure operation with a phase angle close to zero. (A zero degrees phase angle translates to a power factor of one, which indicates optimum utilisation of power).

The temperature on the outer surface of the crucible was measured continuously during each test. This was done to avoid overheating of the metal bath.

Once at least 3 kg of material was fed to the furnace, the temperature profile of the solids bed was measured. This means that the temperature profile was only measured once the furnace was operated for a period longer than the residence time of material in the solids bed (to achieve steady state operation in the furnace). The temperature profile is the variation of temperature with vertical position in the bed. During initial tests, chromel(Ni-Cr)/alumel(Ni-Al) (or type K) thermocouples were used, but during the last series of test, Pt/Pt10%Rh (or type S) thermocouples were used. The reference height for measurements was the height of the crucible lid. The profile was measured by pushing a thermocouple vertically down, (through a 4 mm hole in the crucible lid) into the bed. The thermocouple temperature and the distance by which the thermocouple was lowered into the bed were recorded simultaneously. The thermocouple was lowered 5 mm at a time, and held in position until the measured temperature approached a constant value.

The height of the metal bath was measured by inserting a 3 mm mild steel rod 300 mm deep into the crucible, through the hole that was used for measuring the temperature profile. Upon extrusion of the rod, the height of the metal bath (relative to the height of the lid) could be seen. This is similar to the "dip rod" method used

to determine the bath level in pilot plant furnaces. Note further that the temperature profile was also measured relative to the height of the lid. With these measurements the temperature profile of the solids bed was expressed relative to the height of the bottom of the solids bed.

After the temperature profile of the heap was measured, the temperature of the metal bath was also measured. For this a Pt/Pt10%Rh (or type S) thermocouple, shielded in a Metamic 829 sheath was used. These types of sheaths comprise 70 % molybdenum and 30 % alumina, and are normally used in vacuum melting furnaces.

At the end of the experiment, the crucible was lifted from the induction furnace and left to cool to ambient temperature, as shown in ***Figure 47***. A custom made, pliers-like, tool was used for lifting and transporting of the hot crucible.

Figure 47: *Crucible removed from the furnace for cooling.*

After cooling, the mass of the crucible with its content was weighed. The loose material in the crucible was poured out of the crucible, and the material remaining in the crucible was impregnated with cold-setting Araldite M Resin containing 20% Araldite HY 956 hardener. Once solidified, the refractory was removed from the sample (with a hammer and chisel) and the sample was cut in vertical slices, to reveal a picture of the bottom of the solids bed. Some of the samples were polished to a mirror-like finish. Final polishing was done with 3µm diamond paste. Typical images obtained are shown in ***Appendix F.***

3.4.2.3 Temperature control of the liquid bath

The method used to monitor changes in the bath temperature was based on a method used by Duca[54], who measured the refractory temperature to determine the extent of wear of the induction furnace refractories.

The furnace temperature was regulated manually according to the change in temperature of the outer surface of the removable crucible. Three Pt/Pt10%Rh (or type S) thermocouples were installed to measure the temperature on the outer surface of the crucible. Two of these were placed along the sides of the crucible, at the height of the metal bath, while the third was placed, in the centre, below the crucible. The thermocouples were made of 0.38 mm diameter thermocouple wire, which was certified to be accurate within one degree, by the suppliers, Johnson & Matthey.

A combination of an "Adams 4017 data acquisition module" and an "Adams 4520 RS 232 to RS 422 / RS 485 converter" was used to convert the milli-volt output, of the thermocouple to a RS 232 digital signal. This signal was recorded with custom made software, and exported to an excel spreadsheet. The data acquisition and recording equipment is shown in ***Figure 48***.

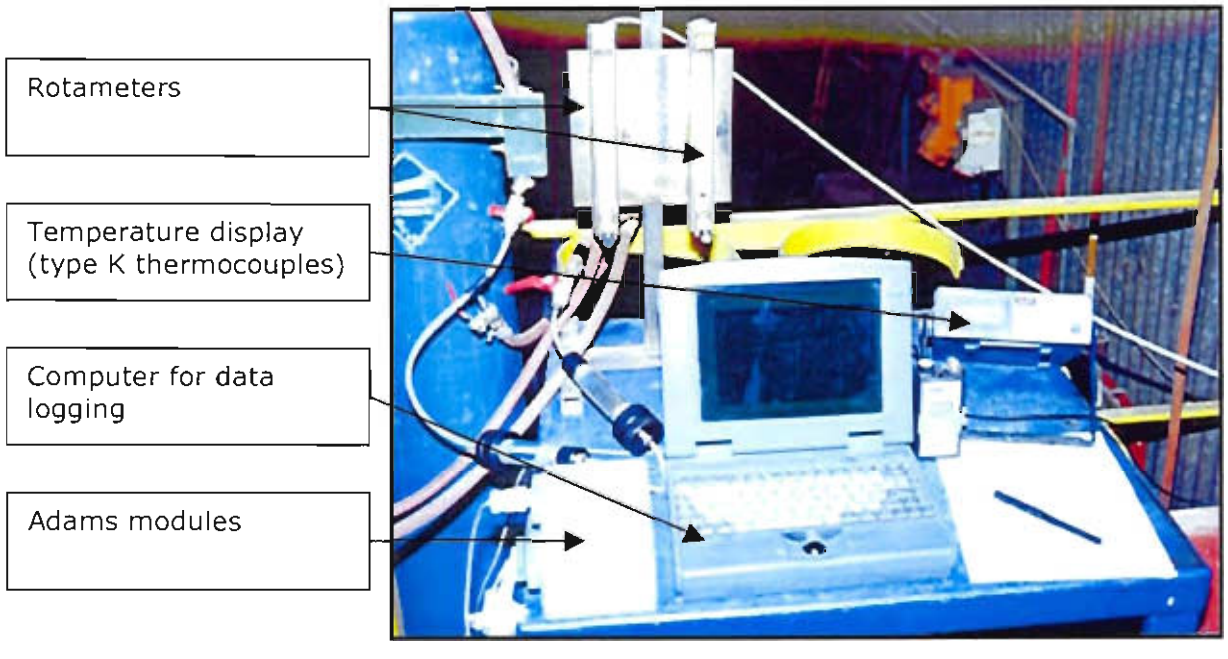

Figure 48: *The data acquisition and recording equipment*

Variations of the temperatures of the outer surface of the crucible, reflected variations of the bath temperature. This means that when the temperature of the bath increased, the recorded temperature also increased, and vice versa. At the start of each test, the bath temperature was directly measured using a sleeved Pt/Pt10%Rh (or type S) thermocouple. The directly measured bath temperature was used as a reference for the temperature measurements on the outer surface of the crucible.

3.4.3 Results and discussion

3.4.3.1 Bridging of solids bed

From time to time, the solids bed stuck to the walls of the crucible, thereby forming a "bridge" in the crucible. This resulted in heat from the metal bath being transferred by radiation to the bottom of the solids bed. The model was accordingly changed to simulate this condition. (The gap that formed between the solids bed and liquid bath is seen in the visual sections of the solids bed, shown in ***Appendix F***)

Bridging of the solids bed also resulted in poor control regarding the production rate. When the energy input to the furnace was increased, the bath temperature increased, which resulted in an increase in production rate. Changing the production rate, while maintaining a constant bath temperature was therefore problematic. The approach with the experiment therefore changed from regulating the production rate to measuring the production rate, in order to obtain data that could be compared to model predictions.

3.4.3.2 Production rates

From the gas analyses (presented in ***Appendix F.5***), the production rates were calculated. Results are presented in ***Figure 49***, ***Figure 50*** and ***Figure 51***.

Sudden increases in the production rate were recorded from time to time. This was due to unsteady operations when too much energy was supplied to the bath, resulting in intermitted moments during which high production rates were observed. In order to achieve stable (near steady state)conditions, production rates in the region of 20 kg Fe/m^2/h had to be maintained

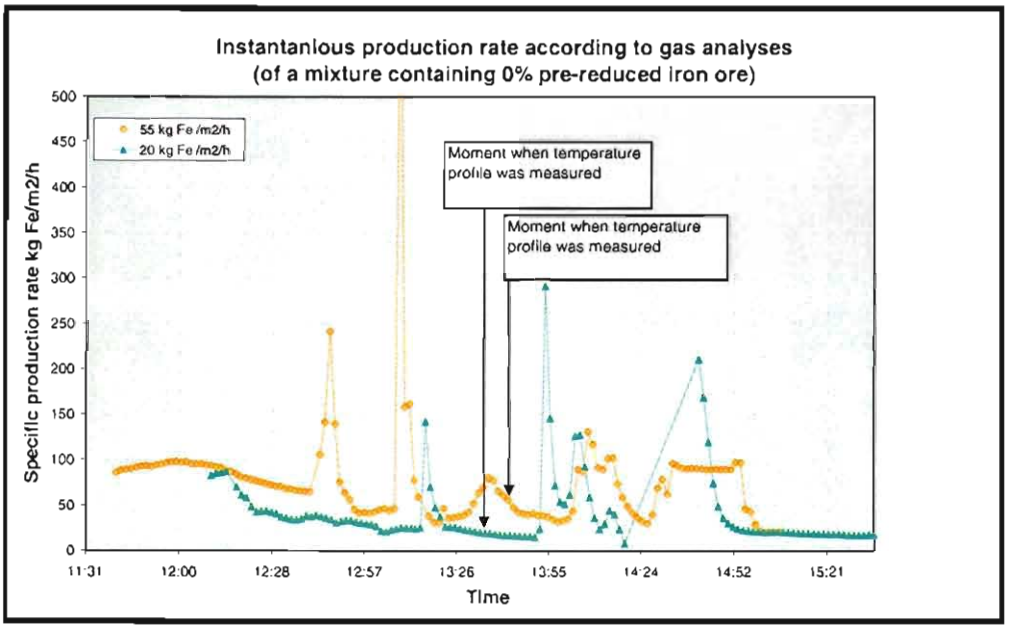

Figure 49: *Specific production rate calculated from gas analyses for tests done with material containing 0% pre-reduced iron ore.*

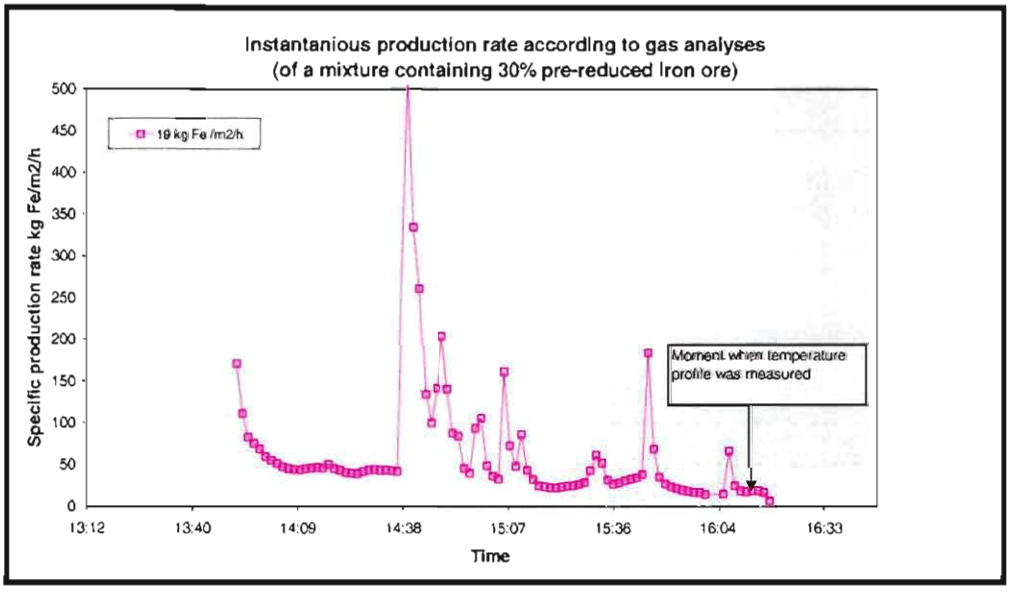

Figure 50: *Specific production rate calculated from gas analyses for tests done with material containing 30% pre-reduced iron ore.*

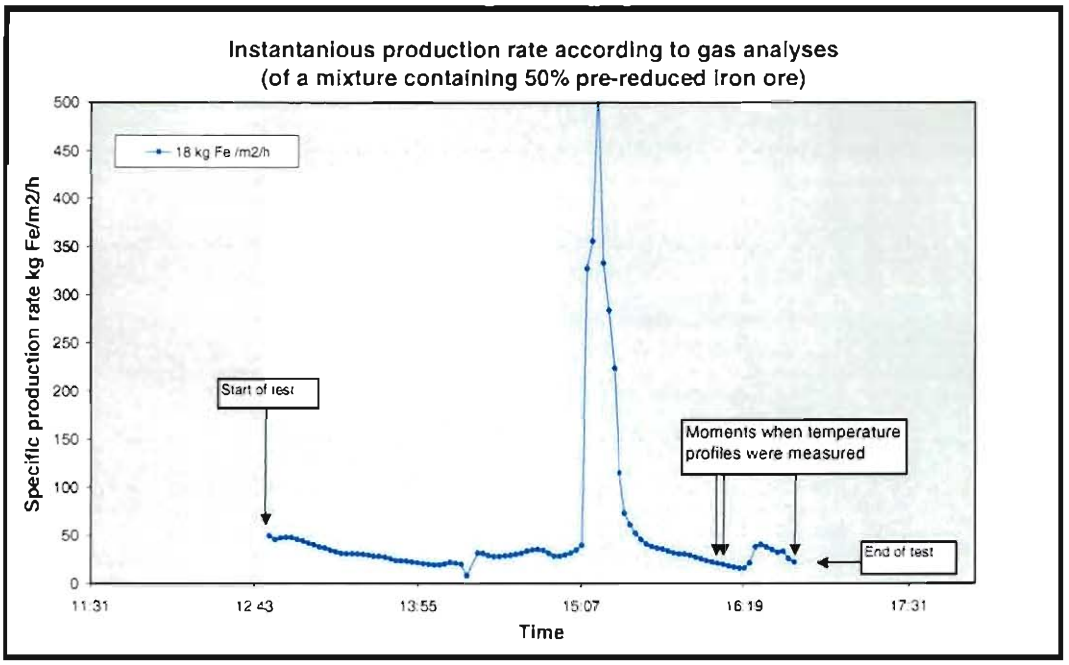

Figure 51: *Specific production rate calculated from gas analyses for tests done with material containing 50% pre-reduced iron ore.*

Figure 49, ***Figure 50*** and ***Figure 51*** show that sudden increases in the production rate from time to time. These increases were mostly observed as slag reactions occurring when part of the solids bed collapsed into the liquid bath.

Times when temperature profiles were measured are also shown in the figures above. From the figures, the actual production rate at the time of the measurement can be seen. These production rates were used as inputs to the model for predicting of the theoretical temperature profiles of the solids bed.

3.4.3.3 Model predictions vs experimental measurements

Figure 52 shows that experimental measurements were repeatable.

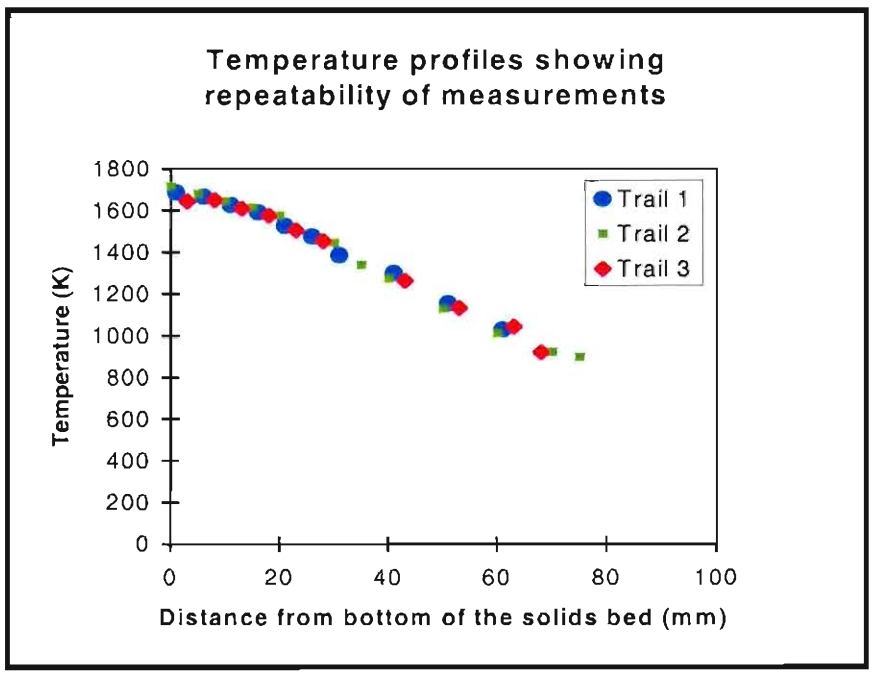

Figure 52: *Experimentally measured temperature profiles of the solids bed, showing repeatability of results. These tests were done with material containing 50% pre-reduced iron ore at a production rate of 18 kg Fe/m^2/h.*

Figure 52 shows that good repeatability of temperature profile measurements were achieved.

Measured temperature profiles are shown in ***Figure 53*** to ***Figure 56***. These figures also show the model simulations of the respective tests. Each test was individually modelled. The production rate and bath temperature that was measured during the test were used as inputs to the model. The model predicted the temperature profile as well as the reduction profile through the solids bed for the specific test.

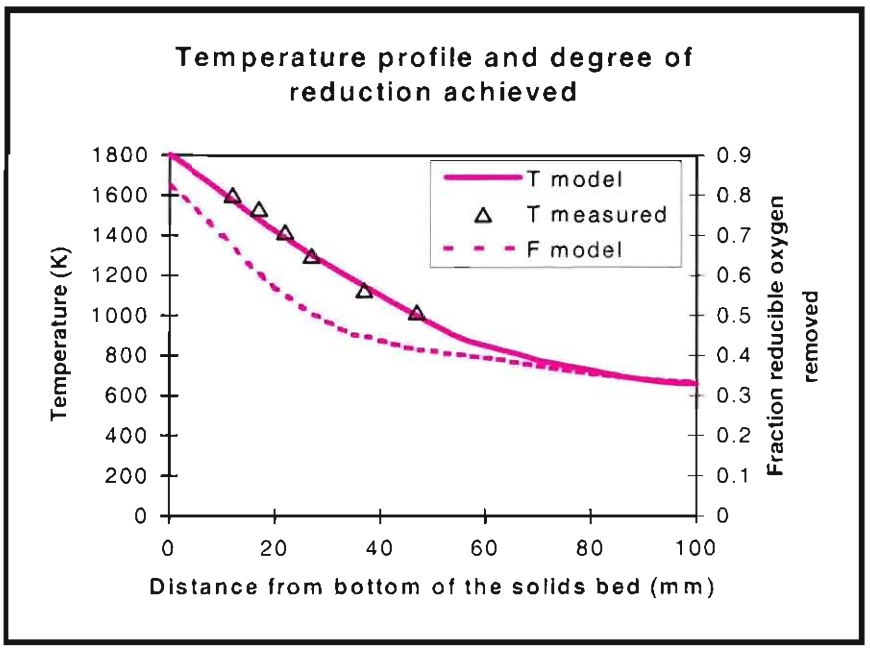

Figure 53: *Comparison between model prediction and experimentally measured temperature profiles of solids bed for a tests done with material containing 30% pre-reduced iron ore at a production rate of 19 kg Fe/m^2/h.*

Figure 53 shows a good correlation between the temperature profile predicted by the model and the actual measured profile. For this test the model predicted that 83% reduction would have been achieved at a production rate of 19 kg Fe/m2/h.

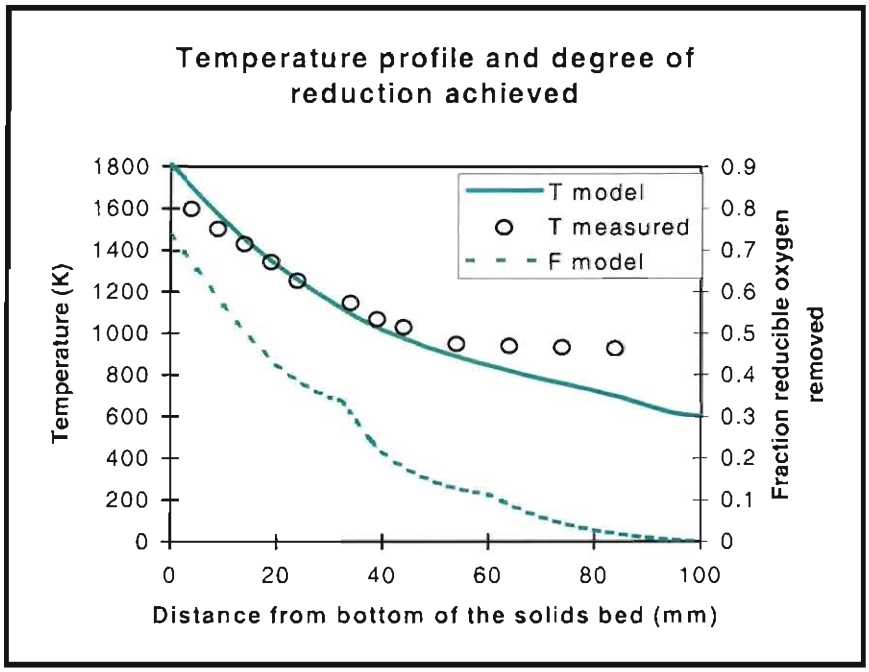

Figure 54: *Comparison between model prediction and experimentally measured temperature profiles of solids bed for a tests done with material containing 0% pre-reduced iron ore at a production rate of 20 kg Fe/m^2/h.*

Figure 54 shows a fair correlation between the temperature profile predicted by the model and the actual measured temperature profile.

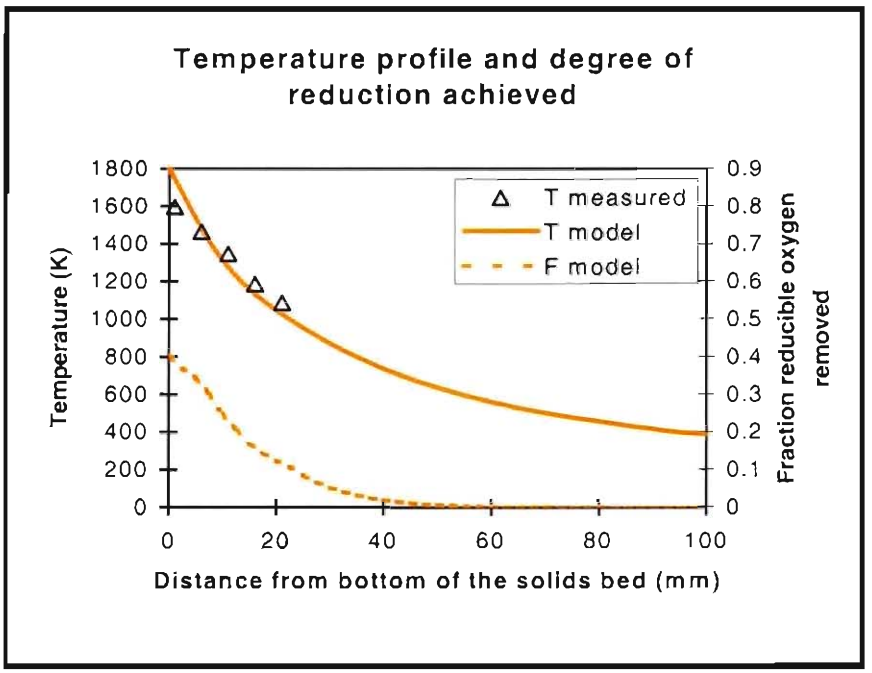

Figure 55: *Comparison between model prediction and experimentally measured temperature profiles of solids bed for a tests done with material containing 0% pre-reduced iron ore at a production rate of 55 kg Fe/m^2/h.*

Figure 55 shows the comparison between the temperature profile predicted by the model and the temperature profile that was measured during the test. The slope of the measured profile is slightly more horizontal than predicted by the model. This is ascribed to movement of the solids bed, due to large amounts of gas being generated below the bed.

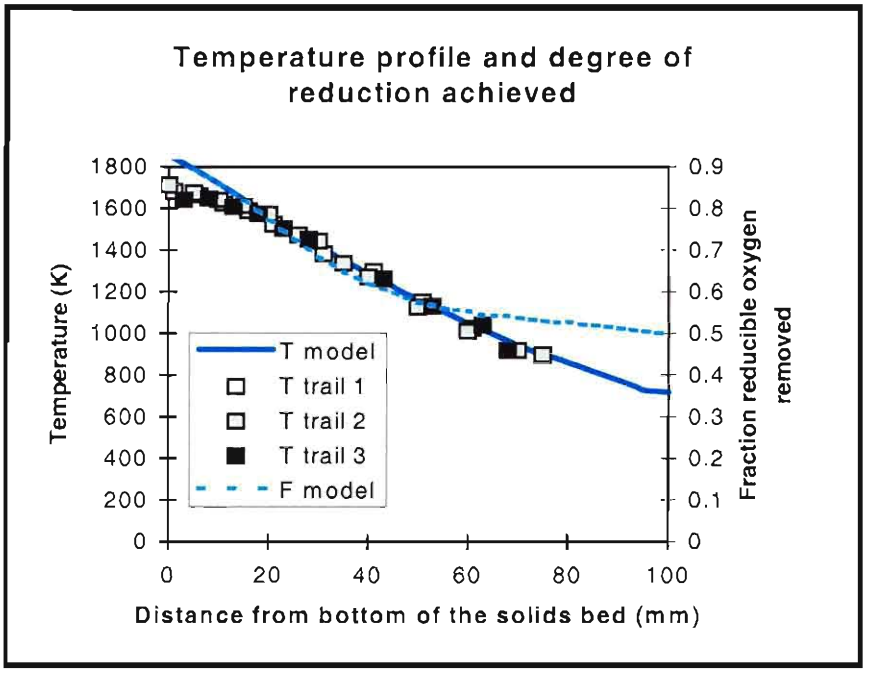

Figure 56: *Comparison between model I prediction and experimentally measured temperature profiles of solids bed for a tests done with material containing 50% pre-reduced iron ore at a production rate of 18 kg Fe/m^2/h.*

Figure 56 shows a good correlation between the temperature profile predicted by the model and the measured temperature profile. The model predicted 92% reduction achieved at the bottom of the solids bed.

3.4.4 Prediction of extent of reduction achieved.

From the previous paragraph it is evident that model predictions were similar to experimental measurements. The model was therefore used to predict the extent of reduction achieved at the bottom of the solids bed, for various degrees of reduction achieved in the upper part of the solids bed. This was done for different production rates, as shown in ***Figure 57***. A "dead zone" temperature of 700°C was assumed for these calculations.

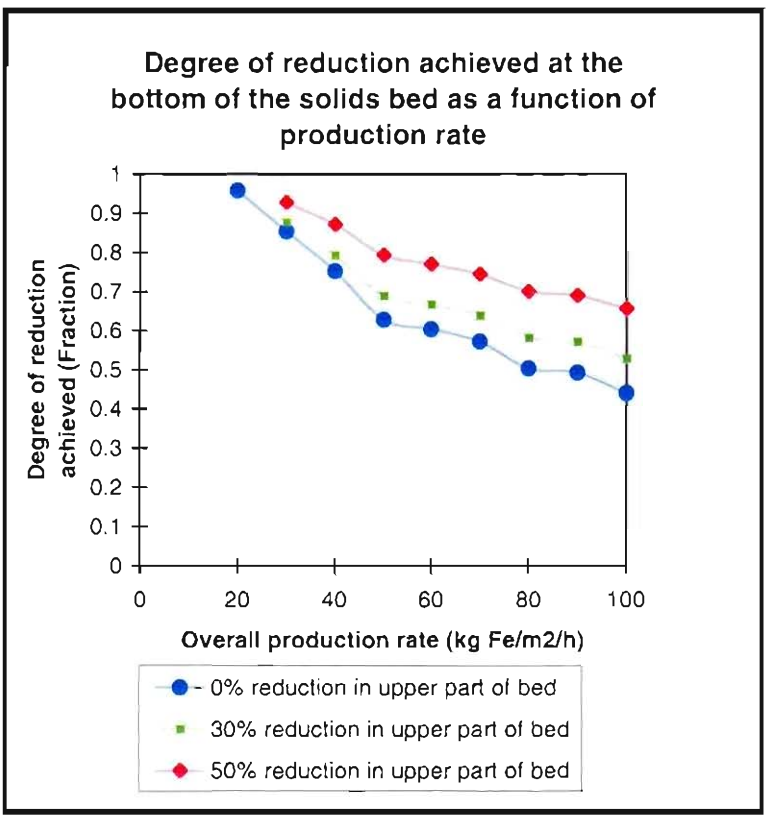

Figure 57: *Model prediction of reduction achieved at the bottom of the solids bed, for various degrees of reduction achieved in the upper part of the solids bed.*

Figure 58 shows the information of ***Figure 57*** fitted onto ***Figure 29.*** ***Figure 58*** therefore compares the degree of reduction achieved in the top part of the solids bed with the total amount of reduction achieved at the bottom of the solids heap, as a function of production rate.

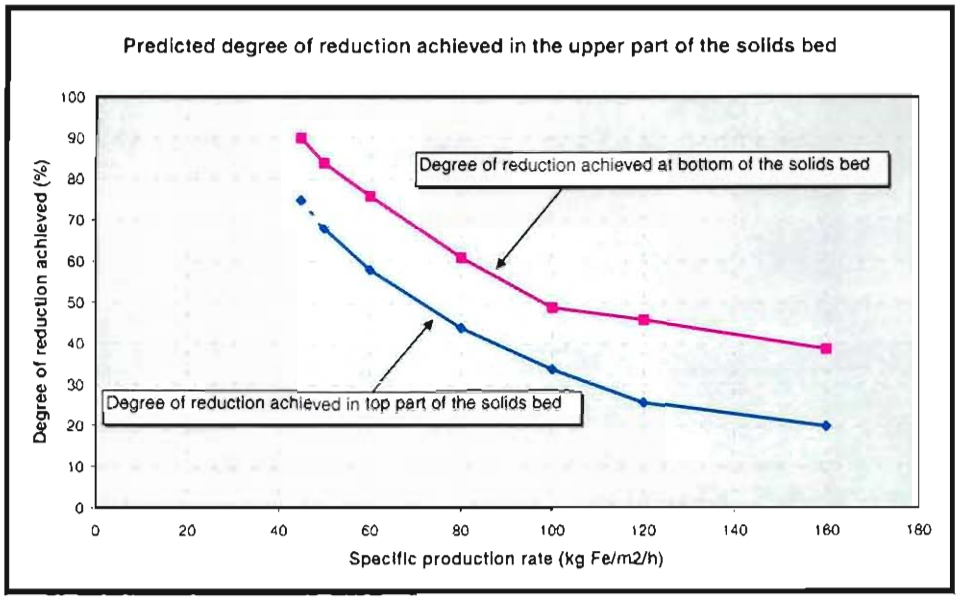

Figure 58: *Anticipated degree of reduction achieved in the upper part of the solids bed (when feeding 40 mm thick batches and with a freeboard temperature of 1500C) as well as the amount of reduction achieved at the bottom of the solids bed.*

At the Ifcon pilot plant facility steel was produced at a rate of 100 kg $Fe/m^2/h$[10,13,16,17]. ***Figure 58*** shows that the anticipated amount of reduction achieved in the upper part of the solids bed was 34 % for a production rate of 100 kg $Fe/m^2/h$, and 49% at the bottom of the solids bed. At a production rate of 100 kg $Fe/m^2/h$, the ore is therefore not fully reduced when reaching the bottom of the solids bed. This implies that final reduction in the Ifcon process did not occur as solid-state reduction. Slag metal reactions therefore must be considered during operation of the Ifcon process.

Since the aim is to achieve 90% reduction in the Ifcon process, the maximum degree of reduction that will be achieved at the top of the solids bed (for these specific conditions) is about 75% at a production rate of 45 kg/m2/h. This is an extrapolated value.

3.5 Conclusions:

In response to technology drivers in the iron and steel industry, various direct reduction- and direct smelting processes were developed. One of these is the Ifcon process, which produces liquid crude steel directly from raw materials.

The reduction rate is significantly increased when the exposure temperature is increased. The presence of volatile matter (in the coal) also increases the rate at which reduction is achieved.

When selecting the optimum feed materials for the process, **ore and coal** should not only be selected according to chemical composition but also according to CO reducibility and CO_2 reactivity. The effect of these parameters on the overall reduction rate is however limited.

The degree of reduction achieved at the bottom of the solids bed (with the current material mixture) depends on the following factors:

- the rate constant of the reduction reaction.
- The thermal conductivity of the solids bed.
- the temperature of the metal bath.
- the production rate .
- the degree of reduction achieved in the upper part of the solids bed.

At a production rate of 100 kg Fe/m^2/h the ore is not fully reduced at the bottom of the solids bed. At this production rate solid-liquid-state reduction accounts for approximately 41% of the total reduction achieved, assuming a final degree of reduction of 90%.

The above only gives insight to the extent to which reactions occur in the solids bed of the process. In order to comment on the final degree of reduction achieved (and production rate), the rate and extent to which solid-liquid-state reduction occurs must be taken into account.

4 References

[1] Y. Gordon, Modern development and future of direct reduction and direct smelting technologies, Hatch: Woodmead presentation, South Africa, 2002.

[2] R. J. Fruehan, C. L. Nassaralla, Alternative oxygen steelmaking processes, Steelmaking and refining, The AISE Steel foundation, Pittsburgh, U.S.A, 1998.

[3] R.J. Fruehan, Future iron and steelmaking in the USA, Scandinavian Journal of Metallurgy, vol 28, 1999, pp. 77-85.

[4] B. Sarma, R. J. Fruehan, A review of coal-based direct iron making processes, ICSTI/Ironmaking conference proceedings, Praxair Inc, Tarrytown, NY, 1998, pp 1537-1548.

[5] R. J. Fruehan, Iron bath smelting-Current status and understanding, Elliot symposium proceedings, pp. 1-10, 1990.

[6] C.P. Manning, R. J. Fruehan, Emerging technologies for iron and steelmaking, http://www.tms.org/pubs/journals/JOM/0110/Manning-0110.html, 2001

[7] R.L. Stephenson, Direct reduced iron, The iron & steel society of AIME, Warrendale, PA, U.S.A. , 1980, pp.9-34

[8] Batelle Europe, Follow-up, Zurich, Switzerland, 1996.

[9] PCT Patent: "Steelmaking process", South Africa, patent number 94/4233, 1994

[10] P. C. Pistorius, An overview of the current understanding of the Ifcon process, University of Pretoria, Pretoria, South Africa, 1996 (not published).

[11] L. Gunnewick, CFD modelling of Ifcon furnace freeboard combustion, Hatch, Mississauga, Ontario, Canada, 2000 (internal report).

[12] P. C. Pistorius, An assessment of electrical energy consumption in the Ifcon, University of Pretoria, Pretoria, South Africa, 1996 (not published).

[13] L. Lourens, Ifcon Demo plant technical specification, Iscor Ltd, Pretoria, South Africa, 2001. (internal report)

[14] O. Knacke, O. Kubaschewski, K. Hesselmann, Thermochemical properties of inorganic substances, Springer-Verlag, Heidelberg, Germany, 1991.

[15] P. C. Pistorius, 1-D Model report, University of Pretoria, Pretoria, South Africa, 1996 (internal report).

[16] C. Janse van Rensburg, Integrated process model specification, Hatch, Woodmead, 2001 (internal report).

[17] L. Lourens, Report on the sixth pilot plant campaigne, Iscor Ltd, Pretoria, South Africa, 1999 (internal report).

[18] J.A. Groenewald, Report on the design, building, commissioning and first campaign of the Ifcon pilot plant, Iscor Ltd: internal report, 1993.

[19] T. Coetsee, Ifcon reduction I simulation experiments, 2000, (Internal report).

[20] Personal communication with R du Plessis, WEDO CC (Coal and Coke technology), 2001.

[21] J. F. Stubington, Release of volatiles from large coal particles in a hot fluidised bed. Fuel, Vol 63, 1984, pp. 1013-1019.

[22] P. Arend, K. H. van Heek, Comparative investigations of coal pyrolysis under inert gas and H_2 at low and high heating rates and pressure up to 10 Mpa. Fuel, Vol 60, September, pp 779-787.

[23] B. H. Huang, W. K. Lu, Kinetics and mechanisms of reactions in iron ore / coal composites. ISIJ International, Vol 33, No 10, 1993, pp 1055-1061.

[24] C. Bryk, W. K. Lu, Reduction phenomena in composites of iron ore concentrates and coals. Ironmaking and Steelmaking, Vol 13, No 2, 1986, pp 70-75,

[25] E.T. Turkdougan, J.V. Vinters, Gaseous reduction of iron oxides: Part I. Reduction of hematite in hydrogen, Metallurgical Transactions B, vol 2, 1971, pp 3175-3188.

[26] E.T. Turkdogan, R.G. Olsson, J.V. Vinters, Gaseous reduction of iron oxides: Part II. Pore characteristics of iron reduced from hematite in hydrogen, Metallurgical Transactions B, vol 2, 1971, pp 3189-3196.

[27] A.K. Biswas, Principles of blast furnace ironmaking, Cootha Publishing House, Brisbane, Australia, 1981, pp 26-48.

[28] P. C. Pistorius, J. M. A. Geldenhuis, Short Course: Pyrometallurgy, University of Pretoria, South Africa, 2002.

[29] J. P. Holman, Heat Transfer, S I Metric Edition, McGraw-Hill Book Co, Singapore, 1989.

[30] T. Coetsee, P.C. Pistorius, E.E. de Villiers, Rate determining steps for reduction of magnetite-coal pellets, Minerals Engineering, vol 15, 2002, pp 919-929.

[31] N. Shivaramakrishna, S. B. Sakar, K. K. Prasad, The role of internal coal in the reduction of composite pellets. SEAISI Quarterly, April 1996, pp 82-95.

[32] R. J. Fruehan, The rate of reduction of iron oxide by carbon. Metallurgical Transactions B, Vol 8, June 1977, pp 279-286.

[33] E.T. Turkdogan, J.V. Vinters, Kinetics of oxidation of graphite and charcoal in carbon dioxide. Carbon, vol 7, 1969, pp 101-117.

[34] S. K. Dutta, A. Gosh, R.J. Belt, Study of non-isothermal reduction of iron ore-coal/char composite pellet. Metallurgical Transactions B, 25B(1), 1994, pp 15-26.

[35] R.J. Tyler, I.W. Smith, Reactivity of petroleum coke in carbon dioxide between 1030 and 1180 K. Fuel, vol 54, 1975, pp 99 – 104.

[36] N.S. Srinivas, A.K. Lahhiri, Studies on the reduction of hematite by carbon. Metallurgical Transactions B, vol 8B, 1977, pp 175-178.

[37] K.L. Trushenski, W.O. Philbrook, Non-topochemical reduction of iron oxides. Metallurgical Transactions B, vol 5, 1974, pp 1149-1158.

[38] S. Sun, W. K. Lu, Building of a Mathematical modelfor the reduction of iron ore in ore/coal composites. ISIJ International, vol 39(2), 1999, pp 130-138.

[39] S. Sun, K. W. Lu, A study of kinetics and mechanisms of iron ore reduction in ore / coal composites. 1996 Steelmaking conference proceedings, 1996, pp 641-647.

[40] S. Sun, W. K. Lu, A non-isothermal mathematical model for reduction of iron ore in ore/coal composites, 10'th RTD proceedings, 1992, pp 403-408.

[41] Q. Wang, Z. Yang, J. Tian, W. Li, J. Sun, Reduction kinetics of iron ore-coal pellets during fast heating, Ironmaking and steelmaking, Vol 25, No 6, 1997, pp 443-447.

[42] Q. Wang, Z. Yang, J. Tian, W. Li, J. Sun, Mechanisms of reduction in iron ore-coal composite pellets. Ironmaking and Steelmaking, Vol 24, No 6, 1997, pp. 457-460.

[43] S. K. Dutta, A. Gosh, A new method for measurement of the degree of reduction in composite pellets of iron ore with carbonaceous matter, ISIJ International, vol 33, No 7, 1993, pp 735-739

[44] S. K. Dey, B. Jana, A Basumallick, Kinetics and reduction characteristicsof hematite-non coking coal mixed pellets under nitrogen gas atmosphere.ISIJ International, Vol 33, No 7, 1993, pp735-739.

[45] T. Sarma, Reduction of iron ore fineswith coal fines. Ironmaking and Steelmaking, Vol 20 No 5, 1993, pp 362-365.

[46] Specification: sample probe, ISO/CD13909-3, 1994

[47] D.R. Lide, Handbook of Chemistry and Physics, 80'th edition, CRC Press, 1999, pp 12-200.

[48] CO reducibility results and CO_2 reactivity results communicated from Iscor ITEC. 1999.

[49] T. Coetsee, P. C. Pistorius, Calculation of gas transfer coefficients (not published)

[50] G. Nabi, W. K. Lu, Reduction kinetics of hematite to magnetite in Hydrogen –water vapor mixtures, Transactions of the metallurgical society of AIME, volume 242, December 1968, pp 2471 -2477.

[51] P.C. Pistorius, T. Coetsee, M de Campos, Ore reducibility and char gasification experiments: IFCON, 2001 (internal report).

[52] T Akiyama, H Ohta, R Takahashi, Y Waseda & J Yagi: "Measurement and modeling of thermal conductivity for dense iron oxide and porous iron ore agglomerates in stepwise reduction." *ISIJ International*, vol. 32, 1992, pp 829-837.

[53] O Kubaschewski, CB Alcock & PJ Spencer: *Materials Thermochemistry*, 6th edition. Pergamon, Oxford, 1993.

[54] W. J. Duca, New method helps to determine when to shut down an inductor, Modern casting, July 1996, pp 27-29.

APPENDIX A

Experimental Aspects: TGA

Page no

A.1. Calibration of rotameters

Calibration of the rotameters, was done with a Bunsen tower. The technique is based on the movement of a frictionless piston by the gas entering a vessel and measuring the time needed to displace a certain volume as indicated by the piston. The Bunsen tower employs a soap bubble moving upwards through a graduated burette. The soap bubble is the frictionless piston, implying that the pressure difference across the bubble is negligible, and the burette is used to measure the volume. The time it takes a bubble to travel along a certain length of the burette (corresponding to a certain volume) is determined with a stop-watch and the flow rate is thus determined. The size of the burette influences the linear velocity of the bubble and therefore affects the accuracy of time measurement and ultimately the flow rate measurement. Two Bunsen towers with different sizes were used to measure different flow rates. For large flow rates a larger burette ($400cm^3$) was used, while a small burette ($50cm^3$) was used for low flow rates.

A.2. Determining of the constant heat zone of the work tube

The temperature profile of the work tube was measured prior to the experimental runs. The profile is simply the variation of temperature with vertical position in the tube and indicates where the hottest area (with constant temperature) is located. Measurements were done by replacing the scale, molybdenum wire and crucible arrangement with a thermocouple. The thermocouple was lowered approximately 5 cm at a time, and held in position for at least ten minutes, while recording the temperature on a recorder. This procedure was repeated until the bottom of the work tube was reached. The temperature profile is shown in

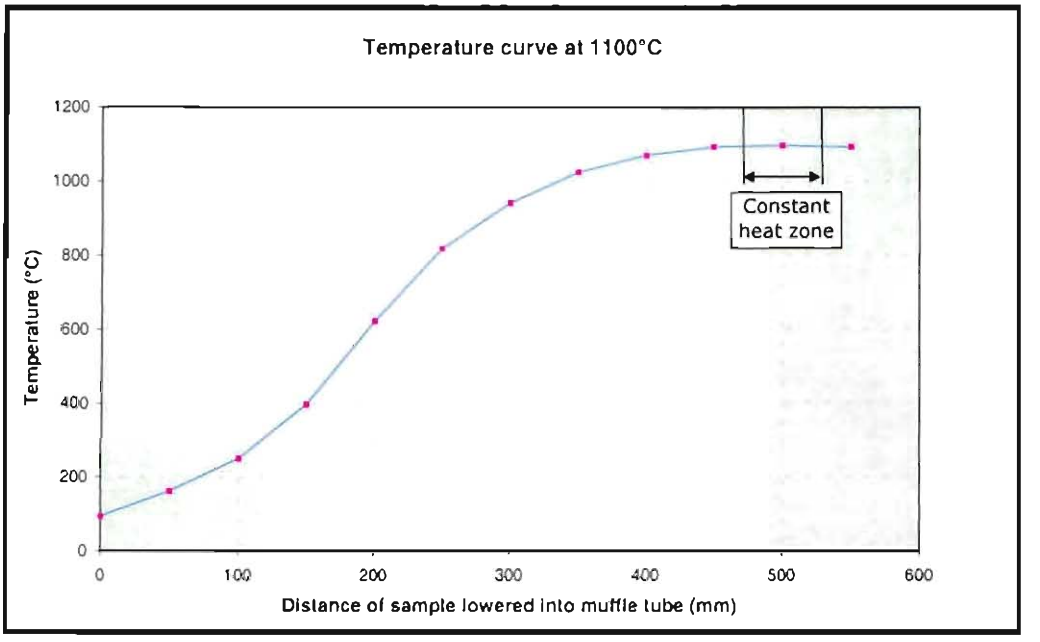

Figure A 1: *Temperature profile of the work tube that was used for thermo gravimetric analyses.*

A.3. Raw material preparation for TGA experiments

The feed materials for this investigation were similar to those used at the Ifcon pilot scale facility. The materials that were used are listed in ***Table A 1***.

Table A 1: *Feed materials used during this investigation.*

Feed Material	Ore
Ore	Iron ore fines (-10 mm) from Kumba's Sishen mine
	Iron ore fines (-10 mm) from Kumba's Thabazimbi mine
Coal	Duff coal from Eikeboom Collieries
	Duff coal from Leeuwpan Collieries
Dolomite	Fine dolomite from Mooiplaas dolomite mine
Limestone	Crushed sinter limestone from PPC Lime

All the materials were air dried for 24 hours. The coal was crushed, using a roller crusher. The gap of the crusher was set at 2 mm, and the material was fed slowly, to avoid choke feeding. Each batch of material was screened into distinct size fractions and each size fraction was weighed to obtain a size distribution for each batch of material. Note that only ore smaller than 6.3 mm, and coal, dolomite and limestone smaller than 2 mm were used. Oversize material was discarded. The screen analyses of the various feed materials are shown in ***Table A 2***.

Table A 2: *Size distributions that were used as standards for material make-up.*

	Mass percentage of material (%)			
Size fraction	**Ore**	**Coal**	**Dolomite**	**Limestone**
- 6300µm + 4750µm	31.12			
- 4750µm + 3350µm	20.62			
- 3350µm + 2800µm	7.50			
- 2800µm + 2000µm	12.07			
- 2000µm + 1400µm	7.75	43.49	13.77	49.73
- 1400µm + 850µm	6.74	23.65	32.08	12.62
- 850µm + 425µm	4.80	15.63	47.10	9.25
- 425µm + 212µm	2.05	17.23		5.88
- 212µm + 106µm	1.42		7.05	6.20
- 106µm	5.93			16.32
TOTAL (%)	**100.0**	**100.0**	**100.0**	**100.0**

These screen analyses were used as standard size distributions for all samples used during the experiments. This means that samples from each material stream was made up in such a way that the size distribution of a sample was similar to the distribution listed in ***Table A 2***. This ensured that the screen analyses of all the samples were similar. For example, the screen analyses of the Thabazimbi ore was modified to be similar to that of Sishen ore, and the screen analyses of the Leeuwpan coal was modified to be similar to that of Eikeboom coal.

Part of the coal was air dried for 24 hours, after which it was charred at 1000°C. The coal was charred until no further mass loss occurred. This was done by heating a 7 kg

batch of coal, at such a rate that 1% mass loss occurred every 10 minutes. Charring was done in a nitrogen atmosphere. After cooling, the char was screened and samples were compiled so that the size distribution of each sample matched the size distribution of the coal in ***Table A 2***.

A.4. Composition of raw materials

Two samples of each type of material were compiled for chemical analysis. The moisture content of the coal was determined by measuring the mass loss of the coal after air-drying the coal for 24 hours. The total carbon-, hydrogen-, oxygen- and nitrogen content of the coal was measured using a LECO analyser. The ash content of the coal and coal char was determined by combusting the coal (or char) with oxygen at 900°C.

Two ore samples, two dolomite samples and two limestone samples were pulverised, by milling each sample for 5 minutes in a pulverising mill. These samples as well as the ash were analysed using ICP (inductively coupled plasma) analyses. The chemical compositions of the ores and fluxes are shown in ***Table A 3*** while the moisture-, ash-, total carbon-, hydrogen-, oxygen- and nitrogen content of the coal and char are shown in ***Table A 4*** and ***Table A 5***. The chemical compositions of the ash from the coal and coal char are shown in ***Table A 6***.

Table A 3: *Average composition of ore and fluxes.*

Raw material	Units	Fe_2O_3	$CaCO_3$	$MgCO_3$	SiO_2	Al_2O_3	Total
Sishen ore fines	%	94.5	0.14	0.04	3.66	1.25	99.59
Thabazimbi ore fines	%	94.1	0.45	0.29	3.91	0.69	99.43
Dolomite	%	0.72	53.36	42.47	2.61	0.17	99.33
Limestone	%	0.21	95.49	2.18	1.13	0.17	99.17

Table A 4: *Ash and moisture content of coal and char.*

Raw material	Moisture (%)	Ash (%)
Eikeboom coal	1.6	12.5
Eikeboom char	0.3	15.7
Leeuwpan coal	1.3	14.8

Table A 5: *Total carbon-, hydrogen, oxygen, and nitrogen content of coal and char.*

Raw material	Units	C (%)	H (%)	O (%)	N (%)	Ash (%)	Total (%)
Eikeboom coal	%	72.9	3.97	8.36	1.88	12.5	99.6
Eikeboom char	%	82.1	0.33	0.37	1.10	15.7	99.6
Leeuwpan coal	%	71.6	3.58	7.58	1.80	14.8	99.3

Table A 6: *Ash composition of coal and char.*

Raw material	Units	Fe_2O_3	CaO	MgO	SiO_2	Al_2O_3	Total
Eikeboom coal	%	4.61	2.06	0.52	51.9	34.9	94.0
Eikeboom char	%	4.30	2.02	0.58	52.1	34.9	93.9
Leeuwpan coal	%	1.48	14.1	3.24	38.2	30.2	87.2

A.5. Analytical techniques

Ore-, lime-, dolomite-, ash-, and slag analyses were done by ICP (inductively coupled plasma) analysis. This method entails the melting of a known mass of the pulverised sample with sodium peroxide and carbonate as fluxes. The glass obtained from the melt is then dissolved in 20M hydrochloric acid. This solution is ionised in an argon plasma, and the intensity of the ionisation wavelengths are measured. Each element has one or more characteristic ionisation wavelengths and the measured intensities are recalculated to obtain the concentration of each element in the sample. The concentrations of the elements are expressed in terms of the most stable oxide (e.g. SiO_2) or simply as the concentration of the element in cases were the exact specie is not known (e.g. Fe which can be in the form of Fe_2O_3, Fe_3O_4, FeO_x or metallic Fe).

The forms of iron (i.e. Fe^0, Fe^{2+}, Fe^{3+}) were determined by wet chemical analyses. This method entails the dissolution of metallic iron (from a pulverised sample) with 10M iron

chloride ($FeCl_3$). The $FeCl_3$ oxidises all the metal iron (Fe^0) to Fe^{2+} ions in solution. The solution is then filtered. The Fe^{2+} content, of the filtrated solution, is determined by titration of the solution with potassium dichromate ($K_2Cr_2O_7$), which oxidises the Fe^{2+} to Fe^{3+}, while the Cr^{6+} from the chromate is reduced to Cr^{3+}. The titration yields the metallic iron content of the sample. The filtration residue, which contains all the Fe^{2+} (originally present as FeO), is dissolved in hydrochloric acid. The Fe^{2+} content of this solution is also determined by titration with potassium dichromate ($K_2Cr_2O_7$), which yields the Fe^{2+} content of the sample. Since the total iron content of the sample is known from ICP analysis, the Fe^{3+} content of the sample is calculated as the difference between the total iron content, the Fe^0 content, and the Fe^{2+} content.

The carbon and sulphur content of samples (excluding coal samples) were determined using a LECO CS 400 analyser, while the carbon, hydrogen and nitrogen content of the coal were determined with a LECO CHN 1000 analyser.

A.6. Raw material mixtures for TGA experiments

The mass ratio of coal to ore in the material mixture depends on the compositions of the coal as well as the composition of the ore. For this reason the atomic ratio of fixed carbon in the coal to reducible oxygen in the material mixture (further referred to as the $FC/O_{(red)}$ ratio) was calculated. The fixed carbon content of the coal was calculated from the total carbon-, oxygen- and hydrogen content of the coal. It was assumed that all the oxygen in the coal was present as moisture[15], while the hydrogen not associated with this moisture was reported as methane. This means that the fixed carbon was calculated as the difference between the total carbon content of the coal and the amount of carbon associated with the volatiles (as methane). The same argument holds for coal char.

The reducible oxygen is the oxygen associated with Fe in the material mixture. This was calculated from ICP analyses combined with the forms of Fe (discussed in ***Appendix A.5***).

The $FC/O_{(red)}$ ratio gives a good indication of the carbon efficiency of the process. In the Ifcon process, the carbon efficiency is determined by the CO/CO_2 ratio of the gas generated in the solids bed, the amount of carbon oxidised on the surface of the solids bed and the amount of carbon that reports to the molten bath[10,13,17]. The correct $FC/O_{(red)}$ ratio will result in just enough carbon at the bottom of the solids bed for complete reduction. When this ratio is too high, excess carbon is present at the bottom of the bed after reduction is completed. Most of this carbon will then dissolve into the

metal, thereby increasing the carbon content of the metal. When the $FC/O_{(red)}$ ratio is too low the material in the solids bed becomes depleted of carbon before reduction is completed. This will result in the production of a slag with high FeO content, which is associated with a low metal yield.

The material mixtures for the TGA tests were chosen so that the results of the experiments could be compared to results from the pilot scale facility and other relevant investigations[15,19].

A.7. Calculation of degree of reduction achieved

Since the mass of the sample was recorded continuously during the test, the degree of reduction achieved was calculated as a function of exposure time. Since exit-gas analyses were not available the quantitative contribution of carbon monoxide, hydrogen and hydrocarbons from volatiles, to the reduction reactions, was not known.

Two methods were used to calculate the degree of reduction achieved. The first method assumed that reducible oxygen was removed as a combination of CO, CO_2 and H_2O. The CO/CO_2 ratio was taken as that corresponding to the equilibrium CO/CO_2 ratio for the reduction of the oxide at 1000°C. 1000°C was an arbitrary estimate of the temperature at which the gas would leave the sample (noting that actual temperatures were not made). In addition, it was assumed that the volatiles acted as reductant, contributing to the reduction reaction. Results obtained by using this method of calculation are shown in ***Appendix C.2***

The second method assumed that oxygen (excluding oxygen present as moisture and CO_2 from calcination of $MgCO_3$) was removed only as carbon monoxide. The method was therefore based on the assumption that the outer surface of the sample heated up quickly to temperatures above 1000°C, and that the CO/CO_2 ratio was in equilibrium with the carbon on the outer surface of the sample. In addition, only the fixed carbon in the coal was considered as a reductant. The results obtained using this method are presented in ***Appendix C.3***.

The following generic assumptions were made for both methods described above:

a) Ca and Mg in the limestone and dolomite were present as $CaCO_3$ and $MgCO_3$ respectively.

b) The analyses were done on dry basis and the difference between the total of the ICP analyses and 100% represented elements not reported. The analyses were therefore normalized.
c) Oxygen in the volatiles was present as H_2O.
d) All hydrogen not accounted for as H_2O was present as CH_4.
e) The difference between the total carbon and carbon present as CH_4 resulted in the fixed carbon content of the coal.
f) Calcination of $MgCO_3$ were completed before reduction started.
g) Calcination of $CaCO_3$ only started once reduction was completed.

With both methods the degree of reduction achieved was calculated as a function of the exposure time.

APPENDIX B

Kinetic model inputs

B.1. Thermal conductivity correlations

The thermal conductivities of the iron oxide and carbon (with units W/m/K) was expressed as follows:

$$K=1/(AT+B) \qquad (B.a)$$

where *A* and *B* are constants shown in ***Table B 1***.

Table B 1: *Constants for calculation of thermal conductivities, with T_{max} signifying the maximum temperature over which the first set of values in the table (for A and B) are valid*[30]

Parameter	Iron oxide as O:Fe ratio			Carbon
	1.5	1.33	1.0	
A	1.84x10-04	1.69x10-04	2.34x10-04	0
B	0	0	0.1136	3.846
Tmax (K)	912	906	825	1600
A	8.32x10-05	2.97x10-06	0	0
B	9.24x10-02	0.1508	0.3062	3.846

Thermal conductivities for iron, the gas phase, lime and calcite(with units: W/m/K) was expressed as follows:

$$K=AT^2+BT+C \qquad (B.b)$$

where *A*,*B* and *C* were constants shown in ***Table B 2***.

Table B 2*: Constants for calculation of thermal conductivities*[30].

Constant	Fe	Gas phase	CaO	CaCO3
A	4.30x10-05	-2.46x10-08	0	0
B	-1.08x10-01	8.75x10-05	0	0
C	1.02x1002	2.05x10-03	1	1

B.2. Equilibrium constants

Expressions used to calculate equilibrium constants are presented in ***Table B 3***.

Table B 3: *Thermodynamic data used in model calculations*[30].

Reaction	Expression for equilibrium constant
$3Fe_2O_3 + CO = 2Fe_3O_4 + CO_2$ (above 564°C)	$pCO2/pCO = 10^{(3.8865-816.29/T)}$
$3Fe_2O_3 + H_2 = 2Fe_3O_4 + H_2O$ (above 564°C)	$pCO2/pCO = 10^{(2.2523-2034.4/T)}$
$Fe_3O_4 + CO = 3FeO + CO_2$ (above 564°C)	$pCO2/pCO = 10^{(0.6601-270.33/T)}$
$Fe_3O_4 + H_2 = 3FeO + H_2O$ (above 564°C)	$pH2O/pH2 = 10^{(2.2523-2034.4/T)}$
$FeO + CO = Fe + CO_2$ (above 564°C)	$pCO2/pCO = 10^{(-1.2239+ 1031.9/T)}$
$FeO + H_2 = Fe + H_2O$ (above 564°C)	$pH2O/pH2 = 10^{(0.4404 -806.56/T)}$
$0.25Fe_3O_4 + CO = 0.75Fe + CO_2$ (below 564°C)	$pCO2/pCO = 10^{(-0.3653+ 412.2/T)}$
$0.25Fe_3O_4 + H_2 = 0.75Fe + H_2O$ (below 564°C)	$pH2O/pH2 = 10^{(1.7157 -1706.95/T)}$
$CO_2 + C = 2CO$	$(pCO)2/pCO = 10^{(14.2423 -9016.9/T)}$
$H_2O + C = CO + H_2$	$pCO\ pH2O/\ pCO = 10^{(12.4224 -7009.2/T)}$

B.3. Enthalpy values

The enthalpy expression that was used was as follows:

$$H = A + BT \qquad (B.c)$$

Where H was the enthalpy (with units: J/mol), A and B were constants, and T was the absolute temperature (with unit: K). Values used for A and B are presented in ***Table B 4***.

***Table B 4**: Values used for the calculation of enthalpies*[30].

Species	A (J/mol)	B (J/mol K)
$FeO_{1.5}$	-435685	73.25
$FeO_{1.333}$	-393789	73.27
FeO	-283919	57.2
Fe	-19267	44.4
CO	-120780	32.33
CO_2	-411040	51.58
H_2	-9414	30.36
H_2O (g)	-254775	39.68
CH_4	-99500	65.58
C	-7924	20.42

B.4. Rate constants used in calculations

Rate constants and activation energies used for model calculations are presented in ***Table B 5***.

***Table B 5**: Rate constants and activation energies used for model calculations*[30].

Reaction	ko (m3/kg s)	EA (J/mol)
$3Fe_2O_3 + CO = 2Fe_3O_4 + CO_2$ (above 564°C)	30	69648
$3Fe_2O_3 + H_2 = 2Fe_3O_4 + H_2O$ (above 564°C)	133	54048
$Fe_3O_4 + CO = 3FeO + CO_2$ (above 564°C)	30	69648
$Fe_3O_4 + H_2 = 3FeO + H_2O$ (above 564°C)	133	54048
$FeO + CO = Fe + CO_2$ (above 564°C)	59	76887
$FeO + H_2 = Fe + H_2O$ (above 564°C)	214	65414
$0.25Fe_3O_4 + CO = 0.75Fe + CO_2$ (below 564°C)	0.20	26307
$0.25Fe_3O_4 + H_2 = 0.75Fe + H_2O$ (below 564°C)	1932	57053
$CO_2 + C = 2CO$	45780	172401
$H_2O + C = CO + H_2$	64	99814
	k (1/s)	EA (J/mol)
Devolatilisation (first step)	1.81x105	74000
Devolatilisation (second step)	8.99x108	157000

B.5. Default conditions for model calculations

Default conditions regarding used during model calculations are presented in ***Table B 6***.

***Table B 6**: Default conditions for model calculations*[30].

Parameter	Value
Furnace temperature	1473 K
Initial Fe content of the mixture	729 kg Fe/m^3
Initial fixed carbon content of the mixture	274 kg C/kg Fe
Volatile content (mass basis, ash free)	23%

APPENDIX C

TGA: Experimental results

C.1. Summary of experimental results

A summary of experimental data from the TGA tests that was used to calculate extent of reduction achieved as a function of time are presented in ***Table C 1*** to ***Table C 3*** below.

Tabel C 1: *Experimental results for base mixture*

Base mix 1 (1100°C)		Base mix 2 (1100°C)		Base mix 3 (1100C)		Base mix 4 (1100°C)	
Time	Mass	Time	Mass	Time	Mass	Time	Mass
(s)	(g)	(s)	(g)	(s)	(g)	(s)	(g)
0	86.62	0	88.08	0	85.98	0	89.36
103	84.75	104	86.28	103	84.40	104	88.08
207	82.40	208	83.98	207	82.13	208	85.72
311	80.53	312	82.04	310	80.28	311	83.83
415	78.98	416	80.45	413	78.72	415	82.21
518	77.77	521	79.19	516	77.46	519	80.86
622	76.73	625	78.13	620	76.38	624	79.74
725	75.85	729	77.23	725	75.47	728	78.77
828	75.11	833	76.48	828	74.72	832	77.92
932	74.45	937	75.83	932	74.07	936	77.22
1035	73.90	1041	75.30	1036	73.54	1040	76.61
1139	73.42	1144	74.83	1139	73.08	1143	76.06
1242	72.99	1248	74.42	1243	72.68	1247	75.61
1345	72.65	1352	74.10	1346	72.33	1351	75.21
1448	72.34	1455	73.83	3120	70.37	1454	74.85
1552	72.07	1559	73.61	3225	69.34	1558	74.55
1655	71.85	1662	73.41	3328	70.80	1661	74.30
1758	71.66	1766	73.26	3432	70.49	1764	74.08
1861	71.50	1869	73.13			1867	73.90
1965	71.36	1972	73.02			1971	73.74
2068	71.23	2075	72.92			2074	73.61
2171	71.13	2204	72.82			2177	73.51
2274	71.04	2307	72.75			2280	73.44
2377	70.96	2411	72.69			2384	73.38
2480	70.89	2513	72.64			2486	73.34
2584	70.83	2617	72.60			2589	73.30
2687	70.78	2720	72.56			2692	73.28
2790	70.73	2823	72.53			2796	73.25
2893	70.69	2926	72.50			2899	73.63
2996	70.65	3029	72.47			3002	73.64
						3105	73.64
						3208	73.64

Tabel C 2: *Experimental results for mixture containing Thabazimbi ore as well as the mixture containing Leeuwpan coal.*

Thabazimbi ore 1 (1100°C)		Leeuwpan coal 1 (1100°C)		Leeuwpan coal 2 (1200°C)	
Time	Mass	Time	Mass	Time	Mass
(s)	(g)	(s)	(g)	(s)	(g)
0	88.64	0		0	85.82
105	88.61	104	86.48	103	84.39
209	88.61	208	85.09	207	82.42
312	88.61	312	83.73	311	80.68
416	88.61	416	82.50	414	79.33
520	88.61	520	81.55	518	78.36
624	88.26	625	80.72	621	77.51
727	85.91	728	79.94	725	76.80
831	83.92	832	79.25	828	76.15
935	82.22	936	78.60	931	75.58
1039	80.80	1040	77.99	1035	75.05
1142	79.65	1143	77.42	1138	74.59
1246	78.70	1247	76.93	1242	74.19
1349	77.90	1350	76.49	1345	73.81
1453	77.22	1454	76.10	1449	73.51
1557	76.62	1557	75.74	1552	73.21
1660	76.12	1661	75.43	1655	72.93
1763	75.68	1764	75.15	1758	72.69
1866	75.30	1867	74.88	1862	72.50
1970	74.97	1970	74.64	1965	72.30
2073	74.67	2074	74.44	2068	72.15
2176	74.41	2177	74.25	2171	72.01
2279	74.20	2280	74.08	2274	71.89
2383	74.00	2384	73.94	2377	71.78
2486	73.83	2487	73.79	2480	71.68
2589	73.71	2590	73.67	2583	71.61
2692	73.59	2693	73.56	2686	71.51
2795	73.50	2796	73.47	2790	71.46
2898	73.40	2900	73.38	2893	71.41
3002	73.33	3002	73.31	2996	71.36
3105	73.27	3106	73.24	3099	71.32
3208	73.21	3209	73.18		
3311	73.16	3312	73.12		

Tabel C 3: *Experimental results for mixture containing Sishen ore with particle sizes as follows: +425 –850 µm, +1400 –2000 µm, +4750 –6300 µm..*

+212 -425 µm (1200°C)		+1400 –2000 µm (1200°C)		+4750 –6300 µm (1200°C)	
Time	Mass	Time	Mass	Time	Mass
(s)	(g)	(s)	(g)	(s)	(g)
0	86.07	0	89.22	0	85.82
104	84.44	104	87.53	104	84.39
208	82.26	208	85.30	207	82.42
312	80.48	312	83.40	310	80.68
415	79.05	416	81.90	413	79.33
519	77.90	520	80.67	516	78.36
623	76.95	624	79.59	619	77.51
727	76.06	728	78.71	722	76.80
831	75.33	831	77.90	825	76.15
934	74.69	935	77.22	928	75.58
1037	74.11	1039	76.63	1032	75.05
1140	73.63	1142	76.15	1135	74.59
1243	73.20	1246	75.73	1238	74.19
1346	72.82	1350	75.38	1341	73.81
1450	72.50	1453	75.06	1445	73.51
1553	72.22	1557	74.82	1548	73.21
1656	71.94	1660	74.60	1651	72.93
1760	71.71	1763	74.43	1754	72.69
1863	71.51	1867	74.30	1857	72.50
1967	71.33	1970	74.18	1960	72.30
2070	71.17	2074	74.08	2064	72.15
2173	71.03	2177	74.00	2167	72.01
2276	70.93	2280	73.93	2270	71.89
2379	70.83	2383	73.87	2373	71.78
2483	70.74	2486	73.82	2476	71.68
2586	70.67	2589	73.77	2579	71.61
2689	70.62	2693	73.73	2682	71.51
2791	70.58	2796	73.69	2785	71.46
2895	70.54	2900	73.65	2888	71.41
2998	70.51	3003	73.62	2992	71.36
3101	70.48	3106	73.59	3095	71.32
3204	70.46	3210	73.56		
3307	70.44	3313	73.54		

C.2. Apparent degree of reduction achieved illustrations (I)

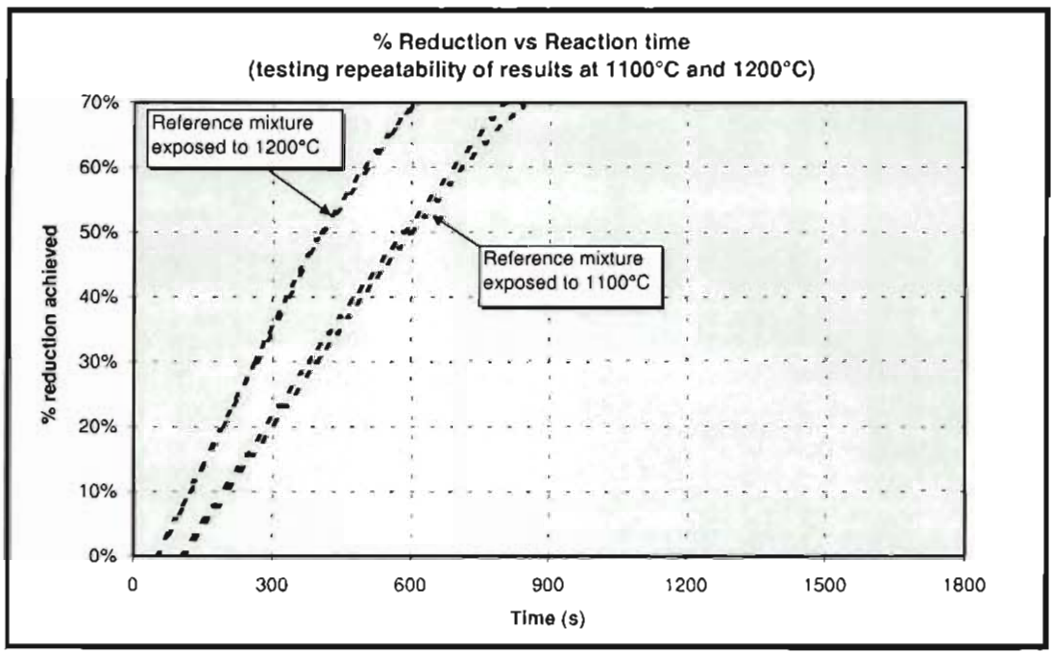

***Figure C 1**: Reduction rate of two runs with the base mixture exposure to 1100°C and two runs with the base mixture exposure to 1200°C, showing the repeatability of results.*

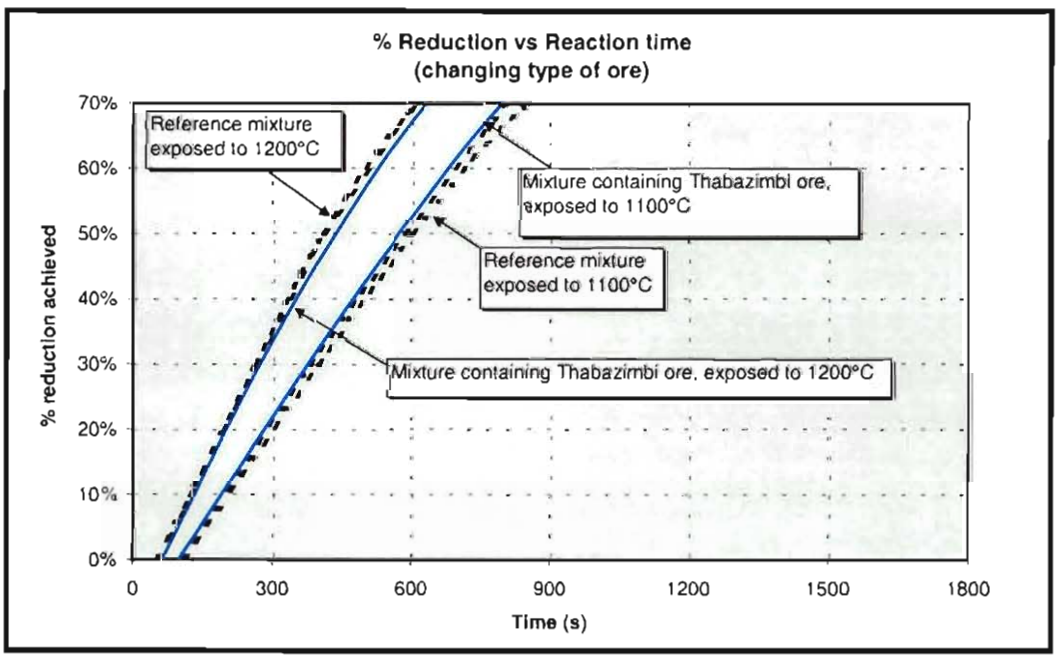

***Figure C 2**: Reduction rate of base mixture and a mixture contalning Thabazimbi fine ore exposed to 1100°C and 1200°C.*

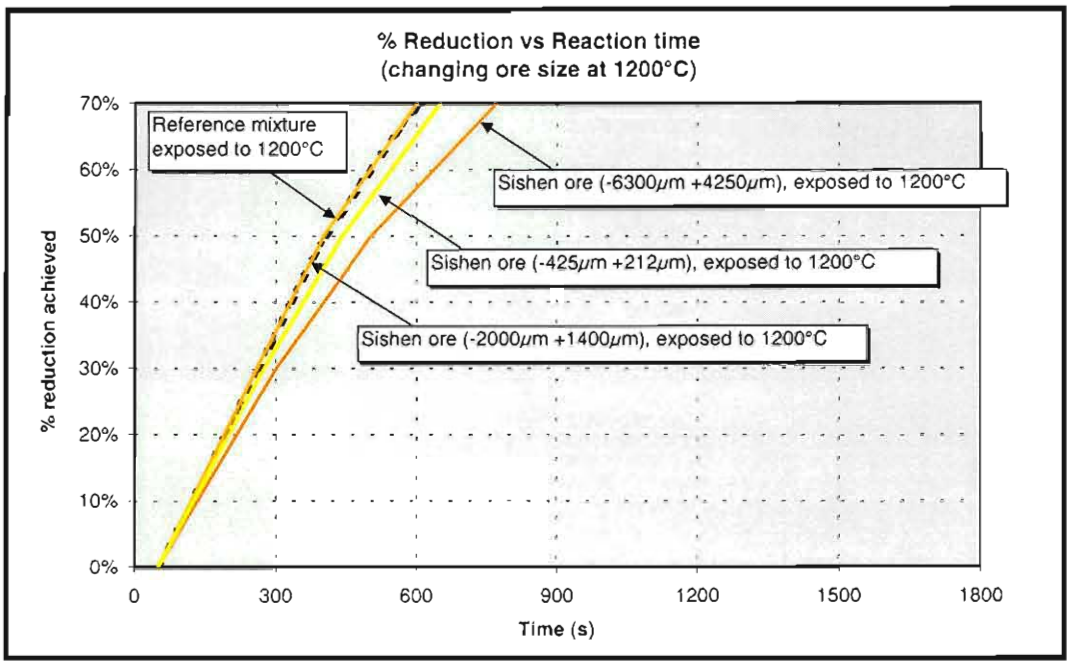

***Figure C 3**: Reduction rate of base mixture and a mixture containing various size fractions of Sishen ore during exposure to 1200°C.*

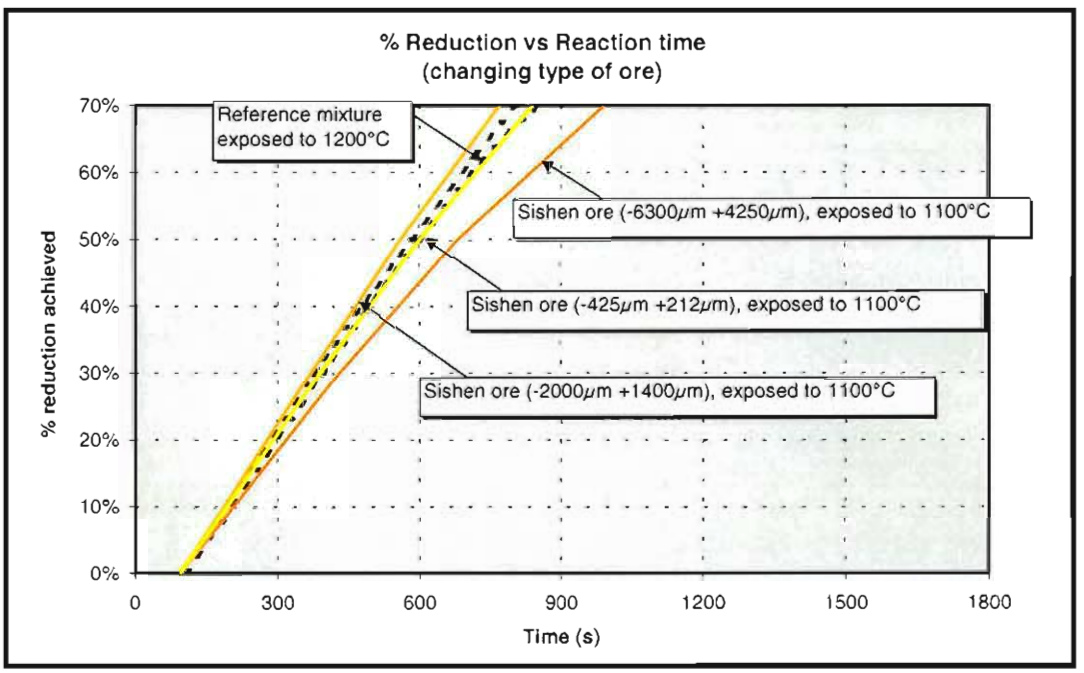

***Figure C 4**: Reduction rate of base mixture and a mixture containing various size fractions of Sishen ore during exposure to 1100°C.*

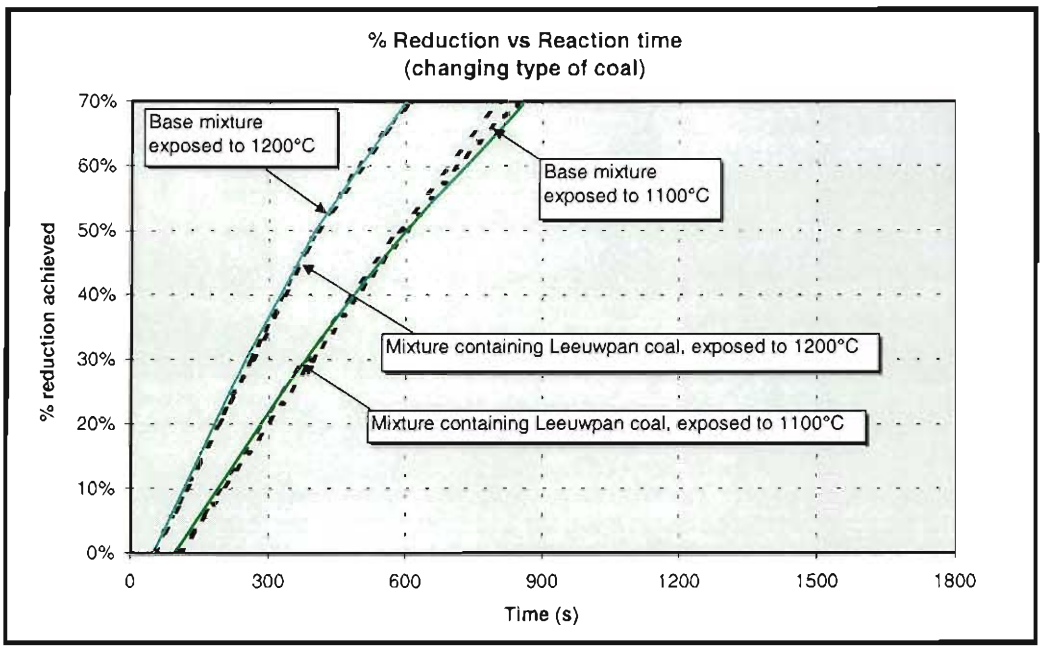

***Figure C 5**: Reduction rate of base mixture and a mixture containing Leeuwpan coal exposed to 1100°C and 1200°C.*

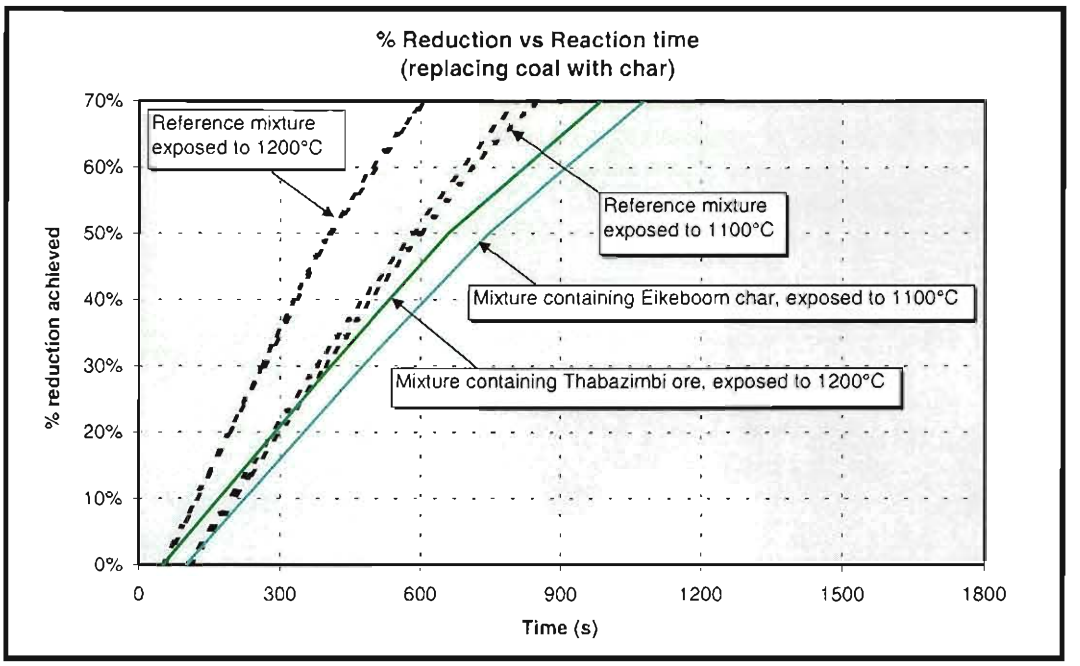

***Figure C 6**: Reduction rate of base mixture and a mixture containing Thabazimbi fine ore exposed to 1100°C and 1200°C.*

Figures C 1 to ***C6*** show the apparent degree of reduction achieved calculated according to the procedure presented in ***Appendix A.7***. The figures show that reduction only started after approximately 2 minutes. This is a result of the assumption that calcinations of $MgCO_3$ is completed before reduction starts. However the results support the findings of ***paragraph 2.4***. These calculations were based on the assumption that volatiles contribute to the reduction reaction and that both CO and CO_2 formed as reduction products. The CO/CO_2 ratio of the product gas was calculated as the CO/CO_2 in equilibrium with iron oxide. This is the one limit regarding the extent of reduction achieved.

The other limit is when calculations are based on the assumption that volatiles do not contribute to reduction and only CO forms as gaseous product (due to reduction). The results when using this approach are presented in ***Figures C 7***to ***C 12*** in ***Appendix C.3.***

C.3. Apparent degree of reduction achieved illustrations (II)

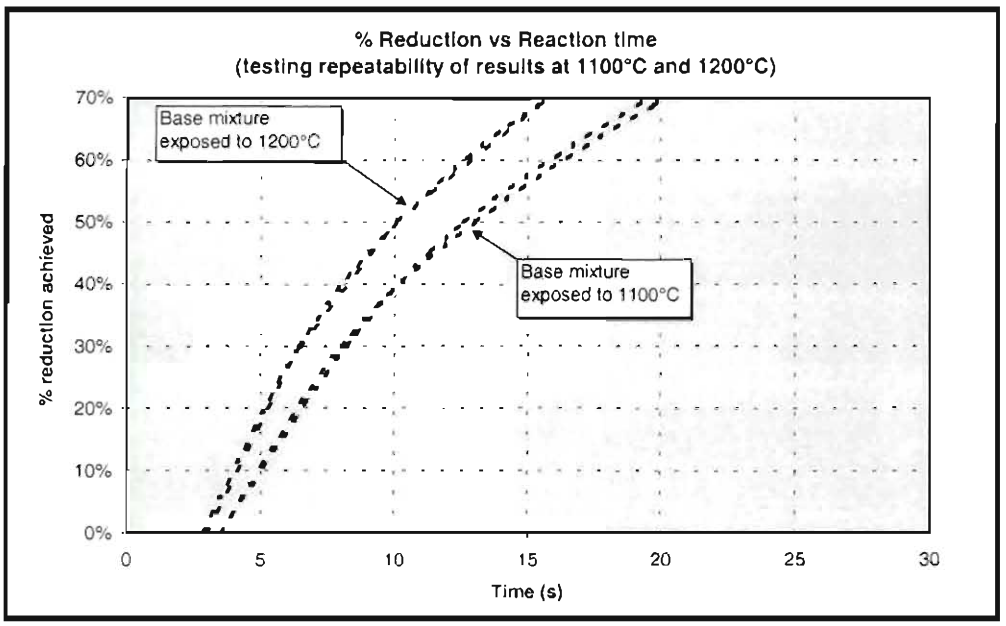

***Figure C 7**: Reduction rate of two runs with the base mixture exposure to 1100°C and two runs with the base mixture exposure to 1200°C, showing the repeatability of results.*

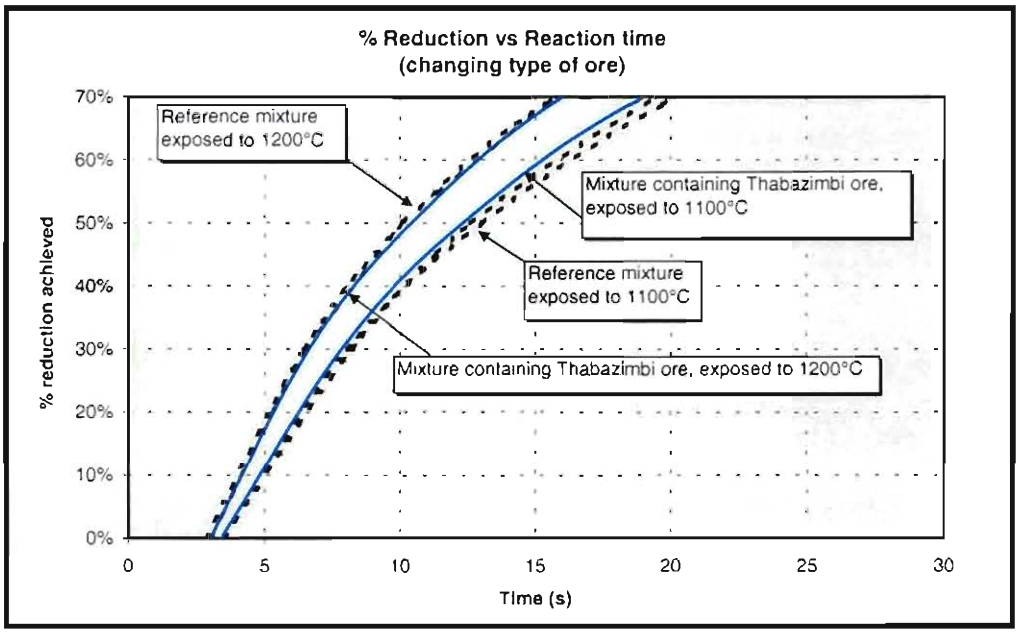

***Figure C 8**: Reduction rate of base mixture and a mixture containing Thabazimbi fine ore exposed to 1100°C and 1200°C.*

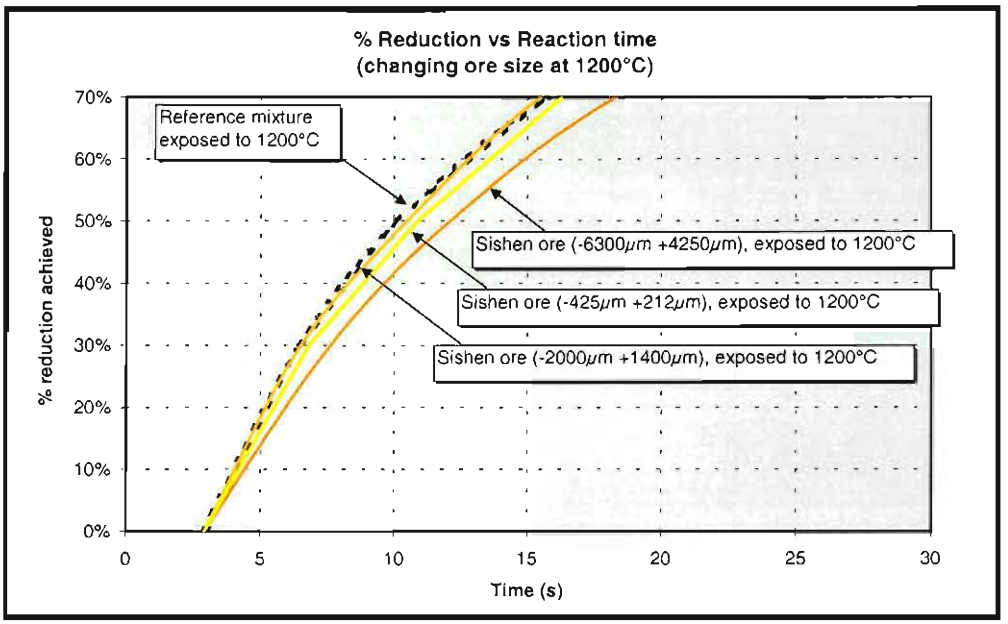

***Figure C 9**: Reduction rate of base mixture and a mixture containing various size fractions of Sishen ore during exposure to 1200°C.*

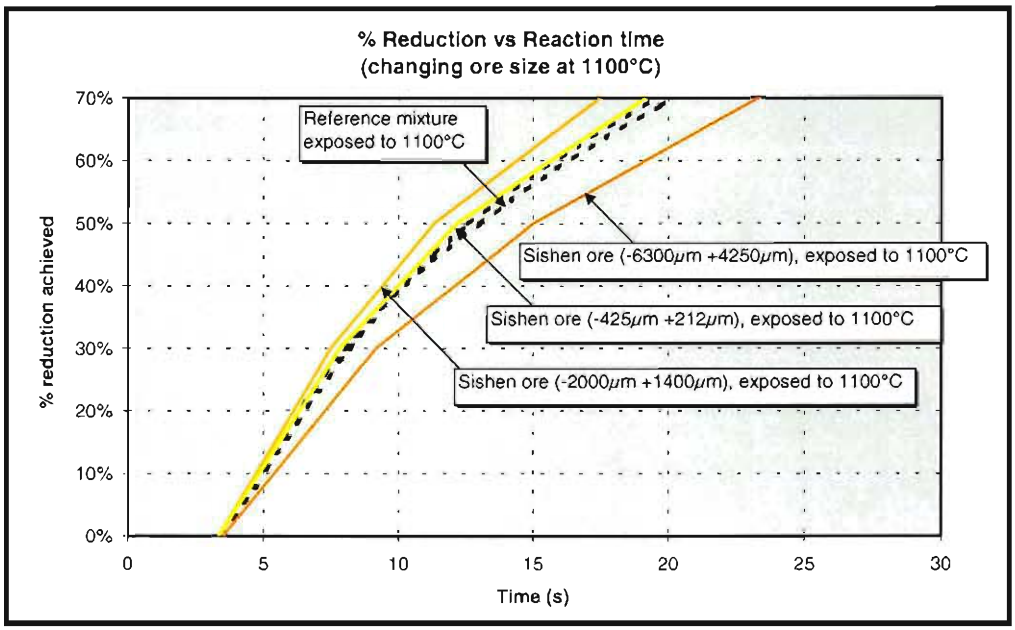

***Figure C 10**:Reduction rate of base mixture and a mixture containing various size fractions of Sishen ore during exposure to 1100°C.*

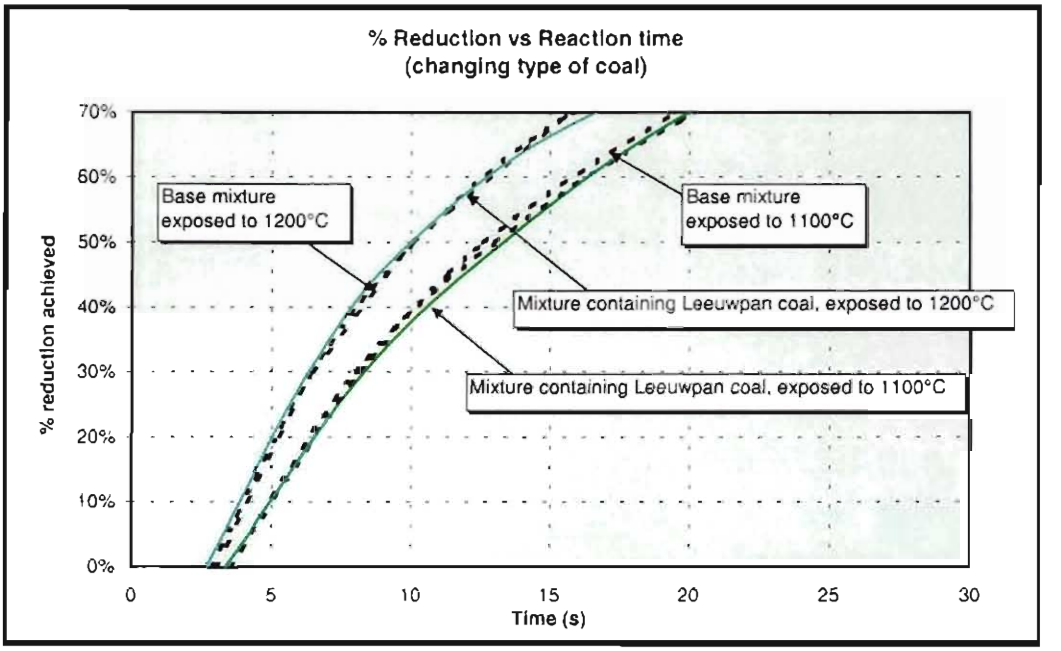

***Figure C 11**: Reduction rate of base mixture and a mixture containing Leeuwpan coal exposed to 1100°C and 1200°C.*

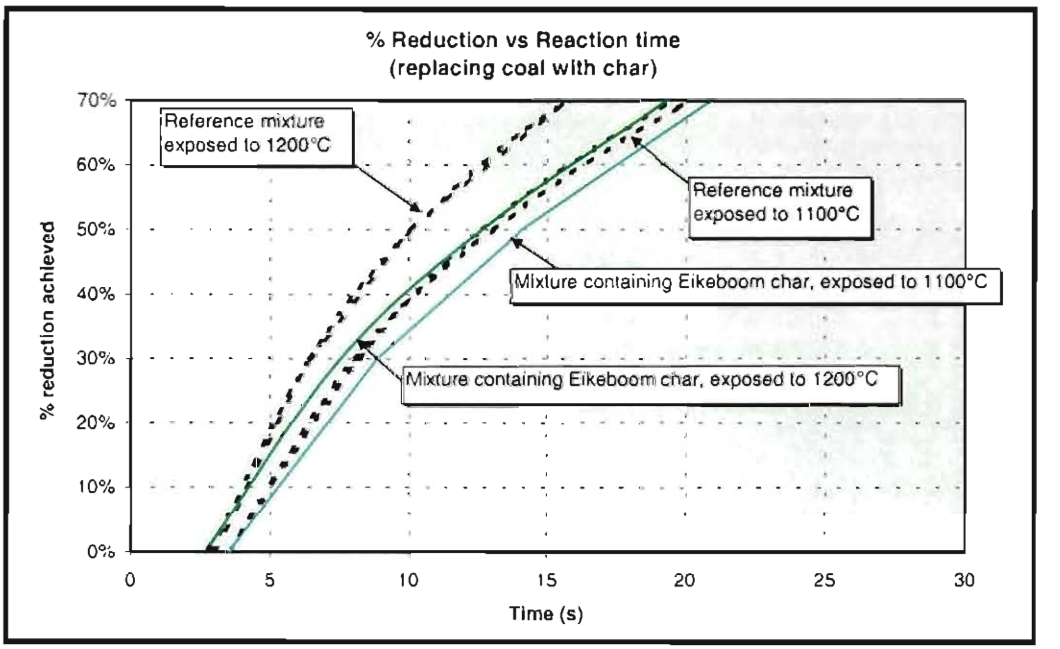

***Figure C 12**: Reduction rate of base mixture and a mixture containing Thabazimbi fine ore exposed to 1100°C and 1200°C.*

The results that are shown in ***Figures C 7*** to ***C12*** show the apparent degree of reduction achieved calculated according to the procedure presented in ***Appendix A.7.*** These calculations were based on the assumption that volatiles did not contribute to the reduction reaction and that only CO formed as reduction products.

The results shown in ***Appendix C.2*** and ***Appendix C.3*** complimented each other , and confirmed results presented from ***paragraph 2.4***. Note that the time before reduction starts is longer when reduction by volatiles are not accounted for, since the initial mass loss accounts for calcinations of $MgCO_3$ and loss of volatiles (without reduction occurring). It should therefore be kept in mind that the results presented in ***Appendix C.2*** and ***Appendix C.3*** are not fundamental reduction rates but rather apparent reduction rates based on specific sets of assumptions.

APPENDIX D

Reaction kinetics

Page no

D.1 Calculation of gas flow rates to overcome mass transfer control

For the fluidization tests, flow rates were selected according to the following requirements[30]

- The flow rate must be at least equal to the minimum flow rate required for fluidisation.
- The minimum fluidisation flow rate should be less than 12 l/min (due to equipment restrictions).
- The mass transfer constant for fluidisation must be at least 10 times the chemical reaction rate constant at the experimental temperature.

D.1.1 Calculation of required flow rate for fluidisation

The minimum fluidisation velocity required for each size fraction at the experimental temperature was calculated using the following equation:[30]

$$u_{mf} = \left[\left((33.7)^2 + 0.0408 \frac{d_p^3 \rho_g (\rho_s - \rho_g) g}{\mu^2} \right)^{1/2} - 33.7 \right] \cdot \frac{\mu}{d_p \rho_g} \qquad \text{(D.a)}$$

where u_{mf} *is the* minimum fluidisation velocity (with unit: m/s), ρ_s is the solids density (with unit: kg/m^3), ρ_g is the gas density (with units: kg/m^3), μ is the gas viscosity (with units: kg/ms), d_p is the particle diameter (with unit: m), g is gravitational acceleration (9.81 m/s^2), k_d is the gas phase mass transfer coefficient (with units: m/s), $D_{A\text{-}B}$ is the binary diffusivity of A in B (with units: m/s^2), Re is the Reynolds number, Sc is the Schmidt number, and Sh is the Sherwood number.

The diffusivity in the binary gas systems was calculated as follows:

$$D_{A-B} = \left(\frac{(1\times10^{-3})T^{1.75}}{P(v_B^{1/3} + v_A^{1/3})^2} \left[\frac{1}{M_A} + \frac{1}{M_B} \right]^{1/2} \right) \times \frac{1}{100} \qquad \text{(D.b)}$$

Where T is temperature (with unit: K), P is pressure (0.86 atm),v_A is the diffusion volume of specie A (with unit: m^3) and M_A is the molecular weight of specie A (with unit: g/mol).

The gas phase mass transfer coefficient was calculated as follows:

$$\mathrm{Re} = \frac{d_p \rho_g u_{mf}}{\mu} \qquad \text{(D.c)}$$

The Reynolds number and Schmidt numbers were used to calculate the Sherwood number from the following equations:

$$Sc = \frac{\mu}{\rho_g D_{A-B}}$$

For 0.1 < Re >15:

$$Sh = 0.374\mathrm{Re}^{1.2} Sc^{1/3} \qquad \text{(D.d)}$$

For 15 < Re >250:

$$Sh = 2.01\mathrm{Re}^{1.2} Sc^{1/3} \qquad \text{(D.e)}$$

The Sherwood number is then used in the following equation to calculate the gas phase mass transfer coefficient:

$$Sh = \frac{k_d d_p}{D_{A-B}} \qquad \text{(D.f)}$$

For the minimum fluidisation velocity and the reactor diameter of 25 mm a minimum fluidisation flow rate was calculated by multiplying the reactor cross sectional area with the minimum fluidisation gas velocity. The gas phase mass transfer coefficient for the minimum fluidisation velocity was then calculated, and this coefficient was compared to the chemical reaction rate constant. If the gas phase mass transfer coefficient was more than ten times larger than the chemical reaction rate constant, the experimental gas flow was assumed sufficient to overcome gas phase mass transfer control.

Only small particle were fluidised. Calculations showed that the gas flow rates required to overcome mass transfer control for the large particles were less than the gas flow rate required for fluidisation of the large particles.

The experimental conditions used for determining the rate constant of each size fraction are shown in ***Table D.1*** and ***Table D.2***.

Table D 1: *Experimental conditions for ore Reduction with CO gas at 800°C, 900°C, 950°C and 1000°C*

Size Fraction (μm)	Gas flow rate for 800°C (l/min) @ STD	Gas flow rate for 900°C (l/min) @ STD	Gas flow rate for 950°C (l/min) @ STD	Gas flow rate for 1000°C (l/min) @ STD	Fluidise/Packed bed
-212 +106	0.45	0.39	0.37	0.35	Fluidise
-300 +212	0.74	0.65	0.61	0.58	Fluidise
-850 +425	4.11	3.63	3.42	3.50	Fluidise
-2800 +2000	1.80	1.80	1.80	1.80	Packed
-6300 +4750	1.80	1.80	1.80	1.80	Packed

Table D 2: *Experimental conditions for char gasification with CO_2 gas at 800°C, 850°C, 900°C, and 950°C.*

Size Fraction (μm)	Gas flow rate for 800°C (l/min) @ STD	Gas flow rate for 850°C (l/min) @ STD	Gas flow rate for 900°C (l/min) @ STD	Gas flow rate for 950°C (l/min) @ STD	Fluidise/Packed bed
-212 +106	0.1	0.1	0.1	0.1	Fluidise
-425 +212	0.5	0.4	0.4	0.4	Fluidise
-850 +425	1.8	1.7	1.6	1.5	Fluidise
-2000 +1400	7.8	7.5	7.1	6.8	Fluidise

D.1.2 Determining of required flow rate for packed bed

For the packed bed experiments, the required flow rate had to be determined experimentally. For this, reduction tests were repeated at the maximum temperature (1000°C) and the flow rate was increased during each test. The minimum flow rate for which the reduction/gasification rate became independent of gas flow rate was the minimum flow rate that was used for the specific set of experiments. This gas flow rate was then used for all of the experiments in the particular size fraction material. ***Figure D 1*** shows the results of the above procedure done for CO reducibility of the ore.

Figure D 1: *Minimum CO flow rate required for iron ore reducibility tests – Stagnant bed*

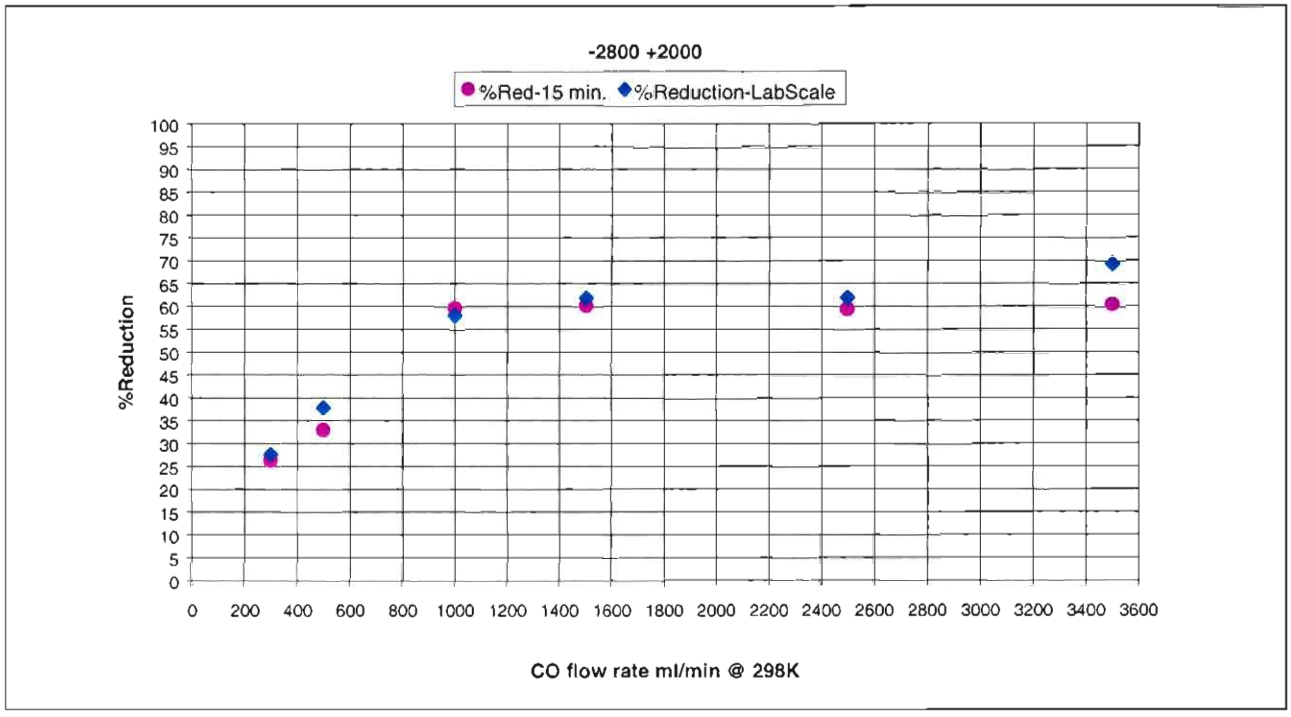

D.2 Summary of kinetic data

This paragraph presents the raw experimental data of the kinetic study.

***Table D.1**: Kinetic data for reduction of -212 +106 µm Sishen ore particles with CO gas.*

900	°C	950	°C	1000	°C
Time (s)	Mass (g)	Time (s)	Mass (g)	Time (s)	Mass (g)
-117	5.766	-150	5.718	-75	5.616
33	5.656	0	5.718	75	5.376
183	5.306	150	5.378	225	4.936
333	4.976	300	5.028	375	4.606
483	4.696	450	4.728	525	4.326
633	4.446	600	4.448	675	4.066
782	4.246	750	4.208	825	3.876
932	4.106	900	4.038	974	3.726
1082	3.976	1050	3.888	1124	3.606
1232	3.856	1200	3.758	1274	3.486
1382	3.746	1350	3.648	1424	3.396
1532	3.646	1500	3.538	1574	3.276
1682	3.566			1724	3.196
1832	3.456				
1982	3.336				
2132	3.246				
2282	3.166				

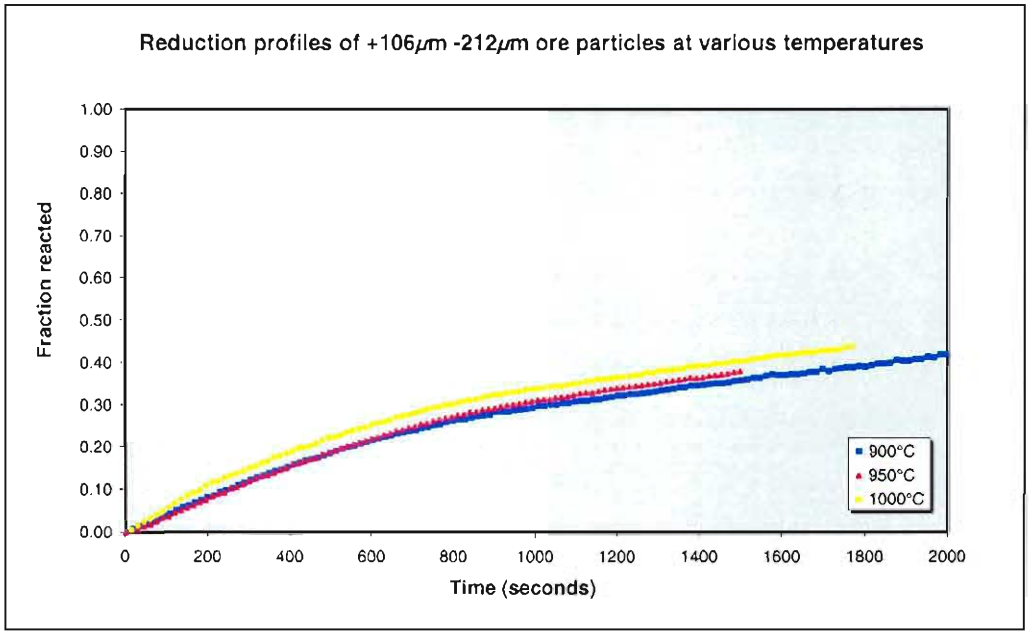

***Figure D 2:** Fraction of reducible oxygen removed as a function of reaction time during reduction of Sishen ore particles (in the size range -212µm +106µm) with CO gas.*

***Table D.2**: Kinetic data for reduction of -300 +212 µm Sishen ore particles with CO gas.*

800	°C	900	°C	950	°C	1000	°C
Time (s)	Mass (g)	Time (s)	Mass (g)	Time (s)	Mass (g)	Time (s)	Mass (g)
15	5.607	105	5.205	0	5.667	3	5.751
165	4.797	255	4.655	150	5.007	153	5.101
315	4.367	405	4.265	300	4.517	303	4.511
465	4.097	555	3.995	450	4.127	453	4.061
615	3.897	705	3.795	600	3.847	602	3.741
765	3.717	855	3.625	750	3.617	752	3.481
915	3.567	1005	3.445	900	3.407	902	3.241
1065	3.397	1155	3.255	1050	3.217	1052	3.001
1215	3.247	1305	3.095	1200	3.027	1202	2.791
1365	3.097	1455	2.945	1350	2.837	1352	2.581
1515	2.957	1605	2.755	1500	2.647	1502	2.381
1665	2.807	1755	2.605	1650	2.467	1652	2.191
1815	2.677	1905	2.475			1802	1.991
1965	2.547	2055	2.315				
2115	2.417	2205	2.155				
2265	2.307	2355	2.025				
		2505	1.905				

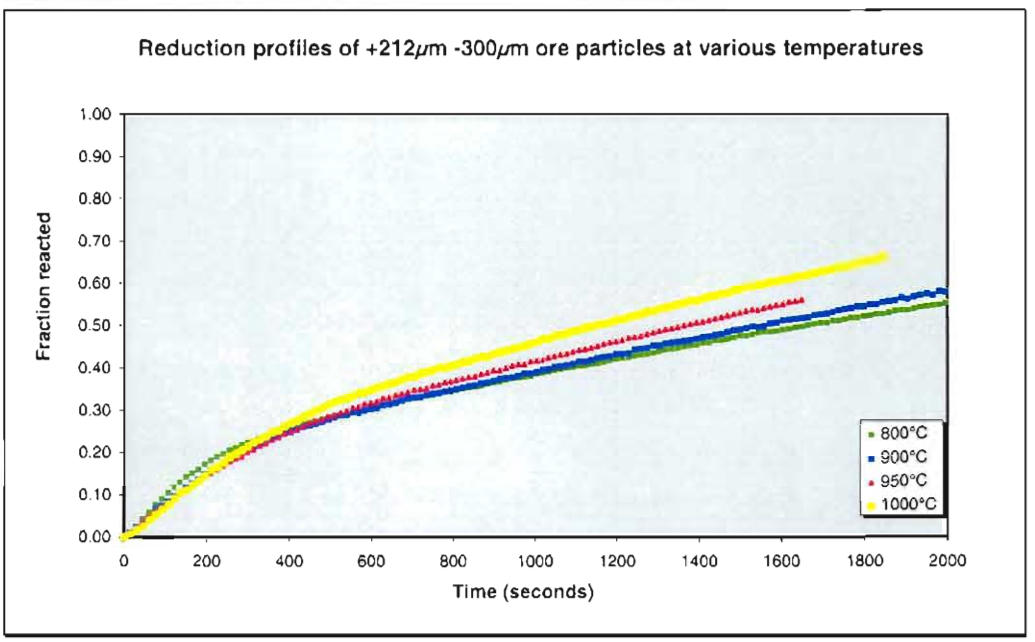

***Figure D 3:** Fraction of reducible oxygen removed as a function of reaction time during reduction of Sishen ore particles (in the size range -300µm +212µm) with CO gas.*

***Table D.3**: Kinetic data for reduction of –850 +425 µm Sishen ore particles with CO gas.*

850	°C	950	°C	1000	°C
Time (s)	Mass (g)	Time (s)	Mass (g)	Time (s)	Mass (g)
0	5.653	90	4.871	59	5.167
50	5.323	240	4.131	209	4.187
100	4.983	390	3.701	359	3.547
150	4.703	540	3.261	509	2.957
200	4.513	690	2.831	659	2.407
250	4.353	840	2.391	809	1.967
300	4.203	990	1.951	959	1.617
350	4.073	1140	1.611	1109	1.397
400	3.963	1290	1.351	1259	1.217
450	3.863	1439	1.171	1409	1.117
500	3.763	1589	1.041	1559	1.047
550	3.683	1739	0.981	1709	0.997
600	3.583			1859	0.957
650	3.513				
700	3.423				
750	3.313				
800	3.263				

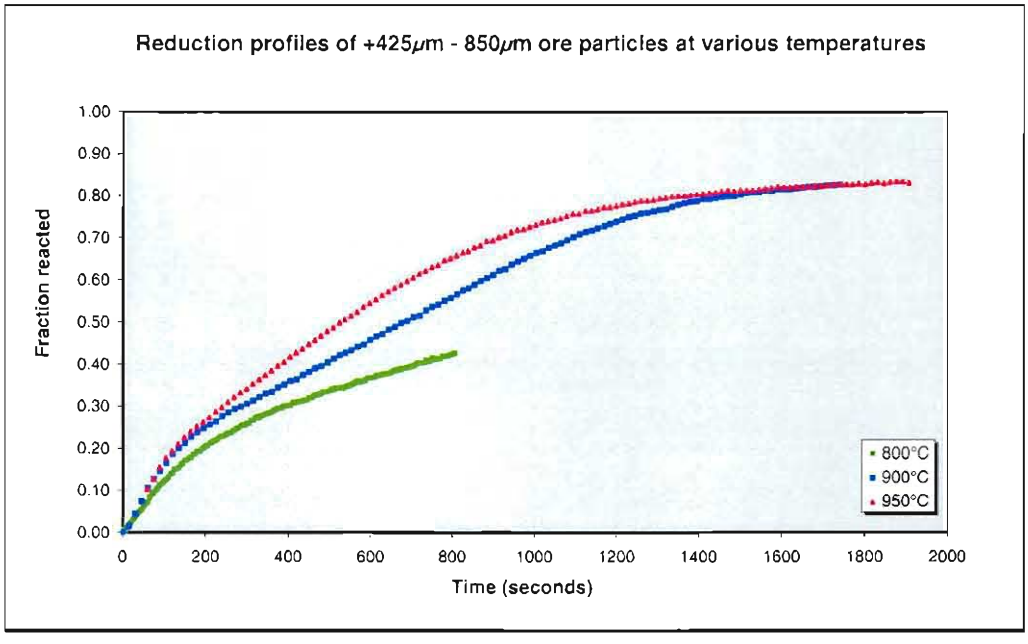

***Figure D 4:** Fraction of reducible oxygen removed as a function of reaction time during reduction of Sishen ore particles (in the size range –850µm +425µm) with CO gas.*

***Table D.4**: Kinetic data for reduction of -2800 +2000 µm Sishen ore particles with CO gas.*

800	°C	850	°C	950	°C
Time (s)	Mass (g)	Time (s)	Mass (g)	Time (s)	Mass (g)
98	5.570	105	5.450	66	5.396
248	5.150	255	4.890	166	4.836
398	4.830	405	4.490	266	4.376
548	4.610	555	4.200	366	3.936
698	4.430	705	3.930	466	3.566
848	4.260	855	3.680	566	3.226
998	4.110	1005	3.410	666	2.926
1148	3.980	1155	3.170	766	2.666
1298	3.850	1305	2.940		
1448	3.720	1455	2.700		
1598	3.580	1605	2.490		
1748	3.440	1755	2.270		
1898	3.360	1905	2.070		

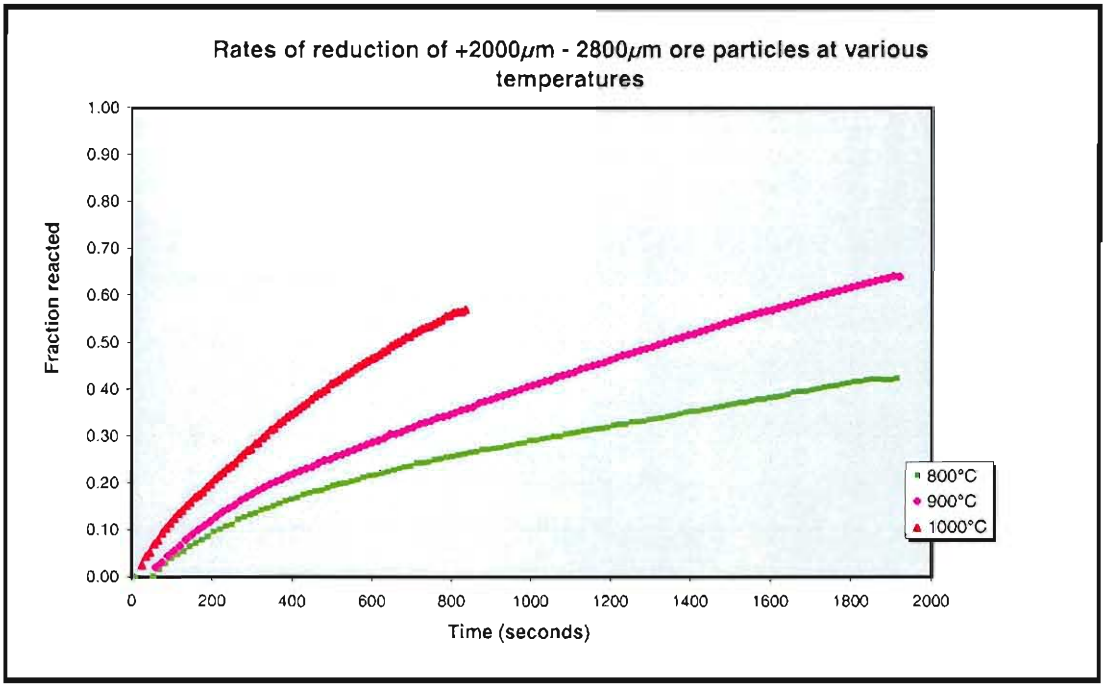

***Figure D 5:** Fraction of reducible oxygen removed as a function of reaction time during reduction of Sishen ore particles (in the size range -2800µm +2000µm) with CO gas.*

***Table D.5**: Kinetic data for reduction of –6300 +4750 µm Sishen ore particles with CO gas*

800	°C	850	°C	950	°C	1000	°C
Time (s)	Mass (g)	Time (s)	Mass (g)	Time (s)	Mass (g)	Time (s)	Mass (g)
95	5.537	75	5.717	90	5.416	75	5.427
245	5.117	225	5.317	240	4.696	225	4.687
394	4.827	375	4.977	390	4.196	375	4.157
544	4.557	525	4.587	540	3.786	525	3.707
694	4.327	675	4.337	690	3.416	675	3.257
844	4.117	825	4.197	840	3.086	825	2.837
994	3.927	975	3.967	990	2.766		
1144	3.777	1125	3.737	1140	2.496		
1294	3.607	1275	3.527	1290	2.226		
1444	3.447	1425	3.377	1440	2.006		
1594	3.307	1575	3.127	1590	1.736		
1744	3.167	1725	3.017	1740	1.536		
1894	3.027	1875	2.807	1890	1.366		
2044	2.907	2025	2.637	2040	1.226		
2194	2.787	2175	2.497	2190	1.056		
2344	2.667	2325	2.407	2340	0.926		
		2475	2.207	2490	0.786		
		2625	2.087	2640	0.696		
		2775	1.967	2790	0.596		
		2925	1.807	2940	0.526		
		3075	1.647	3090	0.446		
		3225	1.547	3240	0.436		
		3375	1.437	3390	0.366		
		3525	1.397	3540	0.336		
		3675	1.297	3690	0.276		

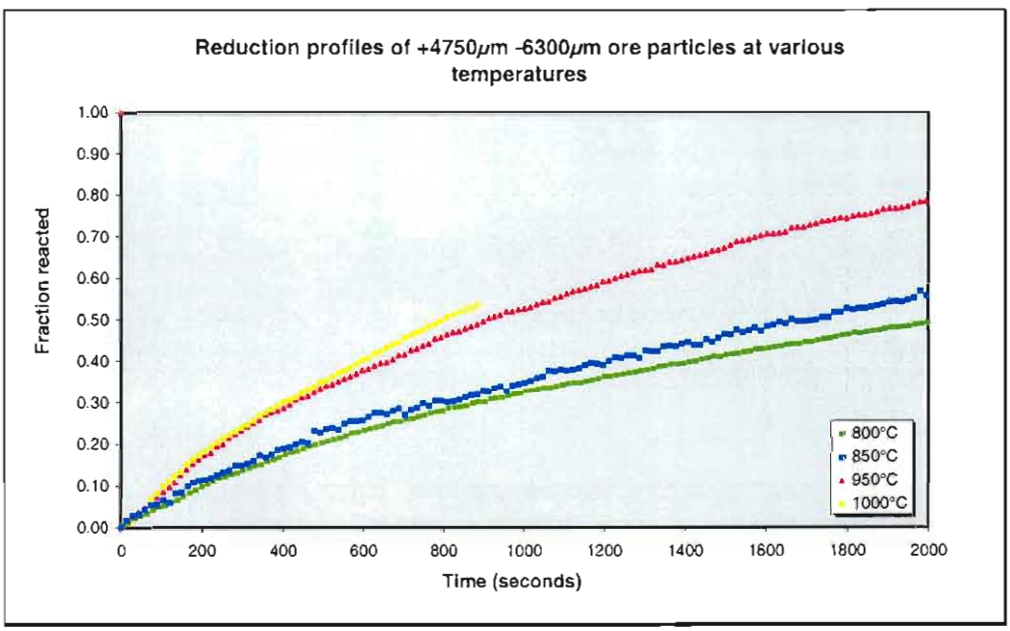

***Figure D 6:** Fraction of reducible oxygen removed as a function of reaction time during reduction of Sishen ore particles (in the size range –6300µm +4750µm) with CO gas.*

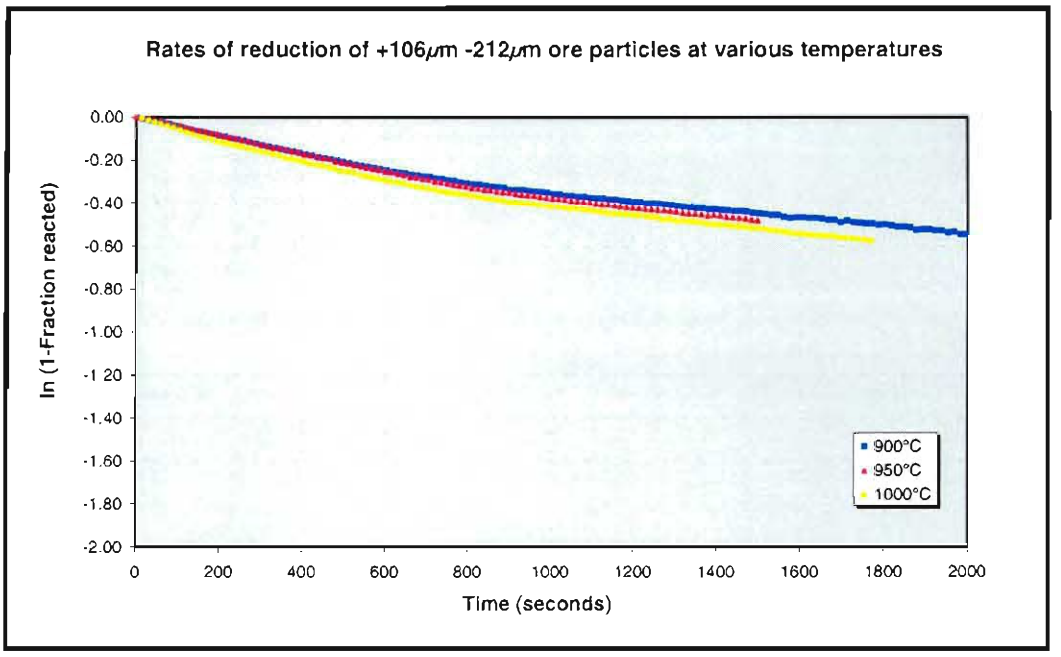

Figure D 2: *ln (1-Fraction of reducible oxygen removed) as a function of reaction time during reduction of Sishen ore particles (in the size range –212μm +106μm) with CO gas.*

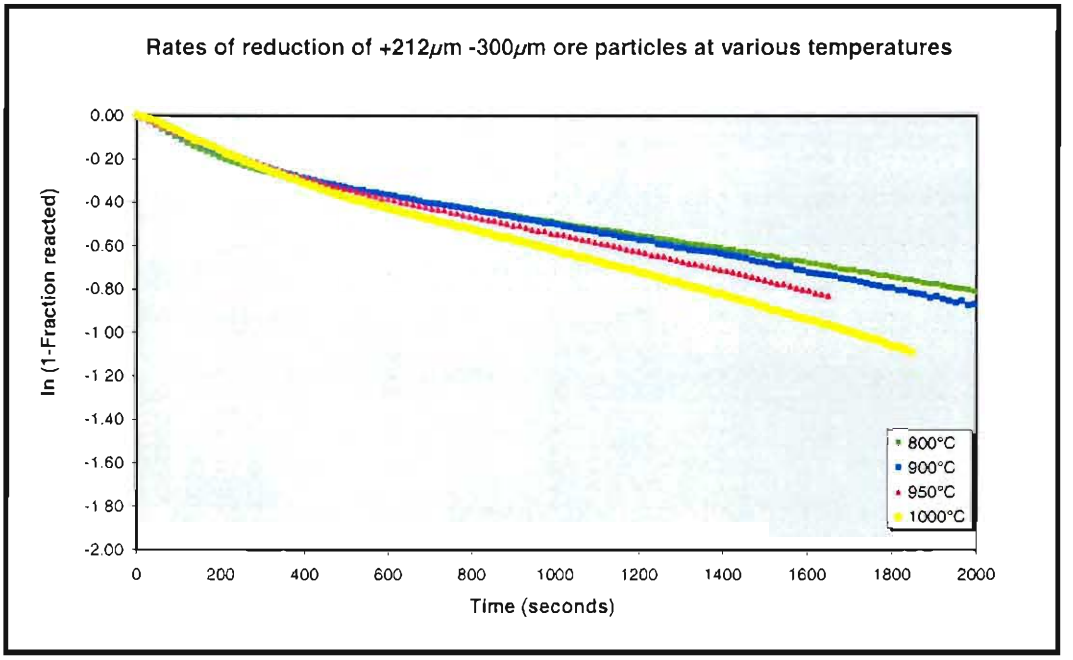

Figure D 3: *ln (1-Fraction of reducible oxygen removed) as a function of reaction time during reduction of Sishen ore particles (in the size range –300μm +212μm) with CO gas.*

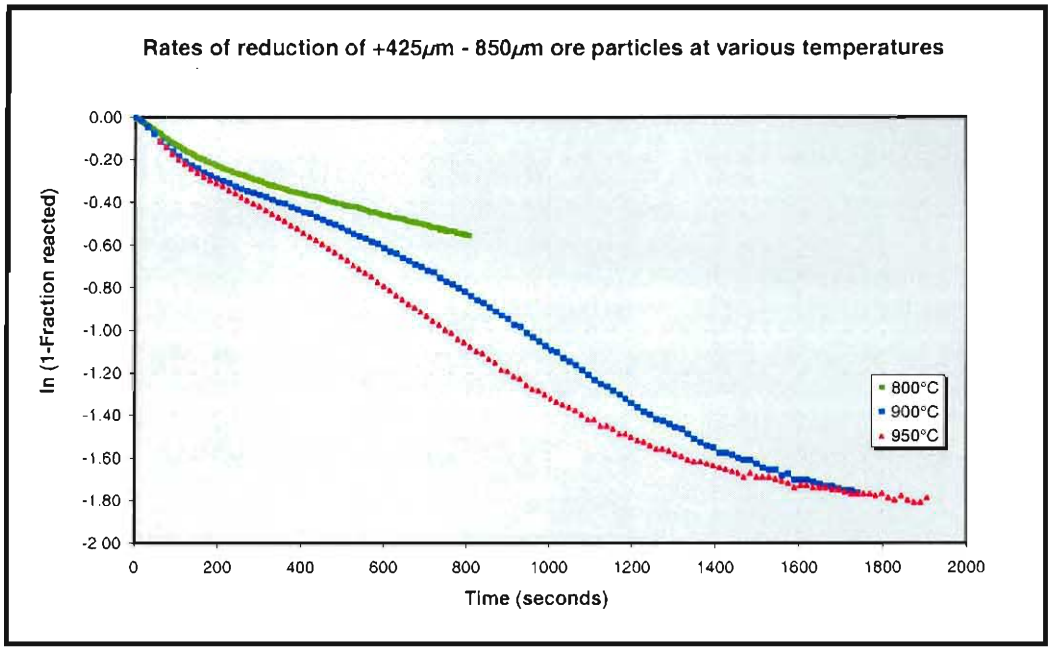

Figure D 4: *ln (1-Fraction of reducible oxygen removed) as a function of reaction time during reduction of Sishen ore particles (in the size range –850μm +425μm) with CO gas.*

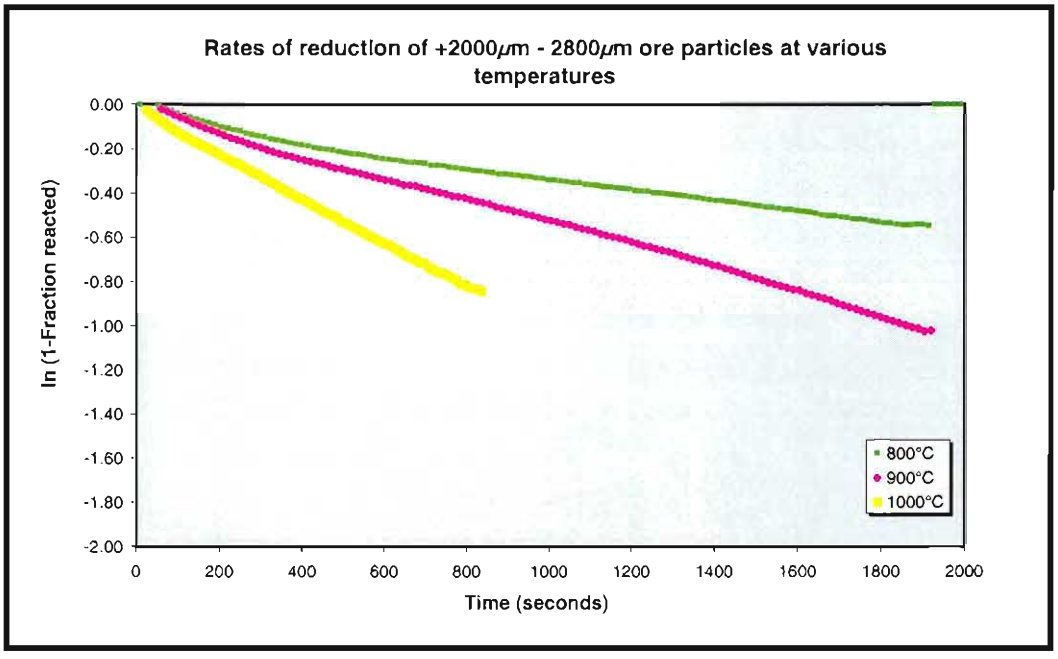

Figure D 5: *ln (1-Fraction of reducible oxygen removed) as a function of reaction time during reduction of Sishen ore particles (in the size range –2800μm +2000μm) with CO gas.*

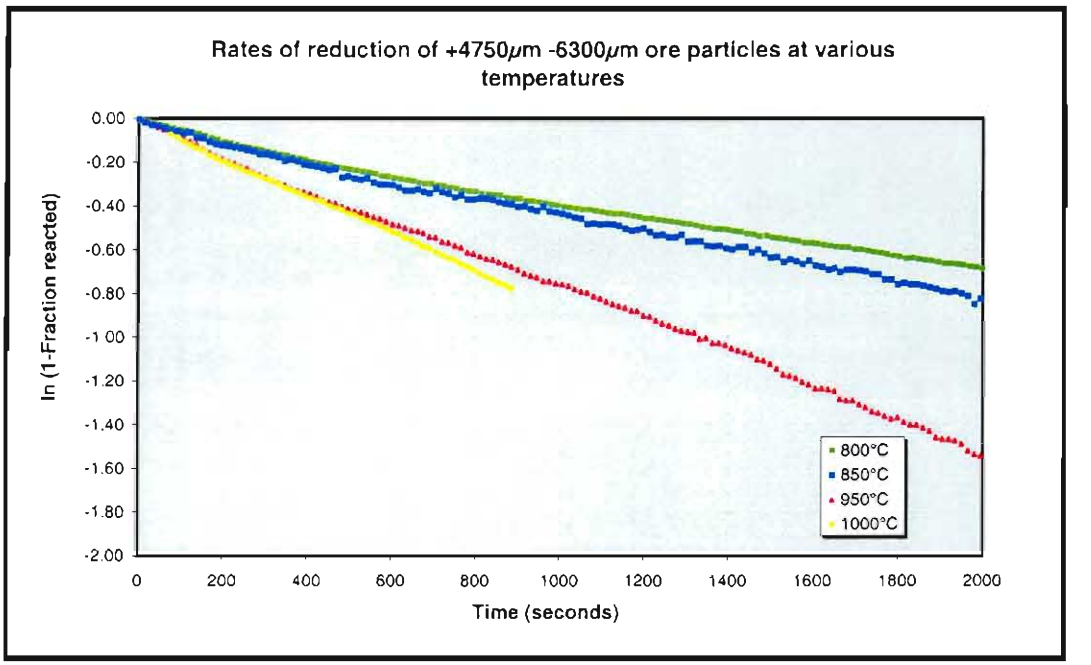

Figure D 6: *Fraction of reducible oxygen removed as a function of reaction time during reduction of Sishen ore particles (in the size range –6300μm +4750μm) with CO gas.*

D.3 Calculation of rate constant and activation energy

Table D.6: *List of rate constants and activation energies calculated from experimental data for degrees of reduction between 0% and 30%.*

0 to 30% reduction

Values of k_{CO}

Particle size range	1/Temperature				
	0.00093	0.00089	0.00085	0.00082	0.00079
+106 -212			9.2E-04	1.1E-03	1.3E-03
+212 -300	1.63E-03		1.8E-03	1.9E-03	2.0E-03
+425-850	2.17E-03		3.2E-03	3.7E-03	
+2000-2800	7.4E-04	1.5E-03		2.9E-03	3.0E-03
+4750-6300	9.6E-04	1.3E-03		2.1E-03	2.6E-03

Values of ln k_{CO}

Particle size range	1/Temperature				
	0.00093	0.00089	0.00085	0.00082	0.00079
+106 -212			-6.99	-6.79	-6.62
+212 -300	-6.42		-6.30	-6.25	-6.19
+425-850	-6.14		-5.76	-5.59	0.00
+2000-2800	-7.21		0.00		-5.81
+4750-6300	-6.95	-6.66		-6.16	-5.94

Interpolated values for ln k_{CO}

Particle size range	1/Temperature				
	0.00093	0.00089	0.00085	0.00082	0.00079
+106 -212	-7.424	-7.195	-6.986	-6.795	-6.617
+212 -300	-6.417	-6.355	-6.299	-6.245	-6.194
+425-850	-6.135	-5.938	-5.759	-5.591	-6.081
+2000-2800	-7.209	-6.494	-6.156	-5.845	-5.805
+4750-6300	-6.948	-6.664	-6.402	-6.161	-5.937

Values of ln k_O and EA

Particle size range	ko (m3/s/kg Fe)	EA (J/mol)
+106 -212	0.10136	45808
+212 -300	0.00676	12667
+425-850	0.00305	3069
+2000-2800	5.61491	79706
+4750-6300	0.59653	57374

Average values for ln k_{CO}

Particle size range	1/Temperature				
	0.00093	0.00089	0.00085	0.00082	0.00079
Average	-6.96104	-6.552775	-6.283238	-6.035427	-5.965703

Average value of ln k_O and EA

	ko (m3/s/kg Fe)	EA (J/mol)
Average	0.53488	56520

Table D.7: *List of rate constants and activation energies calculated from experimental data for degrees of reduction achieved between 30% and 80%*

30 to 80% reduction

Values of k_{CO}

Particle size range	1/Temperature				
	0.00093	0.00089	0.00085	0.00082	0.00079
+106 -212			4.9E-04	5.4E-04	5.9E-04
+212 -300	7.28E-04		1.0E-03	1.2E-03	1.3E-03
+425-850	1.18E-03		2.1E-03	2.7E-03	
+2000-2800	4.8E-04	1.3E-03		3.1E-03	3.2E-03
+4750-6300	5.8E-04	8.8E-04		1.8E-03	2.5E-03

Values of ln k_{CO}

Particle size range	1/Temperature				
	0.00093	0.00089	0.00085	0.00082	0.00079
+106 -212			-7.62	-7.53	-7.44
+212 -300	-7.23		-6.90	-6.75	-6.61
+425-850	-6.74		-6.17	-5.92	0.00
+2000-2800	-7.64		0.00	-5.78	-5.74
+4750-6300	-7.46	-7.04		-6.30	-5.97

Interpolated values for ln k_{CO}

Particle size range	1/Temperature				
	0.00093	0.00089	0.00085	0.00082	0.00079
+106 -212	-7.835	-7.722	-7.619	-7.525	-7.437
+212 -300	-7.225	-7.053	-6.895	-6.748	-6.610
+425-850	-6.743	-6.445	-6.174	-5.921	-6.658
+2000-2800	-7.639	-6.657	-6.201	-5.783	-5.743
+4750-6300	-7.457	-7.039	-6.654	-6.300	-5.972

Values of ln k_O and EA

Particle size range	ko (m3/s/kg Fe)	EA (J/mol)
+106 -212	0.00497	22581
+212 -300	0.03647	34920
+425-850	0.00202	4786
+2000-2800	84.22366	107707
+4750-6300	7.35639	84331

Average values for ln k_{CO}

Particle size range	1/Temperature				
	0.00093	0.00089	0.00085	0.00082	0.00079
Average	-7.454789	-6.890574	-6.520834	-6.181013	-6.098804

Average value of ln k_O and EA

	ko (m3/s/kg Fe)	EA (J/mol)
Average	3.24157	77000

From ***Table D.6.*** and ***Table D.7*** it can be seen that the reduction rate varies significantly with particle size. However, no clear correlation was found between the ore particle size and reaction rate. Reaction rate was therefore found independent of particle size, as would be expected for uniform internal reduction.

As shown in Figure 20 and Figure 21, both uniform and shrinking core reduction patterns were observed for large particles. The reduction rate therefore appears to be influenced more by the morphology of the particles (eg. crack formation, porosity, homogeneity, etc.) than by particle size.

D.4 Model predictions vs measured values

The values of the pre-exponential constant (k_o) and the apparent activation energy (E_a) was used to back-calculate the fraction reacted as a function of time. These graphs were compared to the original data to ensure that the calculated results represented experimental data. These comparisons are shown in ***Figure D.7*** to ***Figure D.11.***

These figures show that the experimental results and model predictions yield similar graphs. This implies that model predictions are representative of the experimentally measured data.

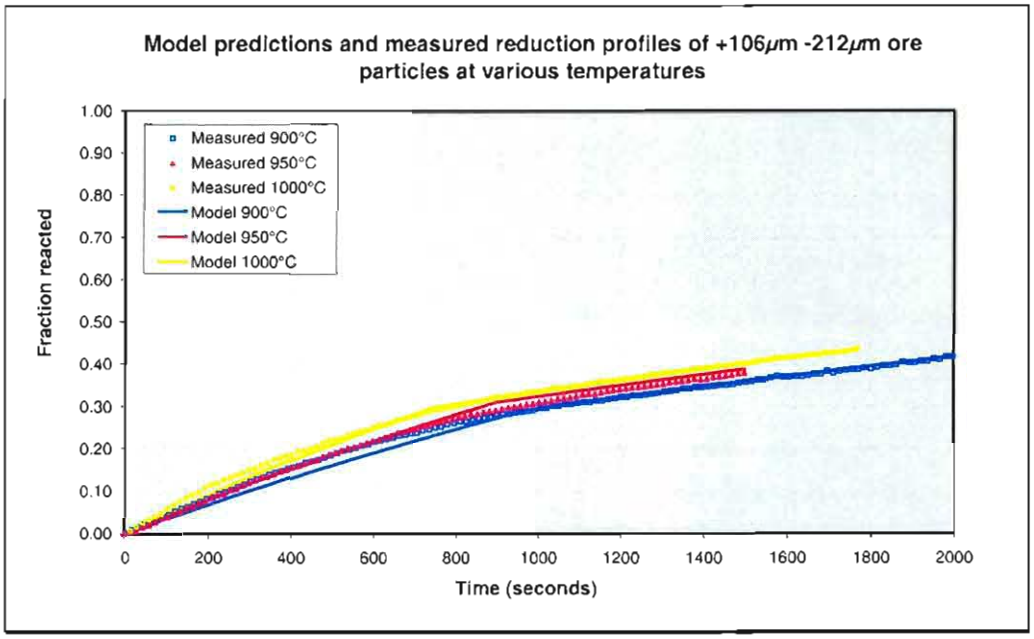

Figure D 7: *Calculated (model) predictions and measured values regarding fraction of reducible oxygen removed as a function of time for ore particles in the size range –212μm +106μm.*

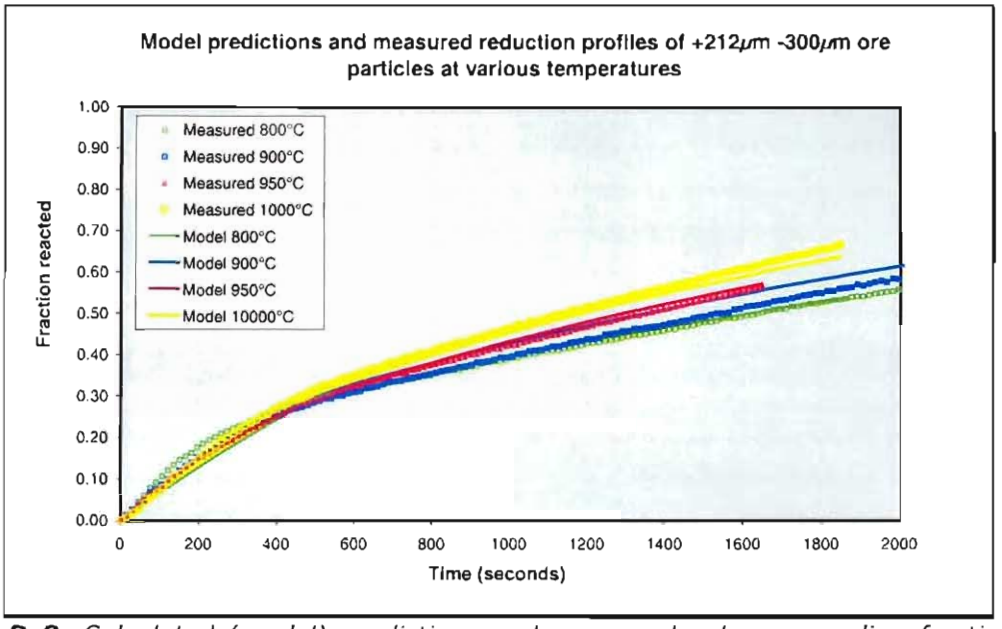

Figure D 8: *Calculated (model) predictions and measured values regarding fraction of reducible oxygen removed as a function of time for ore particles in the size range -300μm +212μm.*

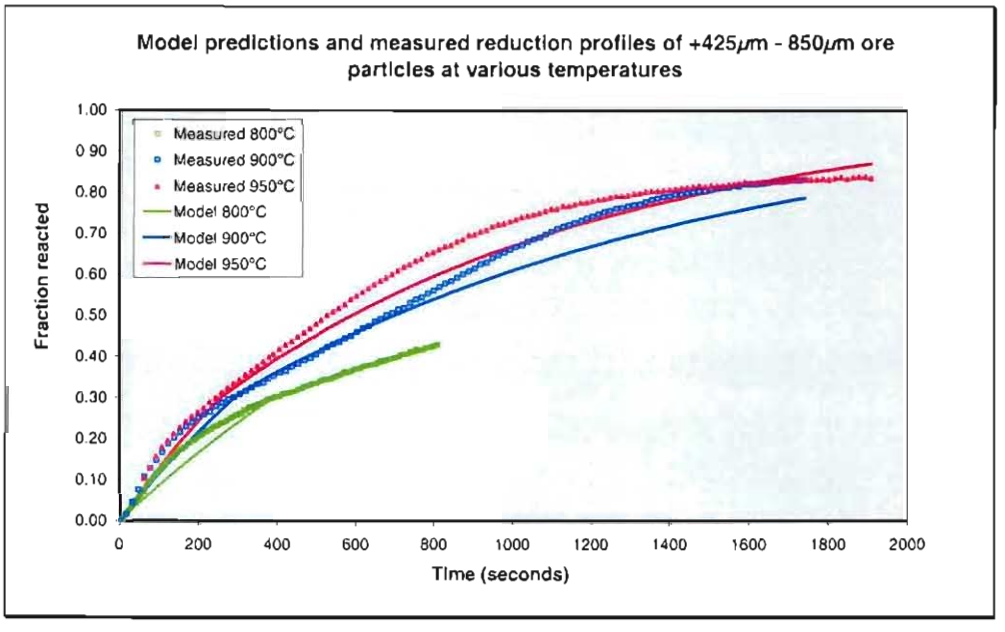

Figure D 9: *Calculated (model) predictions and measured values regarding fraction of reducible oxygen removed as a function of time for ore particles in the size range -850μm +425μm.*

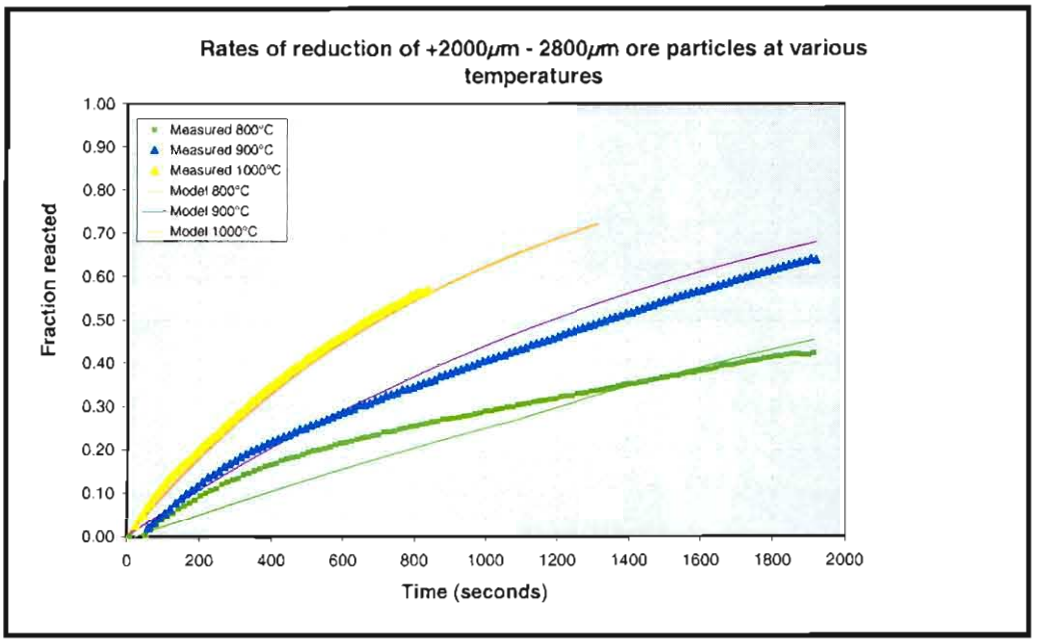

Figure D 10: *Calculated (model) predictions and measured values regarding fraction of reducible oxygen removed as a function of time for ore particles in the size range – 2800μm +2000μm.*

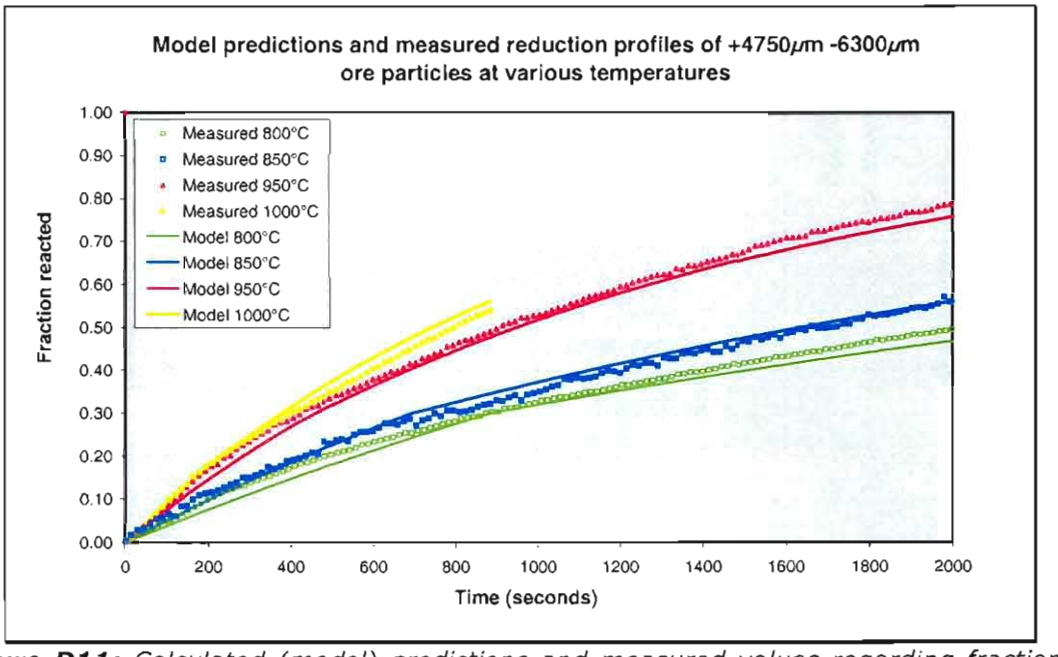

Figure D11: *Calculated (model) predictions and measured values regarding fraction of reducible oxygen removed as a function of time for ore particles in the size range - 6300μm +4750μm.*

APPENDIX E

Model predictions regarding reduction- and temperature profile through the solids bed

E.1 Change in rate constant for the reduction reaction

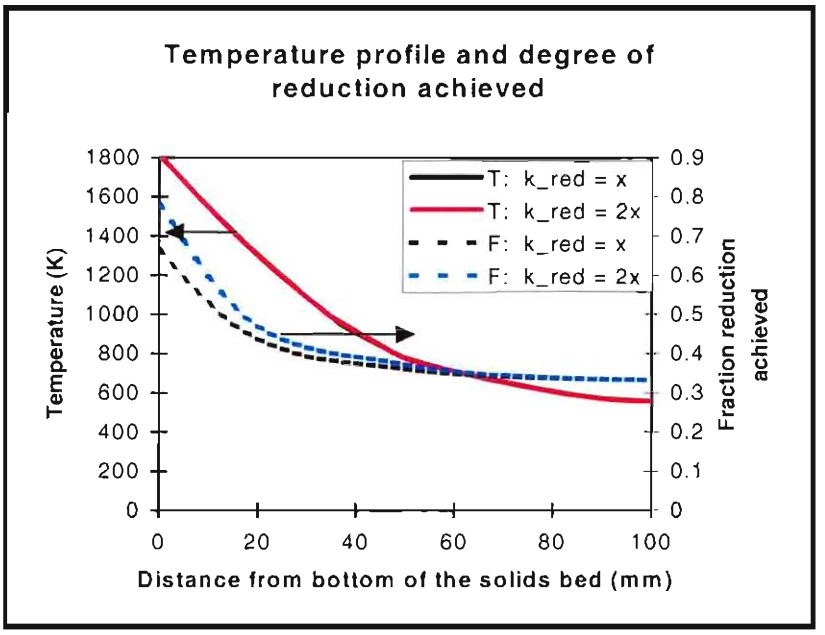

***Figure E 1**: Theoretical profiles of temperature and fraction reduction achieved through a 100mm high solids bed, for a production rate of 30kg/m^2/h, when doubling the rate constant for the reduction reaction.*

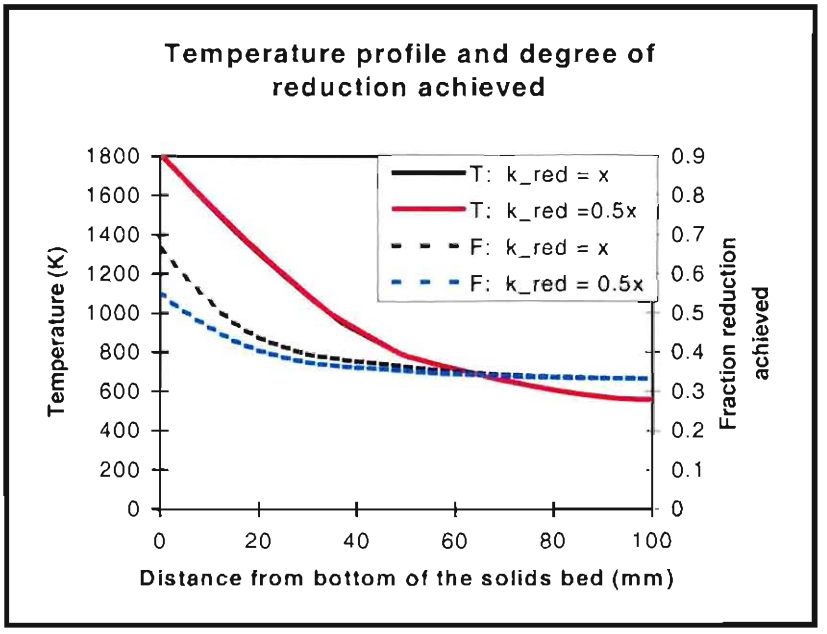

***Figure E 2**: Theoretical profiles of temperature and fraction reduction achieved through a 100mm high solids bed, for a production rate of 30kg/m^2/h, when halving the rate constant for the reduction reaction.*

E.2 Change in rate constant for the gasification reaction

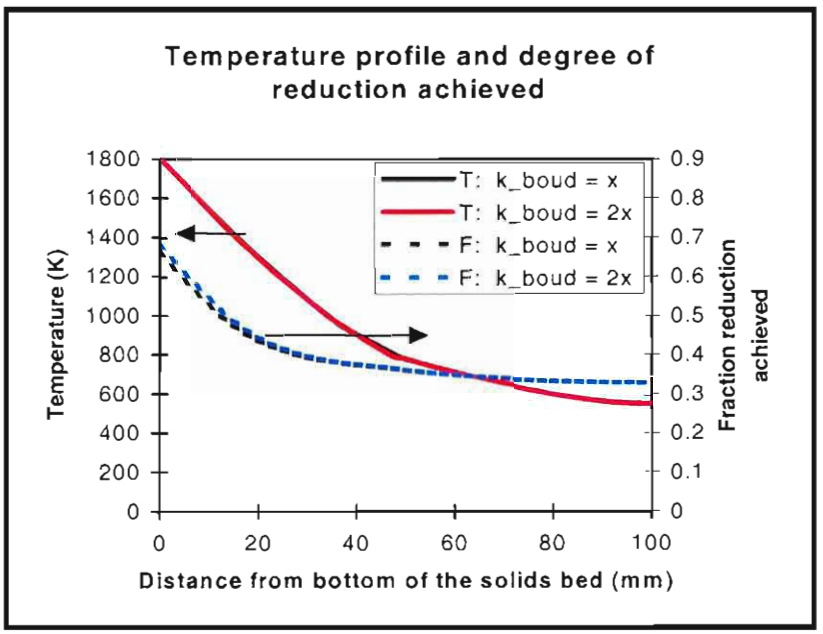

Figure E 3: *Theoretical profiles of temperature and fraction reduction achieved through a 100mm high solids bed, for a production rate of 30kg/m²/h, when doubling the rate constant for the gasification reaction.*

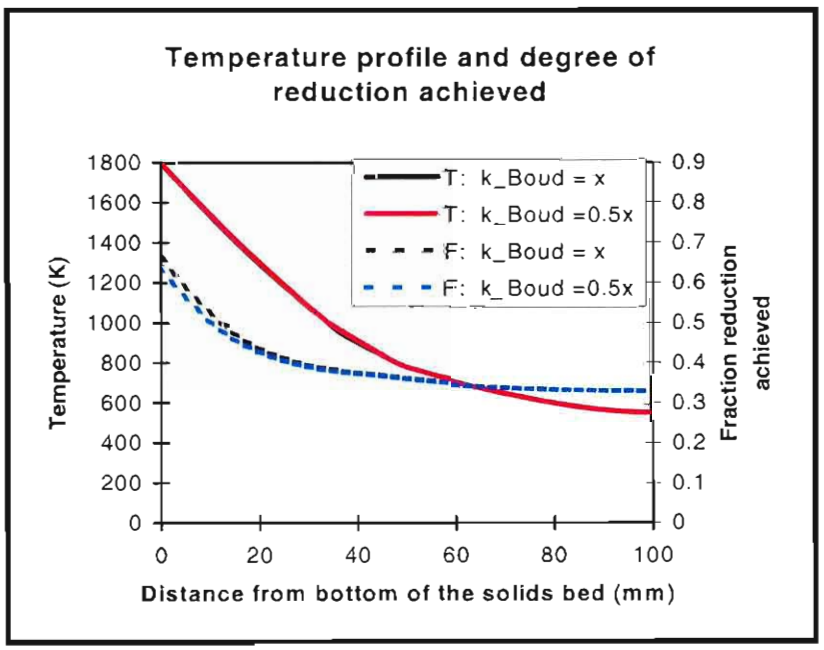

Figure E 4: *Theoretical profiles of temperature and fraction reduction achieved through a 100mm high solids bed, for a production rate of 30kg/m²/h, when halving the rate constant for the gasification reaction.*

E.3 Change in thermal conductivity of the bed

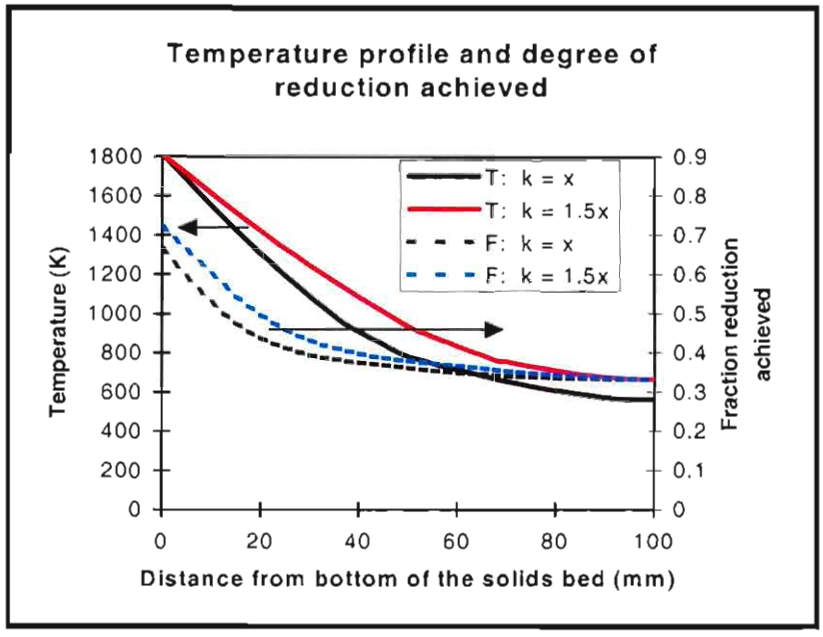

Figure E 5: *Theoretical profiles of temperature and fraction reduction achieved through a 100mm high solids bed, for a production rate of 30kg/m²/h, when increasing the thermal conductivity of the solids bed 1.5 times.*

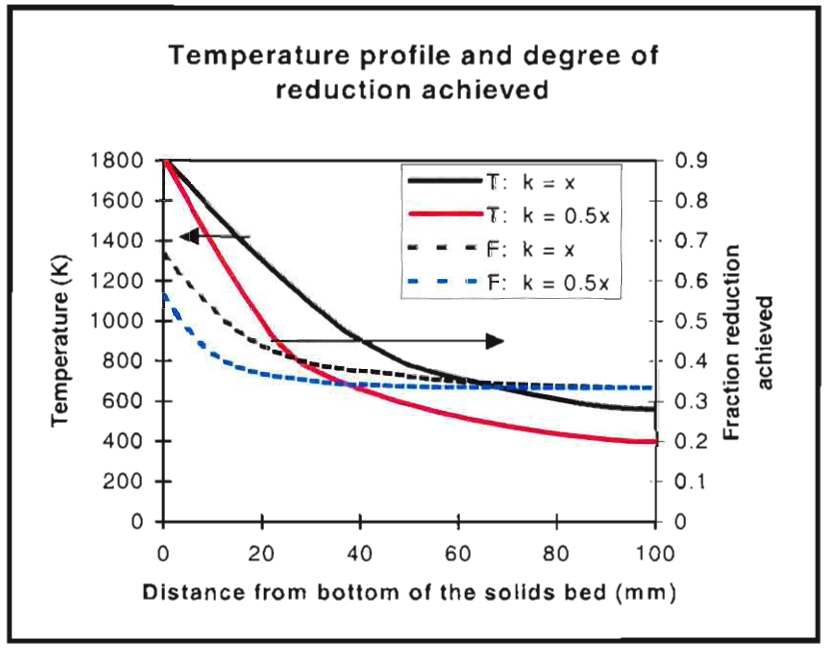

Figure E 6: *Theoretical profiles of temperature and fraction reduction achieved through a 100mm high solids bed, for a production rate of 30kg/m²/h, when halving the thermal conductivity of the solids bed.*

E.4 Change in bath temperature

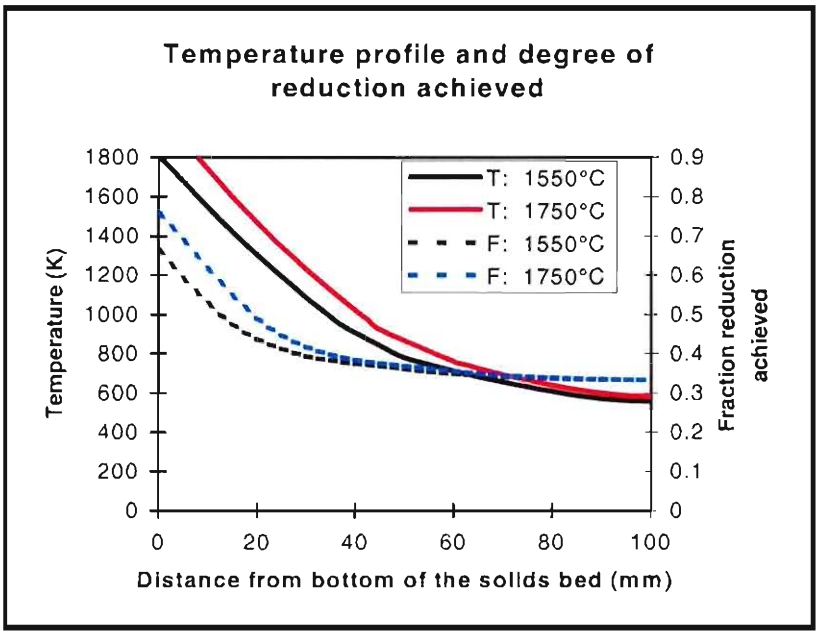

Figure E 7: *Theoretical profiles of temperature and fraction reduction achieved through a 100mm high solids bed, for a production rate of 30kg/m^2/h, when increasing the bath temperature from 1550°C to 1650°C.*

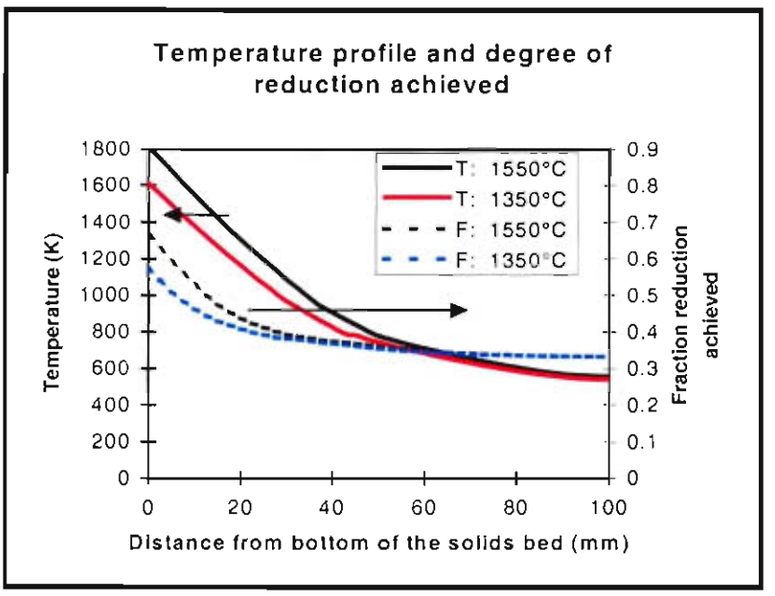

Figure E 8: *Theoretical profiles of temperature and fraction reduction achieved through a 100mm high solids bed, for a production rate of 30kg/m²/h, decreasing the bath temperature from 1550°C to 1350°C.*

E.5 Change in production rate

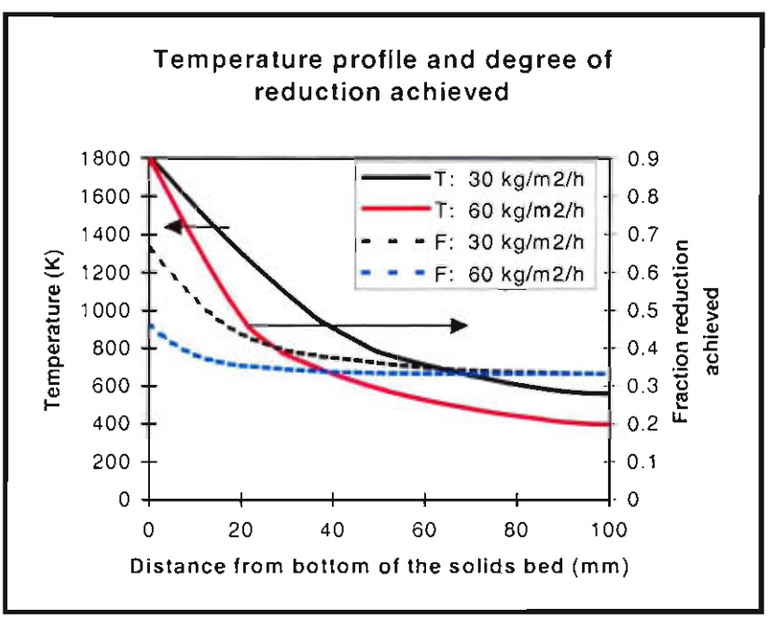

Figure E 9: *Theoretical profiles of temperature and fraction reduction achieved through a 100mm high solids bed, for a production rate of 30kg/m²/h as well as 60kg/m²/h.*

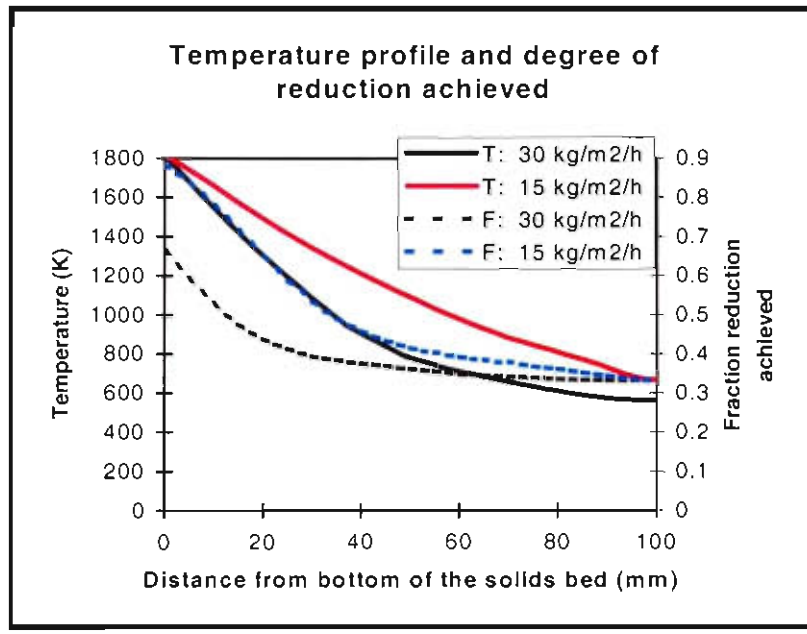

Figure E 10: *Theoretical profiles of temperature and fraction reduction achieved through a 100mm high solids bed, for a production rate of 30kg/m^2/h as well as 15kg/m^2/h.*

APPENDIX F

Experimental aspects: Induction furnace

page no

Appendix F: Experimental aspects: induction furnace

F.1. Raw material mixture selection

Although the $FC/O_{(red)}$ ratio for the feed material at the pilot plant was 1.3, this ratio could not be used for the induction furnace experiments. This is because excess carbon is not oxidised on the outer surface of the solids bed in the induction furnace, as was the case in the pilot plant furnace[10].

To choose the material mixture composition in terms of fixed carbon to reducible oxygen ratio, a thermo gravimetric experiment was done. For this, three samples were compiled, with $FC/O_{(red)}$ ratios of 0.85, 1.0 and 1.15 respectively. The samples comprised of iron ore, char, calcinated dolomite (doloma) and calcinated limestone (lime). Burnt fluxes and char was used because it was assumed that devolatilization and calcinations occurred in the upper part of the solids bed[19]. The samples were reacted in the TGA at 1100°C, since this was the expected average temperature in the lower part of the bed. The experimental equipment and procedures discussed in ***paragraph 2.2*** were used for this test.

The samples were reacted until no further mass loss occurred, after which the samples were removed from the furnace and their respective carbon contents were determined with a Leco CS 400 analyser. From the mass loss (comprising mainly of loss of carbon and oxygen) and the change in carbon content of the sample, the degree of reduction achieved and the amount of excess carbon remaining in the sample was calculated. These results are shown in ***Figure F 1***

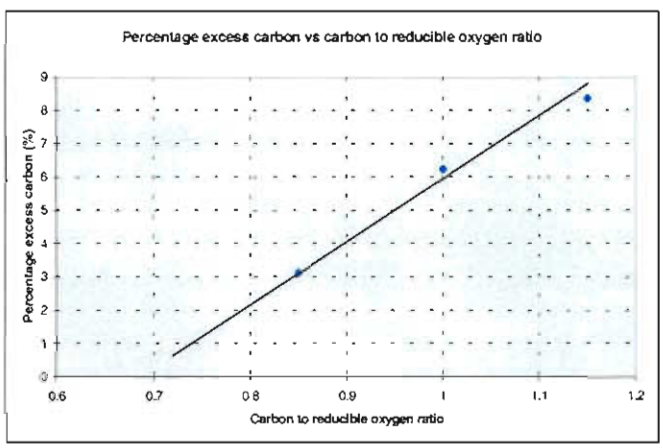

Figure F 1: *Excess carbon in samples as a function of fixed carbon to reducible oxygen ratios*

Figure F 1 shows that a $FC/O_{(red)}$ ratio of 0.7 will yield no excess carbon in the sample. Carbon losses during establishing of the solids bed were estimated at 3% (which was a guess based on pilot plant operations). Accordingly, a fixed carbon to reducible oxygen ratio of 0.85 was chosen for the mixture.

The first seven experiments at the induction furnace (as described in ***paragraph 3.4***) were positioning exercises, during which the experimental equipment and procedure was developed. During these tests the mixture with $FC/O_{(red)}$ ratio of 0.85 was tested to confirm that the mixture would yield a bath with carbon content between 0.01 and 0.1%.

Similar to the way in which the char content of a sample was governed by the $FC/O_{(red)}$ ratio, the doloma and lime content were governed by the anticipated MgO content and basicity of the slag. Since pilot plant trails for the Ifcon process was run with a mixture aiming for 8% MgO in the slag and a CaO/SiO_2 ratio in the slag of 1.4[17], the same criteria was used for this experiment.

The final material mixture selections for simulation of the bottom part of the solids bed in the Ifcon processs are shown in ***Tabel F 1***

Tabel F 1: *Material mixtures used as feed material to the induction furnace*

Feed material	0% pre-reduced mixture	30% pre-reduced mixture	50% pre-reduced mixture
Ore content (%)	78.6	78.2	77.8
Char content (%)	14.3	14.1	14.0
Doloma content (%)	3.4	3.7	3.9
Lime content (%)	3.7	4.0	4.3

F.2. Crucible positioning in the induction furnace

The crucible was positioned so that the surface of the molten bath was at the height of the highest loop of the coil of the inductor. This is the height, above which the induction field deteriorates. Prior to testing, this height was determined by placing six similar mild steel discs in the furnace at various heights, but similar distances from the coil. The

power input to the furnace was set at 20 kW, and the temperature of each metal disc was measured, using a Pt/Pt10%Rh (or type S) thermocouple. From the temperature vs time curves, the heating rate of each disc was calculated. The furnace was cooled and the test was repeated for power inputs of 35 and 50 kW. The results are shown in ***Figure F 2***.

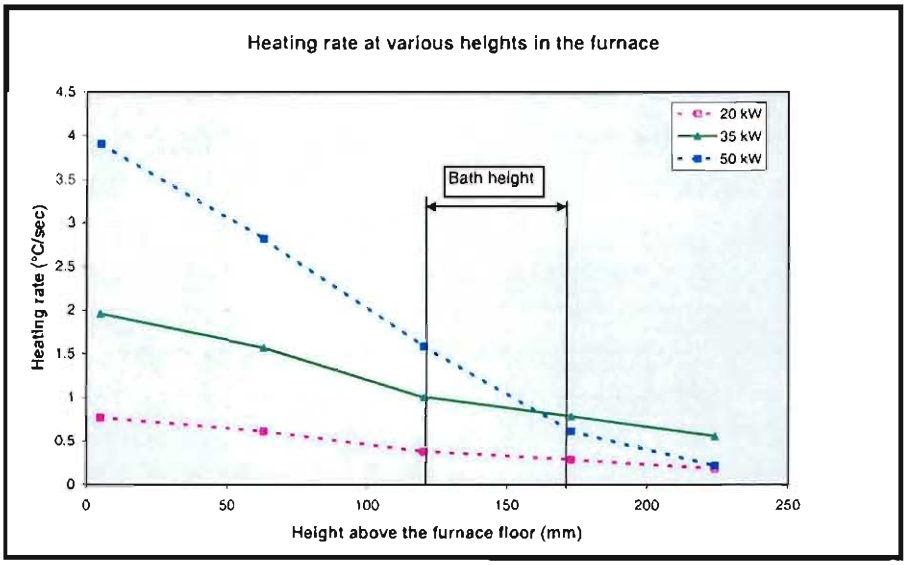

Figure F 2: *Heating rate curve for the induction furnace.*

From the heating rate curves, the height at which the induction field deteriorates (the heating rate curve flattens) was obtained. Since a heat input of about 35kW was anticipated, the bath was established 30 cm below the reference floor height.

During initial test work, attempts were made to establish a metal bath at different heights in the furnace. For this, a trail and error approach was followed. The bath height position determined by this trail and error method was similar to that determined by heating of the discs (as discussed above).

F.3. Calibration of Rotameters with a Bunsen tower.

The method used was similar to the technique discussed in ***Appendix A.1***. However, due to the relatively high flow rates required, a 1000cm^3 Bunsen tower was used. Two rotameters were calibrated, one for the argon purge-gas line and one for the exit-gas line. Since only argon was used as purge gas, the rotameter in the purge-gas line was calibrated with argon. The gas mixture passing through the exit-gas line was expected to be a mixture comprising mainly of argon and carbon monoxide. Accordingly, argon and

carbon monoxide was used to calibrate the rotameter in the exit-gas line. Since the exit gas mainly comprised of argon (± 80%), the calibration curve for argon was used to calculate molar mass flows of species. The calibration curves are shown in ***Figure F 3***.

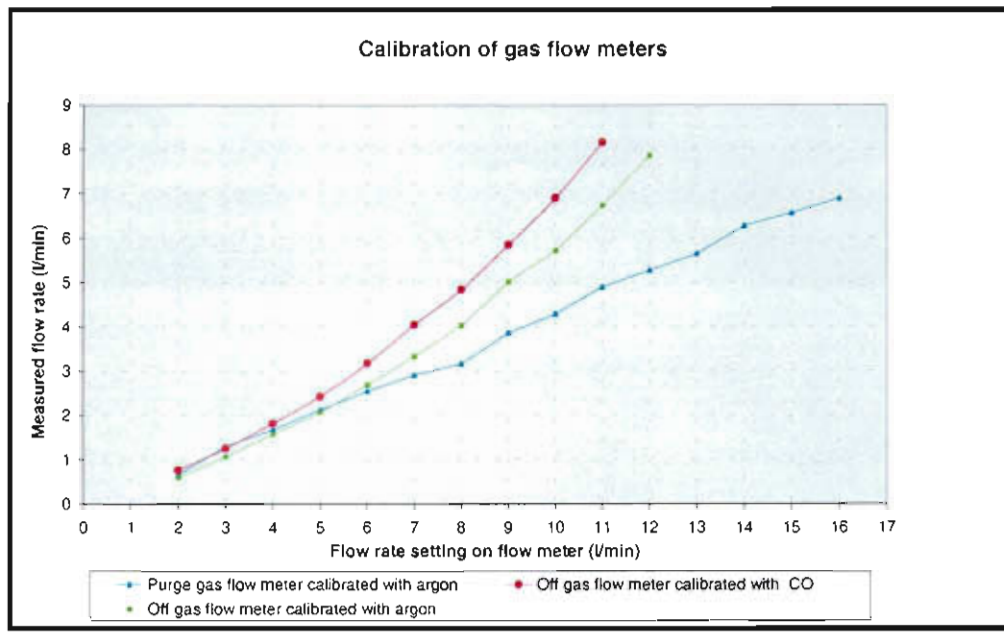

Figure F 3: *Calibration curves for rotameters*

F.4. Visual images from sample cross sections.

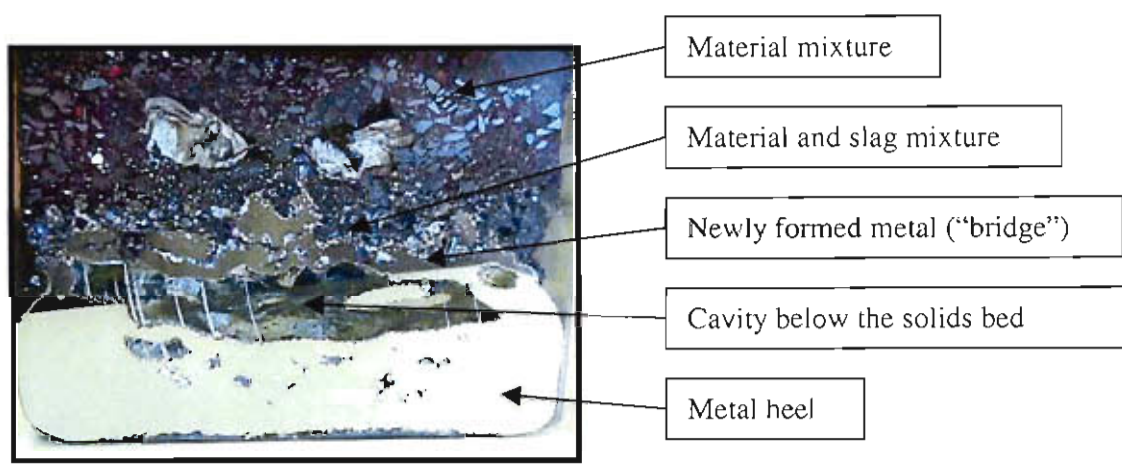

Figure F 4: *Visual image of an impregnated cross section of a sample*

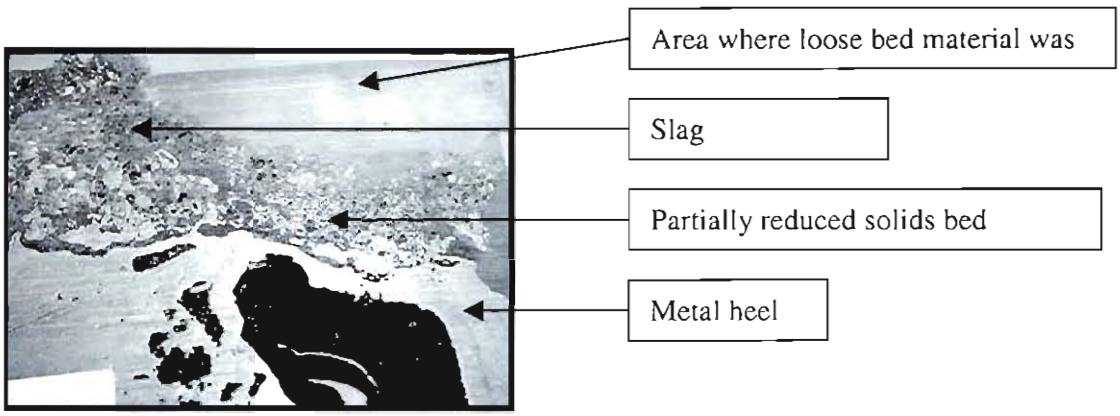

Figure F 5: *Visual image of an impregnated cross section of a sample*

F.5. Gas analyses measured during test work.

The gas analyses obtained are presented in Table F 2 to Table F 5. These analyses were used

Tabel F 2: *Gas analysis from test done with 0% pre-reduced material, during which a production rate of 20 kg Fe /m²/h was achieved.*

Time	Gas composition			
	Ar	CO	CO_2	N_2
	(%)	(%)	(%)	(%)
12:09:46	5.94	5.55	3.69	54.37
12:17:38	42.21	23.97	27.15	4.94
12:23:49	54.15	19.40	20.86	4.19
12:30:00	57.16	14.66	23.70	3.47
12:36:10	61.29	16.52	19.27	1.91
12:42:19	57.04	21.91	18.71	1.60
12:48:32	61.66	19.49	15.37	2.27
12:54:45	62.02	19.11	16.51	1.60
13:00:57	64.98	18.61	14.04	1.71
13:07:09	69.03	12.18	16.05	1.91
13:13:22	68.65	13.81	15.13	1.78
13:19:36	50.44	32.20	15.61	0.87
13:25:48	66.08	17.00	14.34	1.49
13:32:01	70.08	15.26	12.31	1.62
13:38:14	71.81	14.83	10.11	2.51
13:44:27	73.18	15.54	8.52	2.04
13:50:41	73.49	16.69	6.37	2.72
13:56:55	38.69	42.60	15.09	1.44
14:03:07	28.05	45.31	23.75	0.80
14:09:18	54.07	34.67	8.47	1.50
14:15:30	27.45	11.46	8.72	44.65
14:43:06	18.67	41.13	20.63	15.72
14:49:15	57.31	21.25	16.74	3.12

Tabel F 3: *Gas analysis from test done with 0% pre-reduced material, during which a production rate of 55 kg Fe /m²/h was achieved.*

Time	Gas composition			
	Ar	CO	CO_2	N_2
	(%)	(%)	(%)	(%)
11:40:27	5.48	5.22	3.55	55.78
11:46:41	5.88	5.78	4.20	55.95
11:52:53	5.88	5.80	4.38	56.19
11:59:05	5.56	5.76	4.28	56.21
12:05:15	5.29	5.04	4.10	57.34
12:11:21	4.56	4.19	3.42	61.24
12:17:26	3.81	3.15	2.64	66.03
12:23:31	3.33	2.43	2.16	69.15
12:29:36	3.01	1.95	1.84	71.22
12:35:43	2.81	1.62	1.64	72.51
12:43:23	28.02	41.07	18.40	6.89
12:49:34	40.67	30.90	24.93	1.20
12:55:44	56.38	20.24	20.55	1.41
13:01:54	53.36	24.91	19.29	1.17
13:08:04	3.22	55.36	0.98	18.82
13:14:19	46.06	33.27	18.93	1.06
13:22:15	47.64	35.47	11.45	3.72
13:28:27	57.03	22.02	18.03	1.70
13:34:38	41.58	36.24	20.05	1.05
13:40:48	44.14	36.77	16.70	1.08
13:47:00	53.19	31.41	12.99	1.39
13:53:12	54.06	31.50	11.85	1.62
13:59:24	60.01	21.34	15.42	2.09

Tabel F 4: *Gas analysis from test done with 30% pre-reduced material, during which a production rate of 19 kg Fe /m²/h was achieved.*

Time	Gas composition			
	Ar	CO	CO_2	N_2
	(%)	(%)	(%)	(%)
13:52:37	27.05	49.71	15.53	5.95
13:58:51	49.09	35.40	12.05	1.94
14:05:05	57.81	29.86	9.34	1.81
14:11:19	58.56	27.98	9.69	2.27
14:17:32	56.35	30.63	9.90	1.90
14:23:46	60.09	27.18	7.71	3.33
14:30:00	60.13	25.86	10.81	2.05
14:36:13	61.07	25.49	10.23	2.03
14:44:04	32.72	52.71	12.13	0.85
14:50:18	31.10	56.71	9.83	0.90
14:56:32	60.47	30.04	6.06	1.70
15:02:48	62.97	28.11	5.93	1.69
15:09:06	55.23	37.01	4.65	1.45
15:15:23	70.00	21.54	4.44	2.92
15:21:40	71.32	21.19	3.78	2.21
15:27:55	66.81	23.98	4.71	3.16
15:34:10	64.16	26.41	4.55	3.18
15:40:31	64.30	27.53	4.77	2.03
15:46:45	47.26	42.65	7.12	1.74
15:52:58	73.62	18.33	4.60	2.29
15:59:12	76.64	14.61	3.97	3.62
16:08:45	66.92	23.66	2.67	4.75
16:15:02	66.06	12.90	4.44	14.54

Tabel F 5: *Gas analysis from test done with 50% pre-reduced material, during which a production rate of 18 kg Fe /m²/h was achieved.*

Time	Gas composition			
	Ar	CO	CO_2	N_2
	(%)	(%)	(%)	(%)
12:49:57	47.87	13.32	5.45	25.61
12:59:44	46.41	12.43	5.14	27.69
13:09:30	47.29	11.04	4.16	29.25
13:19:04	49.96	9.67	3.59	29.12
13:28:38	48.74	8.31	3.49	30.95
13:38:15	49.51	7.83	3.20	31.29
13:47:51	51.01	6.92	2.71	31.30
13:57:28	51.95	6.19	2.43	31.36
14:07:05	51.71	5.96	2.36	31.87
14:16:41	51.42	2.09	1.06	36.99
14:28:43	46.43	6.90	3.18	34.72
14:38:21	45.23	7.45	3.23	35.25
14:47:58	43.10	8.62	3.44	35.83
14:57:41	43.97	6.69	3.02	36.83
15:07:19	40.79	9.01	3.73	37.08
15:16:54	11.91	30.08	5.17	41.67
15:26:30	28.14	14.21	3.35	43.22
15:36:12	34.14	8.17	3.06	43.52
15:45:50	36.28	7.03	2.70	43.24
15:55:28	37.49	6.51	2.36	42.91
16:05:11	39.62	5.26	1.86	42.69
16:14:49	41.59	4.27	1.46	42.15
16:24:33	36.01	8.51	2.65	42.27

F.6. Temperature profiles through the solids bed.

The Temperatures measured in the solids bed of various experiments are presented below.

Tabel F 6: *Temperature profile of 0% pre-reduced material with which a production rate of 20 kg Fe /m²/h was achieved.*

Trail 1	
Height above metal bath	**Temperature**
(mm)	**(°C)**
84	653
79	
74	660
69	
64	667
59	
54	677
49	
44	757
39	795
34	873
29	
24	980
19	1068
14	1155
9	1228
4	1324

Tabel F.7: *Temperature profile of 0% pre-reduced material with which a production rate of 55 kg Fe /m²/h was achieved.*

Trail 1	
Height above metal bath	**Temperature**
(mm)	**(°C)**
21	814
16	913
11	1074
6	1193
1	1323

Tabel F 8: *Temperature profile of 30% pre-reduced material with which a production rate of 19 kg Fe /m²/h was achieved.*

Trail 1	
Height above metal bath	**Temperature**
(mm)	**(°C)**
47	744
42	
37	856
32	
27	1027
22	1145
17	1260
12	1329
7	
2	

Tabel F 9: *Temperature profile of 50% pre-reduced material with which a production rate of 18 kg Fe /m²/h was achieved.*

Trail 1		Trail 2		Trail 3	
Height above metal bath	Temperature	Height above metal bath	Temperature	Height above metal bath	Temperature
(mm)	(°C)	(mm)	(°C)	(mm)	(°C)
61	755	75	625	68	650
51	880	70	650	63	770
41	1025	60	740	53	860
31	1110	50	855	43	990
26	1200	40	1000	28	1180
21	1250	35	1065	23	1230
16	1315	30	1170	18	1300
11	1350	25	-273	13	1335
6	1390	20	1300	8	1375
1	1410	15	1340	3	1370
		10	1370		
		5	1405		
		0	1440		

Reduction of iron ore fines in the Ifcon furnace

by

Leon Lourens

A dissertation submitted in fulfilment of the requirements for the degree

Masters in Engineering [Metallurgical Engineering]

in the Faculty of Engineering, Built Environment and Information Technology

University of Pretoria

PRETORIA

Supervisor: Prof. J.M.A. Geldenhuis

October 2002

Abstract

This work involved an investigation into the mechanisms governing the reduction of material in the solids bed of the Ifcon® process. Thermo gravimetric analyses were done to investigate the influence of various operational parameters on the rate of solid state reduction. The experiments were modeled, and model predictions were compared to experimental results. Kinetic data was analised and the reduction rate constants were calculated. The rate constants were used as inputs to a model, which describes the reduction behaviour and temperature profile in a composite solids bed (similar to that in the Ifcon® process). High temperature reduction- and melting tests were done in an 150 kW induction furnace, to simulate final reduction in a solids bed. The temperature profile through the solids bed was measured and results were compared to model predictions. Finally the extent to which solid state reduction occurs in the solids bed was estimated as a function of production rate.

Keywords: Ifcon®, thermo gravimetric analyses, reduction and melting, model, kinetics, induction furnace, temperature profile, production rate.

Opsomming

Hierdie werk behels 'n ondersoek na die meganismes ter sprake in die gepakte bed van die Ifcon® proses. Termogravimetriese analises is gedoen om die invloed van verskeie bedryfsparameters op die reduksietempo van komposiet-mengsels te ondersoek. Kinetiese data is geanaliseer, en tempokonstantes asook waardes vir aktiveringsenergie is bereken. Hierdie kinetiese data is as insette gebruik vir 'n model wat die mate van reduksie behaal asook die temperatuurprofiel in 'n gepakte bed voorspel. Hoë temperatuur reduksie-en smeltingstoetse is in 'n 150 kW induksieoond gedoen om reduksie in die gepakte bed van die Ifcon® proses te simuleer. Die temperatuurprofiel deur die gepakte bed is gemeet. Die gemete waardes is met modelvoorspellings vergelyk, en 'n raming is gemaak van die mate waartoe vaste toestand reduksie in 'n gepakte bed verloop, as 'n funksie van produksietempo.

Sleutelwoorde: Ifcon®, termogravimetriese analise, reduksie en smelting, model, kinetiese data, induksie oond. temperatuurprofiel, produksietempo.

Acknowledgements

I am indebted to the following persons and institutes for their support and guidance:

Professor J.M.A. Geldenhuis, my supervisor, for his support and efforts.
Professor P.C. Pistorius for his advice as well as for the use of his kinetic model.
Professor R.J. Fruehan for his advice.
Brian van Rooyen, the IFCON team and Kumba Resources for the opportunity and financial support.
All the others who offered advice and help at some stage.

TABLE OF CONTENTS

Page no

LIST OF TABLES

LIST OF FIGURES